POLITECNICO DI TORINO

FACOLTÀ DI INGEGNERIA

CORSO DI LAUREA MAGISTRALE IN INGEGNERIA AEROSPAZIALE

Tesi di Laurea Magistrale

Use of advanced co-simulation tools for CFD-Multibody modeling and analysis of a Landing gear

Relatore:

Prof. Ing. Francesco Larocca

Candidato:

Marco Carotenuto
Matr. 234917

Tutor aziendale:

Ing. Daniele Catelani

Ing. Elia Cipolato

Anno Accademico 2018/2019

Contents

List of figures

Introduction

This thesis work has been written as outcome of the activity carried out at the MSC Software company in Turin.

The following analysis will present the study of an aeronautical landing gear during the landing phase. During the aforementioned phase, that is the extraction of the landing gear from the appropriate compartment, in order to pass from the rest condition to the fully extended configuration, mechanical forces and torques will be required. Beyond this aspect, it must be considered that in the meantime the aircraft is moving inside a viscous fluid, or air, and that therefore aerodynamic forces will arise which influencing the landing gear extraction process.

The main purpose of this thesis work is to reconcile these two aspects in order to carry out a more accurate analysis, and this has been possible thanks to the use of MSC Adams and scFLOW software.

With Adams it has been possible to take care of the kinematic and dynamic aspect of the problem by considering the landing gear, in accordance with the philosophy of "multibody" analysis, as a set of rigid bodies connected to each other through a series of kinematic constraints.

On the other hand scFlow, has been used for modelling and simulating what happens by entering the body into a fluid stream moving at a certain speed.

The key element that allowed the two codes to communicate with each other and therefore to obtain results taking into account both the physical phenomena is a so-called engine code, still under development and testing, MSC Cosim.

The current work, after a brief theoretical discussion of the equations implemented within the codes, is divided into four sections.

The first one involves the creation of the Adams model, constituted by a set of bodies and constraints defining the landing gear and the setup of applied motion through mathematical function. The model of the landing gear basically can be split in three groups with relative movement between them, i.e. an upper connecting rod which acts as a connection between the wing and the landing gear, a lower rod connecting the

upper rod to the landing gear leg and, at the end, the landing gear leg provided with the tire.

The second section of the work, similarly, involves the realization of the scFLOW model in which a preliminary phase of defeaturing and improving the CAD model is carried out to avoid problems in the calculation phase followed by the preparation of the actual CFD analysis: it consists of a transient analysis that exploits the $k - \omega$ turbulence model and the incompressible flow hypothesis due to the low velocities under examination. Since there are three moving parts it has been necessary to build, in addition to the main mesh, three "slave meshes" integrated with the moving components.

The third section consists in the actual calculation in which the use of the "co-simulator" is fundamental: it has the task of putting in communication the two models and therefore exchanging information such as displacements and forces between the codes.

Finally, we analyze the obtained results by making also a comparison with the results relating to an analysis in which the effect of the aerodynamic forces during the landing gear extraction are neglected.

It is necessary to point out that the presented work must be considered as a first preliminary investigation since the used co-simulation software is still in the development phase and, in order to better explain the physical phenomena involved, it would have been required a more accurate calculation grid.

Chapter 1

Introduction to the principles of multibody simulation

1.1 Introduction

It should be noted that, in this chapter, the formulation of the equations have been presented with reference to [1].

The simulation of Multibody systems consists in the study of the motion of mechanical systems caused by external forces. It is characterized by large displacements and large movements of the system, that is the amplitude of the relative movement between the components is comparable to the general dimensions of the system. In a mechanical system both rigid and flexible bodies can be found, connected to each other through kinematic constraints. These simulation codes, including Adams (Automated Dynamic Analysis of Mechanical Systems), are mainly based on the principles of the Lagrangian dynamics. Although the theory was already known in the eighteenth century, until recently, the complexity of the Lagrangian equations did not allow the study of various applications. With the development of high-speed computers correlated with the new sophisticated numerical calculation methods for solving algebraic and differential equations, it led to the concrete use of the Multibody programs.

MSC ADAMS allows to perform different types of analysis according to the needs of designer, in particular:

- Initial conditions analysis – it is the starting point before tha static, almost-static or dynamic analysis. Adams verifies that the system state, relative to displacements and velocities, is compatible with constraint equations.
- Kinematic analysis – it allows to determine the motion of the system.

- Static analysis – it allows to determine the equilibrium configuration of the system intended as a balance between internal and external forces when there is no motion or inertial forces

- Dynamic analysis – it describes the multibody mechanism by providing the temporal solution of DAE system.

- Linear analysis – Linearization of non-linear equations system around an operative point. The resolution of linear system allow to obtain the eigenvalues, eigenvectors and the state matrix. The eigenvalues are relative to the frequencies while the eigenvectors to the vibration modes of the system.

The analyzes described, moment by moment, in output provide data such as:

- ➢ Displacements
- ➢ Velocities
- ➢ Accelerations
- ➢ Reaction force
- ➢ Applied force
- ➢ User-defined variables
- ➢ User-defined results
- ➢ State matrix of linearized system
- ➢ Eigenvalues and eigenvectors

Thanks to this calculation flexibility Adams finds different fields of application including:

- Automotive industry

- Aeronautic and aerospace industry

- Mechanic industry

Below is a brief description of the equations solved in Adams.

1.2 Cordinates used in Adams

Considering a generic rigid body its position can be defined by 3 Cartesian cordinates:

$$p = \begin{bmatrix} x \\ y \\ z \end{bmatrix} \qquad (1.2.1)$$

The orientation of a rigid body is defined by a set of 3 Euler angles that correspond to the 3-1-3 sequence rotation. These 3 angles are stored in an array in the following form:

$$\epsilon = \begin{bmatrix} \psi \\ \phi \\ \theta \end{bmatrix} \qquad (1.2.2)$$

The cordinates relative the position and the orientation of a rigid body i in ADAMS is denoted with:

$$q_i = \begin{bmatrix} p_i \\ \epsilon_i \end{bmatrix} \qquad (1.2.3)$$

According to this choice the body longitudinal and angular velocity can be written as:

$$u = \dot{p} \qquad (1.2.4)$$

$$\bar{\omega} = B\dot{\epsilon} = B\xi \qquad (1.2.5)$$

Where

$$B = \begin{bmatrix} sin\phi \ sin\theta & 0 & cos\phi \\ cos\phi \ sin\theta & 0 & -sin\phi \\ cos\theta & 1 & 0 \end{bmatrix} \qquad (1.2.6)$$

In which $\bar{\omega}$ is expressed in body local coordinate system.

Considering a complex mechanical system containing nb bodies, the writing become:

$$q = [q_1^T \ q_2^T \ \dots \ q_{nb}^T]^T = [q_1 \ q_2 \dots q_n]^T \qquad (1.2.7)$$

In which $n = 6 \cdot nb$ describes at a given time the position and orientation of each body in the system.

1.3 Joints in Adams

Joints in ADAMS take on the configuration of displacement and rotation constraints around the three axis. From a mathematical point of view a constraint can be defined as:

$$\Phi(q) = 0 \qquad\qquad (1.3.1)$$

By extending writing for a system having more constraints:

$$\Phi(q) = [\Phi_1^T(q)\ \ \Phi_2^T(q) \dots \Phi_{ni}^T(q)]^T = [\Phi_1^T(q)\ \ \Phi_2^T(q) \dots \Phi_m^T(q)]^T \qquad (1.3.2)$$

Where ni is the number of joints present in the system while m is the sum of the number of constraints induced by each joint (Typically $m < n$). By doing the derivative of Eq.(1.3.2), the velocity kinematic constraint equations are obtained as:

$$\Phi_q \dot{q} = 0 \qquad\qquad (1.3.3)$$

By differentiating again the Eq.(1.3.3), the acceleration kinematic constraint equations are obtained as:

$$\Phi_q \ddot{q} = -\left(\Phi_q \dot{q}\right)_q \dot{q} = \tau \qquad\qquad (1.3.4)$$

The position, velocity and acceleration kinematic constraint equation are conditions that the Eq.(1.2.7) with its frist and second time derivatives must satisfy in order to ensure a sense to the evolution of mechanical system.

1.4 Motions in Adams

The motions can be defined as the explicit dependence from time of the generalized coordinates or an expressions which depends on the generalized coordinates.

Then, from a mathematical point of view, a motion can be rapresented as a constraint equation in which time dependence appears:

$$\Phi(q, t) = 0 \qquad (1.4.1)$$

By differentiating the new velocity and acceleration kinematic constraint equations are obtained and them with the position one must be satisfied at any time t.

$$\Phi_q(q, t)\dot{q} = -\Phi_t(q, t) \qquad (1.4.2)$$

$$\Phi_q(q, t)\ddot{q} = -\left(\Phi_q\dot{q}\right)_q \dot{q} - 2\Phi_{qt}(q, t) - \Phi_{tt}(q, t) \qquad (1.4.3)$$

Defined these three equations, it can be introduced the definition of consistent generalized coordinates if they satisfy the position kinematic constraint equations. In the same way if a set of generalized velocities satisfy the velocity kinematic constraint equation can be considered consistent.

1.5 Dynamic Analysis

1.5.1 Definition of physical quantities

To define the equations of motion is necessary to introduce some physical quantities:

- M – generalized mass matrix
- $\bar{J}$ – generalized inertia matrix relative to the principal local reference frame
- K – kinetic energy

The kinetic energy is defined as:

$$K = \frac{1}{2} u^T M u + \frac{1}{2} \bar{\omega}^T \bar{J} \bar{\omega}^T \qquad (1.5.1.1)$$

- $\lambda \in R^m$ – array of Lagrange multipliers
- $(q, \dot{q}, t) = \begin{bmatrix} f \\ \bar{n} \end{bmatrix} \in R^6$ – the vector of applied forces
- $Q(q, \dot{q}, t) \in R^6$ – the generalized force acting on the body (by projecting the applied force upon the generalized coordinates)

The generalized force can be expressed as:

$$Q = \begin{bmatrix} (\Pi^P)^T f \\ (\Pi^R)^T \bar{n} \end{bmatrix} \qquad (1.5.1.2)$$

$$\Pi^P = \frac{\partial v^P}{\partial u} \qquad (1.5.1.3)$$

$$\Pi^R = \frac{\partial \bar{\omega}}{\partial \xi} \qquad (1.5.1.4)$$

- v^P – the velocity of the point of application of the external force

1.5.2 Equation of Motion (EOM) in Adams

According to the Lagrange formulation the equation of motion is a second order differential equation which can be written as:

$$\frac{d}{dt}\left[\left(\frac{\partial K}{\partial \dot{q}}\right)^T\right] - \left(\frac{\partial K}{\partial q}\right)^T + \Phi_q^T \lambda = Q \qquad (1.5.2.1)$$

Remembering the definition given in the Eq.(1.2.3), the equation of motion becomes:

$$\frac{d}{dt}\begin{bmatrix}\left(\frac{\partial K}{\partial u}\right)^T \\ \left(\frac{\partial K}{\partial \xi}\right)^T\end{bmatrix} - \begin{bmatrix}\left(\frac{\partial K}{\partial p}\right)^T \\ \left(\frac{\partial K}{\partial \epsilon}\right)^T\end{bmatrix} + \begin{bmatrix}\Phi_p^T \lambda \\ \Phi_\epsilon^T \lambda\end{bmatrix} = \begin{bmatrix}(\Pi^P)^T f \\ (\Pi^R)^T \bar{n}\end{bmatrix} \qquad (1.5.2.2)$$

With

$$\frac{d}{dt}\left[\left(\frac{\partial K}{\partial u}\right)^T\right] = M\dot{u} \qquad (1.5.2.3)$$

$$\frac{d}{dt}\left[\left(\frac{\partial K}{\partial p}\right)^T\right] = 0 \qquad (1.5.2.4)$$

While the angular moment is defined as

$$\Gamma = \frac{\partial K}{\partial \xi} = B^T \bar{J} B \xi \qquad (1.5.2.5)$$

According to these definitions the EOM are reformulated in Adams as

$$M\dot{u} + \Phi_p^T \lambda = (\Pi^P)^T f$$
$$\dot{\Gamma} - \frac{\partial K}{\partial \epsilon} + \Phi_\epsilon^T \lambda = (\Pi^R)^T \bar{n} \qquad (1.5.2.6)$$

These two frist order differential equations are called kinetic differential equations and they express how external forces determine the time variation of the angular and translational momentum.

The numerical solution of dynamic analysis of a mechanical system is provided by Adams throught a set of 15 equations obtained from the union of kinetic and kinematic differential equations. These equations are:

$$M\dot{u} + \Phi_p^T \lambda = (\Pi^P)^T f \qquad (1.5.2.7)$$

$$\Gamma - B^T \bar{J} B \xi = 0 \qquad (1.5.2.8)$$

$$\dot{\Gamma} - \frac{\partial K}{\partial \epsilon} + \Phi_\epsilon^T \lambda - (\Pi^R)^T \bar{n} = 0 \qquad (1.5.2.9)$$

$$\dot{p} - u = 0 \qquad (1.5.2.10)$$

$$\dot{\epsilon} - \xi = 0 \qquad (1.5.2.11)$$

It is necessary that the solution of this system must also satisfy the kinematic constraint equations of Eqs.(1.4.1) through (1.4.3).

1.5.3 Numerical Solution in Adams

The differential and constraint equations form a set of equations called Differential-Algebric Equations (DAE). A DAE is characterized by an index which indicates the difficult to find the numeric solution, the dynamic analysis problem seen in this chapter has index 3.

In ADAMS solver there are two methods of resolution:

- A direct index 3 DAE solver
- The algorithm SI2

SI2 Algorithm reduces the index of problem from 3 to 2 and it solves the velocity level kinematic constraint equation of Eq.(1.4.2) with the kinematic differential equations. This kind of solver is typically slower than the index 3 but it can be more accurate and robust.

The index 3 method decreases the number of unknow factors throught a backward approximation of time derivatives. The equations system is solved at discrete istants of time, starting from the solution at the instant t_n an interpolant polynome is used to predict the value of the function and its derivative at the instant t_{n+1}.

The integration process proceeds until the convergence criteria are satisfied or if the corrector has reached the maximum number of iterations. If the corrector doesn't reach the convergence, the integration interval is modified and the predictor-corrector algorithm integrates again the DAE system respecting the error tollerance (imposed by user) between the predicted function value and the corrected one.

Chapter 2

Introduction to the principles of fluid-dynamic simulation

2.1 Introduction

The study of fluids, their evolution and related physical phenomena are objects of interest in the branch of fluid dynamic.

With the development of technology, the study of fluid dynamic has become an inseparable aspect of engineering research, however very high costs related to the use of implants such as wind tunnels were also linked to this type of research.

The need to carry out this type of analysis together with the need to reduce costs has led to the development of CFD (Computational Fluid Dynamics) software, which thanks to the development of ever more performing computers have become a fundamental tool for industries.

The typical approach requires:

- The definition of the model that typically consists of a fluid domain in which a body that represents an obstacle can be contained
- The discretization of the fluid domain in elementary cells obtaining a calculation grid (mesh)
- Application in specific points of the grid of iterative resolution methods in order to solve the Navier-Stokes equations.

In this chapter the theoretical aspects of the physical phenomena studied through a fluid dynamic analysis will be presented, introducing the equations used by the scFLOW software during the calculation phase.

2.2 Navier-Stokes Equations

The knowledge of the convection processes of a fluid and in particular of how its properties vary over time can be acquired from the study of particular equations called "Navier-Stokes equations".

These equations are based on three fundamental hypotheses:

- continuous fluid
- chemically homogeneous and non-reactive fluid
- fluid with no electric charges

The Navier-Stokes equations that we will present can be seen as the mathematical modelling of three physical principles that characterize fluids:

- principle of conservation of mass (continuity equation);
- second principle of dynamics (momentum balance);
- first principle of thermodynamics (conservation of energy).

For this reason the Navier-Stokes equations are often called balance equations.

By neglecting the terms of production, the equations can be written as:

$$\frac{\partial \rho}{\partial t} + \frac{\partial}{\partial x_i} \rho u_i = 0 \tag{2.2.1}$$

$$\frac{\partial \rho u_i}{\partial t} + \frac{\partial u_j \rho u_i}{\partial x_j} = \frac{\partial \sigma_{ij}}{\partial x_j} + \rho g_i \tag{2.2.2}$$

$$\frac{\partial \rho H}{\partial t} + \frac{\partial \rho u_j H}{\partial x_j} = \frac{\partial p}{\partial t} + \frac{\partial u_j p}{\partial x_j} + \sigma_{ij} \frac{\partial u_i}{\partial x_j} + \frac{\partial}{\partial x_j} K \frac{\partial T}{\partial x_j} + \dot{q} \tag{2.2.3}$$

The following equations, with appropriate boundary conditions, perfectly describe the behavior of a fluid in both laminar and turbulent conditions. However, due to the spatial scales introduced in the motion field, a direct calculation approach is admissible but involves an exorbitant computational cost; from these exigencies are therefore born models for the resolution of a turbulent field that turn out to be less expensive. Before presenting the used model, it is necessary to introduce some concepts relating to turbulence.

2.3 Turbulence Model

2.3.1   Principles of Turbulence

A fluid motion field can be defined in a turbulent regime when the viscous forces are not enough to contrast the inertia ones. It can be introduced an adimensional number which express this relationship called "Reynolds Number", it is defined as:

$$Re = \frac{\rho v D}{\mu}$$
(2.3.1.1)

Where:

- ρ – is the density $\left[\frac{kg}{m^3}\right]$
- v – is the macroscopic velocity $\left[\frac{m}{s}\right]$
- D – is the characteristic length of the considered phenomenon $[m]$
- μ – is the dynamic viscosity $\left[\frac{N \cdot s}{m^2}\right]$

Through the calculation of this number is possible to understand the nature of the motion field which can be distinguished between laminar and turbulent.

For example, in the case examined, the tire of the landing gear can be considered like to a cylinder (blunt body) and then can be made a distintion between laminar and turbulent regime in this way:

- $Re < 2 \cdot 10^5$ – Laminar regime
- $Re \cong 2 \cdot 10^5$ – Transition regime
- $Re > 2 \cdot 10^5$ – Turbulent regime

 The main difference between turbulent and laminar regime is that the particles present in the motion field no longer have an orderly trend but they move in a chaotic and unpredictable manner. Within the fluid field, structures similar to vortices are immersed, these structures range from dimensions that can be compared to those of the geometric structures present in the domain (integral scale) until it characterizes the smallest existing structures in the motion field (dissipative scale). According to Kolmogorov turbulence theory the mechanic energy of fluid ,provided to the integral scale through external process such as pressure gradients, is progressively degraded

through a waterfall of scales from the integral to the dissipative; at last it is dissipated in thermal energy by viscous frictions. The presence of these different scales in particular the dissipative one doesn't allow the application of direct calculation method in a CFD analysis, thus it arises the need to introduce turbulence models which alleviates computational cost.

The turbulence model used will be presented below.

2.3.2   Reynolds equations

In most engineering applications, what needs to be obtained is not the microscopic structure of eddies but the influence of turbulence to mean velocity distribution and heat transfer. From this standpoint has born the concept of turbulence modelling, in particular in the RANS (Reynolds-Averaged-Navier-Stokes) model the state of turbulent flow is averaged within certain duration of time (long enough to smoothen the fluctuation). Turbulence modeling applies element division regardless of small eddies and remarkably reduces the number of mesh elements.

What needs to be ascertained is not the detailed structure of turbulence but the effect that turbulence has on mean quantities. Therefore, instantaneous velocity u_i, pressure P, temperature T and enthalpy H are expressed by a combination terms of mean value and fluctuation , respectively:

$$u_i = \bar{u}_i + u_i' \qquad\qquad (2.3.2.1)$$

$$P_i = \bar{P} + P' \qquad\qquad (2.3.2.2)$$

$$T = \bar{T} + T' \qquad\qquad (2.3.2.3)$$

$$H = \bar{H} + H' \qquad\qquad (2.3.2.4)$$

The symbol $\bar{}$ denotes the time-averaged value, whose time is longer than the turbulent time scale and shorter than the variation time of average value. If these values are substituted into momentum conservation and energy conservation, respectively, and are averaged, in the hypothesis of incompressible flow the followings can be obtained:

$$\frac{\partial \overline{u}_i}{\partial x_i} = 0 \tag{2.3.2.5}$$

$$\rho \frac{\partial \overline{u}_i}{\partial t} + \rho \frac{\partial \overline{u_j u_i}}{\partial x_j} = \frac{\partial}{\partial x_j}\left(\overline{\sigma_{ij}} - \rho \overline{u_j' u_i'}\right) + \rho g \tag{2.3.2.6}$$

$$\rho \frac{\partial \overline{H}}{\partial t} + \rho \frac{\partial \overline{u_j} \overline{H}}{\partial x_j} = \frac{\partial \overline{P}}{\partial t} + \frac{\partial \overline{u_j} \overline{P}}{\partial x_j} + \overline{\sigma_{ij}} \frac{\partial \overline{u}_i}{\partial x_j} + \frac{\partial}{\partial x_j}\left(\overline{q_j} + \rho \overline{u_j' H'}\right) + \dot{q} \tag{2.3.2.7a}$$

$$\rho \frac{\partial C_p \overline{T}}{\partial t} + \rho \frac{\partial \overline{u_j} C_p \overline{T}}{\partial x_j} = \frac{\partial}{\partial x_j}\left(k \frac{\partial \overline{T}}{\partial x_j} - \rho C_p \overline{u_j' T'}\right) + \dot{q} \tag{2.3.2.7b}$$

The eq. (2.3.2.6) is the Reynolds equation, is necessary to underline that a turbulent flow produces shear stress, which is denoted by $-\rho \overline{u_j' u_i'}$ and called "Reynolds shear stress", while the terms $\rho \overline{u_j' H'}$ and $\rho C_p \overline{u_j' T'}$ indicate the energy transported by turbulent flow. Because these equations are not in complete form and cannot be solved alone, in practice, these terms need to be determined by the known variables before turbulence analysis is performed.

Reynolds stress, according to molecular viscosity in laminar flow expression, is treated in the same way:

$$-\rho \overline{u_j' u_i'} = \mu \left(\frac{\partial \overline{u}_i}{\partial x_j} + \frac{\partial \overline{u}_j}{\partial x_i}\right) - \frac{2}{3} \mu_t \frac{\partial \overline{u_k}}{\partial x_k} \delta_{ij} - \frac{2}{3} \rho k \delta_{ij} \tag{2.3.2.8}$$

where,

$$k = \frac{1}{2} \overline{u_i' u_i'} \tag{2.3.2.9}$$

$$\delta_{ij} = \begin{cases} 1 & (i = j) \\ 0 & (i \neq j) \end{cases} \tag{2.3.2.10}$$

The Reynolds stress is assumed to be proportionl to the spatial gradient of mean velocity. The proportionality constant, in this case μ_t is referred to as the eddy viscosity. Note that equation (2.3.2.8) has as unfamiliar term $\frac{2}{3} \rho k \delta_{ij}$. If the normal

stress (i = j) is calculated using only the first term on the right-hand side of equation (2.3.2.8), the normal stress is eliminated from the mass conservation equation for incompressible fluids, resulting in some inconvenience. The third term on the right-hand side of equation (2.3.2.8) was introduced to assure the existence of the normal stress and acts in the same way as pressure; however, if the pressure in the second term is made to $\bar{P} + \frac{2}{3}\rho k$, it will no longer be an unknown value. Therefore, in equation (2.3.2.8), μ_t is the only item of data that needs to be given.

2.3.3   SST $k - \omega$ model

The idea of eddy viscosity is widely used and highly effective; however, as the eddy viscosity changes with the state of flow and its location, it needs to be redefined for each problem. To improve the situation different kind of models based on the resolution of further differential equations in order to obtain the "fundamental quantities of turbulence" through which the eddy viscosity can be calculated have been made. This quantities are the following turbulence energy k and the dissipation rate per unit turbulence energy ω.

$$k = \frac{1}{2}\overline{u_i' u_i'} \qquad (2.3.3.1)$$

$$\omega = \frac{\epsilon}{k} \qquad (2.3.3.2)$$

where ϵ is the turbulent dissipation rate and is defined as:

$$\epsilon = \nu \frac{1}{2}\overline{\frac{\partial u_i'}{\partial x_j} \frac{\partial u_i'}{\partial x_j}} \qquad (2.3.3.3)$$

As a two-equation turbulence model the k-ω model has been proposed by Wilcox et al. [Reference 7-1]. Instead of directly solving for turbulence dissipation ε the dissipation rate per unit turbulence energy ω, that has the dimension of frequency $[1/s]$, is

treated. In practice, the invers of ω represents the mean residence time of a turbulent structure inside the previously defined waterfall.

 This model has the advantages in reproducing near-wall turbulence behavior; it does not require damping functions to obtain a near-wall velocity profile and provides a better estimation of boundary layer separation under adverse pressure-gradients. However, its strong dependence on boundary conditions such as inflow or free-stream turbulence values has been a known problem, and the model lacks reliability in the outer free-stream layer.

The SST (Shear-Stress Transport) model developed by Menter [Reference 7-2] solves the two equations for k and ω with a zonal treatment; in particular the conventional k-ω equations are solved in near-wall regions and differently from the conventional method they are shifted toward outer regions, which promises an accurate and robust computation. Also, the employed concept of Shear-Stress Transport avoids the over-estimation of eddy viscosity under adverse pressure-gradients, and properly reproduces complicated separation phenomena that the conventional eddy viscosity models may fail to capture.

In the k-ω model, the eddy viscosity is expressed as:

$$\mu_t|_{k-\omega} = \rho \frac{k}{\omega} \qquad (2.3.3.4)$$

The k transport differential equation has the following expression:

$$\rho \frac{\partial k}{\partial t} + \rho \frac{\partial u_i k}{\partial x_i} = \frac{\partial}{\partial x_i}\left(\frac{\mu_t}{\sigma_k}\frac{\partial k}{\partial x_i}\right) + G_s + G_T - \rho C_\mu k\omega \qquad (2.3.3.5)$$

The ω transport differential equation is written as follows:

$$\rho \frac{\partial \omega}{\partial t} + \rho \frac{\partial u_j \omega}{\partial x_j} = \frac{\partial}{\partial x_j}\left[\left(\mu + \frac{\mu_t}{\sigma_\omega}\right)\frac{\partial \omega}{\partial x_j}\right] + \frac{\gamma\rho}{\mu_t}G_s - \beta\rho\omega^2 \qquad (2.3.3.6)$$

The model constants are listed below. The subscripts 1 and 2 indicate the inner and the outer, respectively.

$$C_\mu = 0.09$$

$$\sigma_{k_1} = 1.18 \qquad \sigma_{k_2} = 1.0$$

$$\sigma_{\omega_1} = 2.0 \qquad \sigma_{\omega_2} = 1.17$$

$$\beta_1 = 0.075 \qquad \beta_2 = 0.0828$$

$$\gamma = \frac{\beta}{C_\mu} - \frac{\kappa^2}{\sigma_\omega \sqrt{C_\mu}} \kappa = 0.41$$

Furthermore, the Shear-Stress Transport is represented by the following eddy viscosity expression:

$$\mu_t|_{SST} = \rho \frac{a_1 k}{\Omega} \qquad\qquad (2.3.3.7)$$

In this relation $a_1 = 0.31$ and Ω is the magnitude of mean vorticity. In the computation, both expressions (2.3.3.4) and (2.3.3.7) are interpolated by another blending function that has wall distance and turbulence quantities as its argument.

Chapter 3

Cosimulation Theory

3.1 Communication Architecture

The MSC CoSim engine code (master code) implements a simple control algorithm allowing a variable asynchronous communication of the application software codes such as Adams, scFLOW, and Marc (slave codes) at each time integration step. All slave codes simulate using their best settings and exchange data with the master code at the end of every successful time integration step. In principle, all codes may have different time integration steps. This architecture does not require setting a communication interval like in some other co-simulation standards. The communication with the MSC CoSim engine code is at every time integration step. This means the communication is more frequent if the co-simulation solution is difficult to compute and requires small time step. Similarly, the communication with the MSC CoSim engine code will be less frequent when the codes are taking larger step sizes.
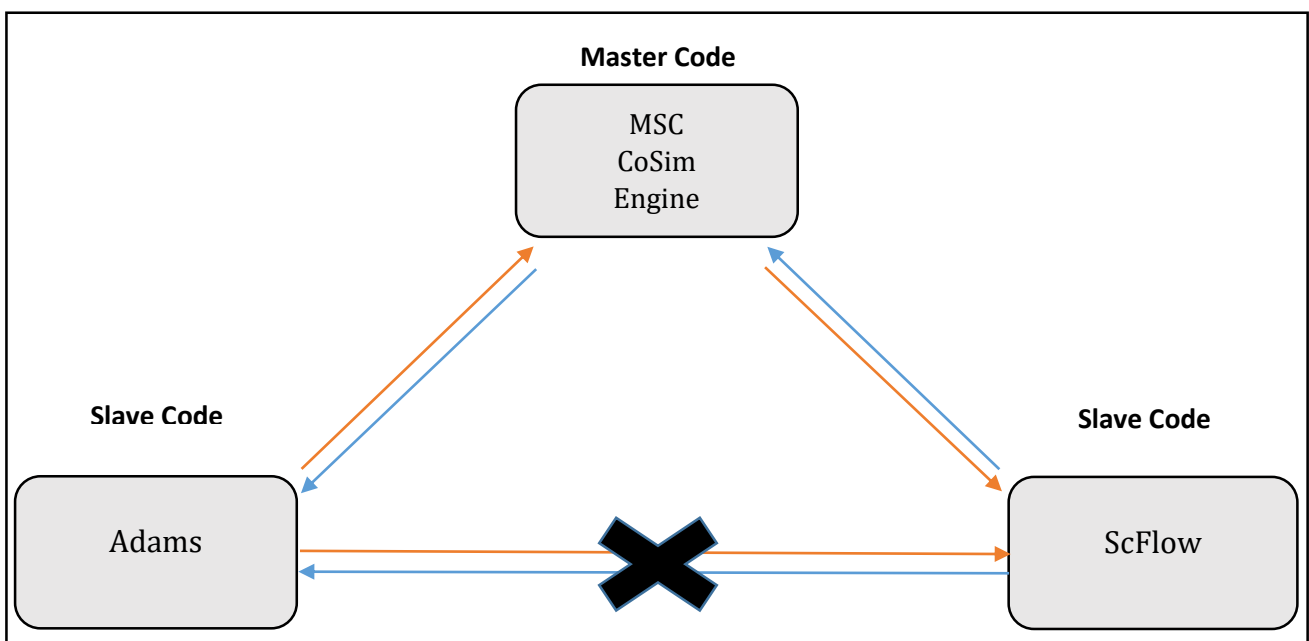

Figure 3.1: Communication Process between codes.

Slave codes can have different time steps to suit respective solver convergence criteria:

 a. If time step is same, communication will happen at every time step.
 b. If time step is different, data will be interpolated based on "time integration" selected by user.

Currently three time integration methods are available:

- Quadratic – This option uses the past history of a signal (force or displacement) to exactly fit a quadratic curve through the available points. The MSC Cosim engine coe keeps a history of the data from all the slave codes.

- Linear – This option uses a linear fit using the latest two data.

- Constant last – This option uses the latest value in the history of the signal.

In particular if the choice is the "constant last" time interpolation method the values exchanged(like the position, force or moment) through the two software will be the same, while if the "linear" or "quadratic" ones are used these two values will be different.

3.2 Adams-scFLOW physical quantities

The exchange of data between the two codes through the co-simulator involves particular physical quantities whose are calculated in the two software in the imposed time step.

The following value is calculated in Adams coordinates system.

- Coordinates of rotational center [m]
- Euler angles [radian] (Body-fixed Z-X'-Z'' system)
- Integral value of Force on surface [N]
- Integral value of torque on surface [Nm]

ScFLOW requires the information of Adams coordinates system as input.

Otherwise, Adams requires as input the information related to the calculation of pressure forces by scFLOW.

The exchanged physical quantities can be monitored through a specific file which rapresents an output of co-simulator. Here the quantities are characterized through numerical ID.

For a vector quantity such as Position, the tenth's digit is for physical quantity ID and the unit's digit is for component ID. For example, 101 means the first component of Position. The following physical quantities are supported by MSC CoSim.

Displacement	Physical quantity ID=1
Force	Physical quantity ID=2
Pressure	Physical quantity ID=6
Position	Physical quantity ID=10

Figure 3.2: Physical Quantities ID

The physical quantities of interest between Adams and ScFlow will be:

- The first component of coordinate of rotational center: **101**
- The second component of coordinate of rotational center: **102**
- The third component of coordinate of rotational center: **103**
- The first component of Euler angle: **104**
- The second component of Euler angle: **105**
- The third component of Euler angle: **106**
- The first component of force: **21**
- The second component of force: **22**
- The third component of force: **23**
- The first component of torque: **24**
- The second component of torque: **25**
- The third component of torque: **26**

Chapter 4

ADAMS Model

4.1 Description of Landing gears types

Before introducing how the ADAMS Model has been made it is interesting to explain whose are the main landing gears diffused into aeronautical industry.

A first differentiation can be done looking at the mechanism typology; it can be subdivided into two main categories:

- Fixed Landing gear
- Retractable Landing gear

The first one is typical of little dimension aircrafts and it is fixed under the fuselage or the aircraft wings; The exposition to the air flow during the whole flight generates a lot of aerodynamic resistence but has the advantage to be less heavy and needs a less frequent maintenance operations because of a easier mechanism.

Figure 4.2: Fixed Landing gear.

The retractable landing gear has the possibility to be retracted into the fuselage or the aircraft wings with the advantages to obtain a great reduction of aerodynamical drag during the flight. Obviously, the higher mechanism complexity leads to an increase of production and maintenance costs.

Figure 4.3: Retractable Landing gear.

Defined the two main categories, a second differentiation is relative to the construction configurations. The most important configurations will be described below.

– Conventional or "taildragger" landing gear: it has only two main wheels under the fuselage or the aircraft wings in a slightly advanced position compared to the center of gravity and a little tail wheel. This type of landing gear is called "conventional" because is the main choice on the firsts aircraft models, however it has been replaced by the introduction of the tricycle

Figure 4.3: Taildragger Configuration.

model. Its main advantage is the possibility to land and take off from runways not in optimal conditions thanks to the robustness of its wheels.

– Tricycle Landing gear: It has an anterior wheel under the aircraft nose and two or more wheels situated under the fuselage or wings. Thanks to this kind of configuration and to the position of center of gravity, the aircraft acquires greater maneuverability, stability and greater tolerance to lateral gusts.

31
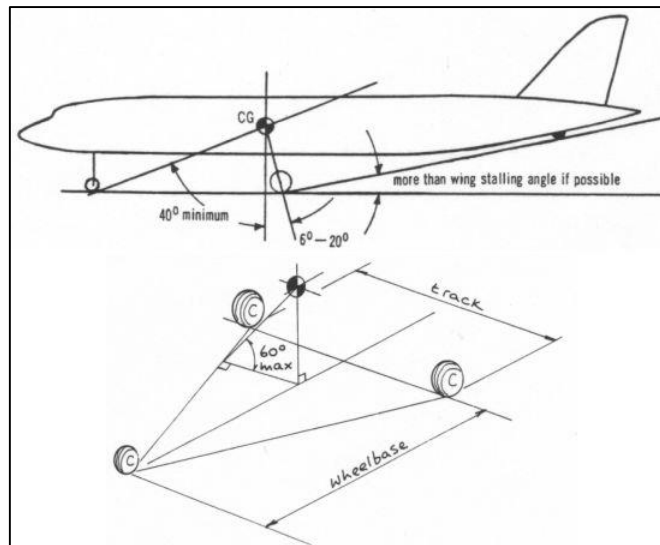
Figure 4.4: Tricycle Configuration.

– Tandem Landing gear: It has two legs with one or more wheels lined up under the fuselage. This configuration is used when to assemble the landing gear under the aircraft wings is not possible because of weapons presence or to have larger fuel tanks.

Figure 4.5: Tandem Configuration.

– Quadricycle Landing gear: It has four wheels situated on the lateral side of fuselage, usually this kind of configuration is applicated on cargo aircrafts but it requires a flat set up in the landing phase.

Figure 4.6: Quadricycle Configuration.

– Multi-bogey Landing gear: It has an anterior leg with two wheels and two lateral series of wheels placed under the fuselage. This configuration is used when more security is needed or for the transport of heavy goods.

Figure 4.7: Multi-bogey Configuration.

4.2 Introduction to the Model – The parts

The model creation is the first step to make for preparing a simulation inside of Adams interface.

Each model is made up of several parts, which do not have to be intended as geometries but as rigid or flexible bodies whose mass is concentrated in specif points called center of gravity. They are the moving components of model and they can have a mass, inertia, initial position, initial velocity and they are made up of geometric elements of any size or shape.

In the particular case of landing gear, neglecting the details, it can be made up of six main elements:

- Side-stay assembly
- Main strut
- Angled strut
- Piston
- Torque arms
- Wheel
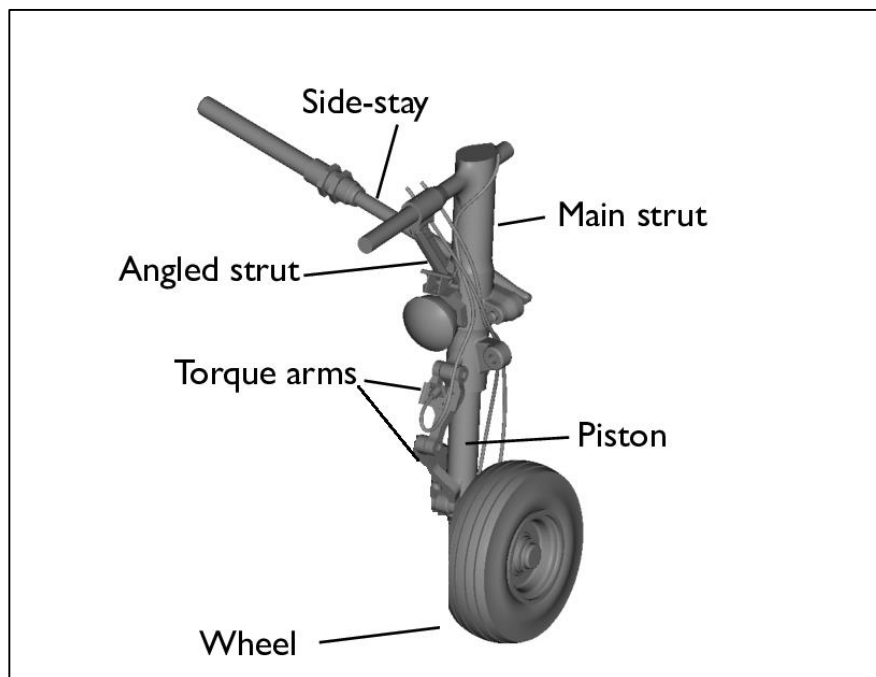
Figure 4.8: Landing gear main parts

Each of the elements mentioned constitutes a part inside Adams, having its own mass and inertia.
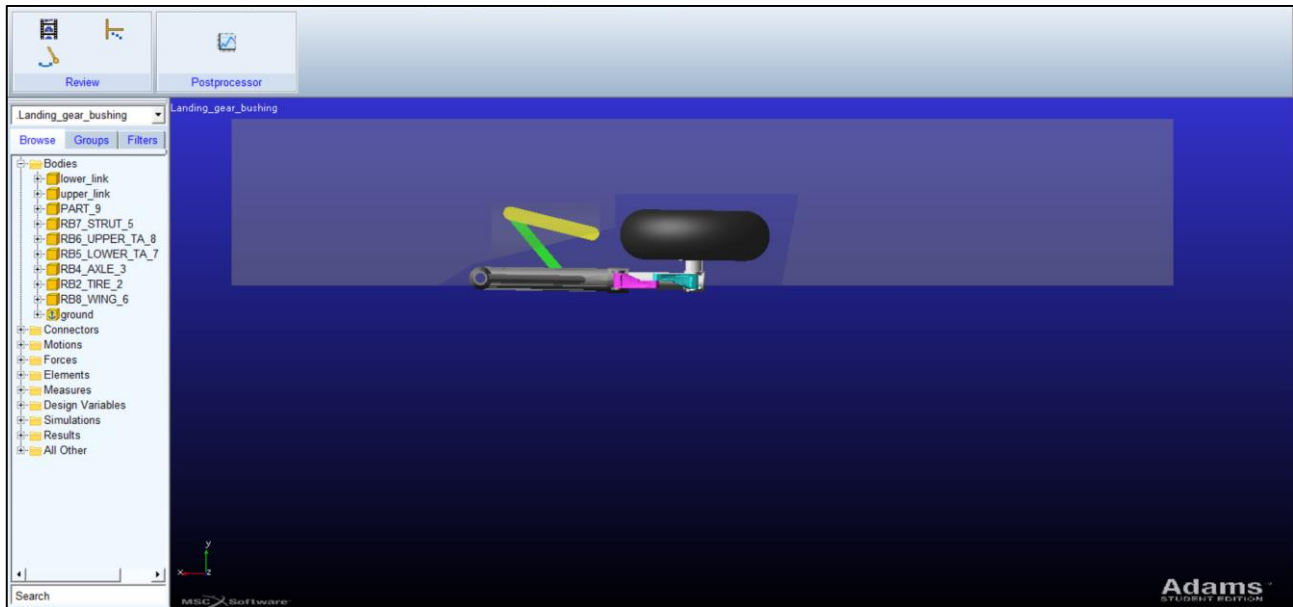
Figure 4.9: Adams model in the initial condition.

As shown in the figure, in addition to the elements described, there are three further parts; "Part_9" is a part without mass, it has been created only to have reference points on model called "marker", they are useful for creating measures or as points of application of forces or constraints.
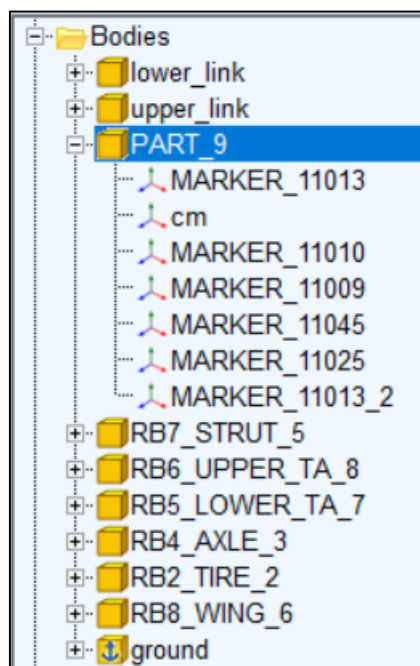
Figure 4.10: Tree of Parts.

"RB8_WING_6" has created to simulate the wing of the plane with the appropriate compartment in which the landing gear is inserted. Its weight or size is not an important element as it does not participate in the simulation.

The "ground" part refers to the entire three-dimensional grid on which it is possible to construct parts and fix them.

It is advantageous to introduce some data, because they can be useful later:

- Landing gear material – Steel
- Landing gear mass – 190.3 kg
- Landing gear length (from the upper of the strut to the lower part of the wheel) – 1.8 m
- Wheel diameter – 0.6 m
- Wheel width – 0.28 m

4.3 Connector and Motions

In this section the connectors and the movements set on the model will be presented. The connectors are a fundamental part of the model because they allow the parts to be connected to each other, imposing also which are the admissible relative displacements or rotations. Instead the motions are two different kind of displacement, the translational and the rotation. These can be set in relationship with a connector and they can be modelled through specific mathematical functions like the step or the impulse.

In the model presented, first of all, it is necessary to constrain the wing with the ground in order to have a fixed element, which is not affected by the action of gravity force.

This kind of connector is called "Fixed Joint", in the particular it locks two parts together so they cannot move with respect to each other, removing all degrees of freedom.
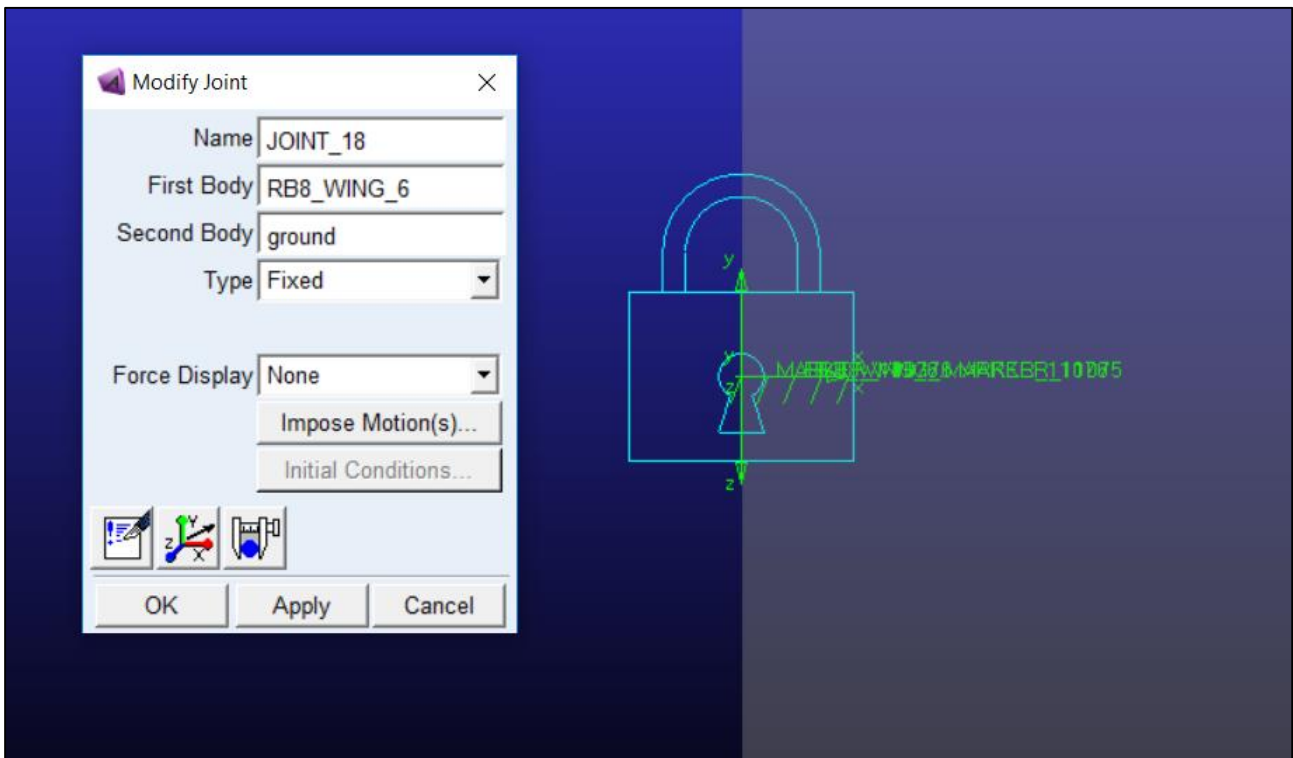
Figure 4.11: Fixed Joint between Wing and Ground parts.

The second joint created is a "Revolute Joint" between the wing and the upper connecting rod, it allows the rotation of one part with respect to another part about a common axis constraining the other five degrees of freedom.
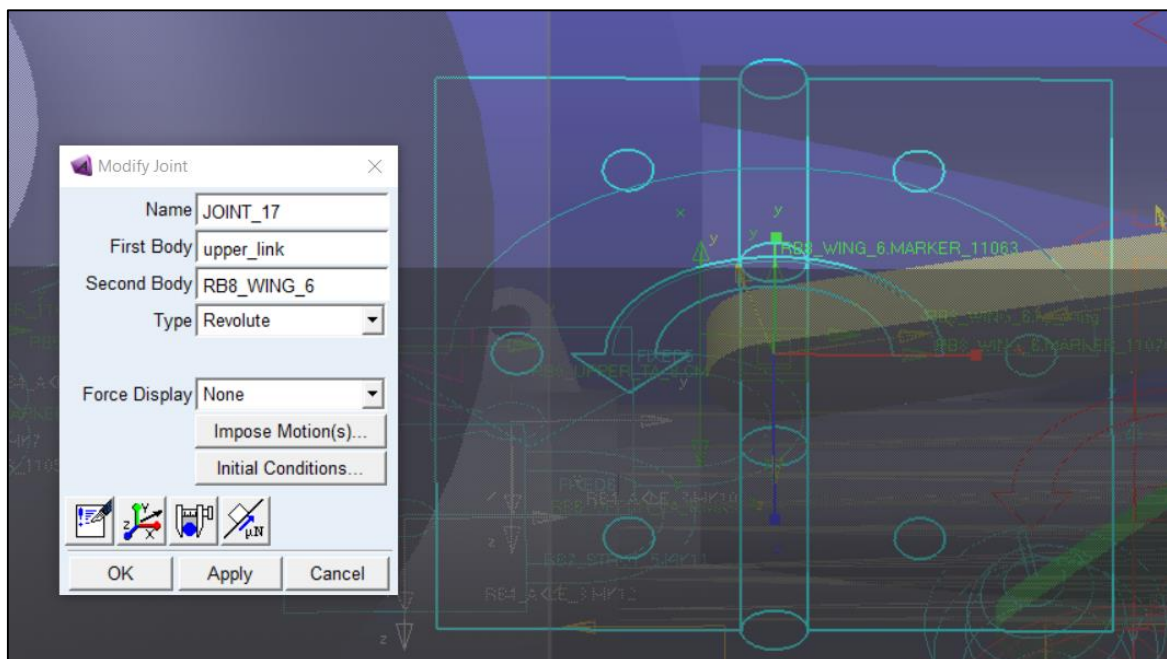

Figure 4.12: Revolute Joint between Upper Link and Wing.

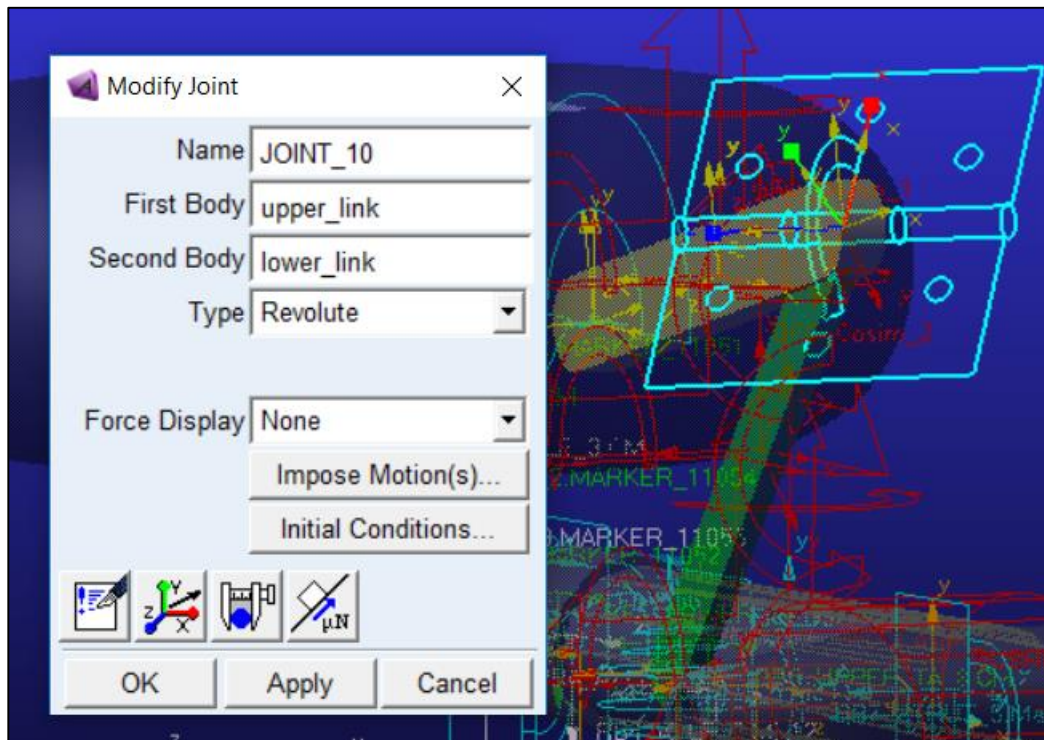A second "Revolute Joint" is necessary to allow the relative rotation between the two connecting rods.

Figure 4.14: Revolute Joint between Upper and Lower Link.

To connect the landing gear leg to the lower connecting rod is a "Spherical Joint".
It allows the free rotation about a common point of one part with respect to another part. The location of the spherical joint determines the point about which the joint's parts can pivot freely with respect to each other, it constraints the three displacements along three axis leaving the rotations free.
The other present joints are necessary to connect and fix of all landing gear leg elements from the strut to the wheel; for this purpose several "Fixed Joint" have been chosen.
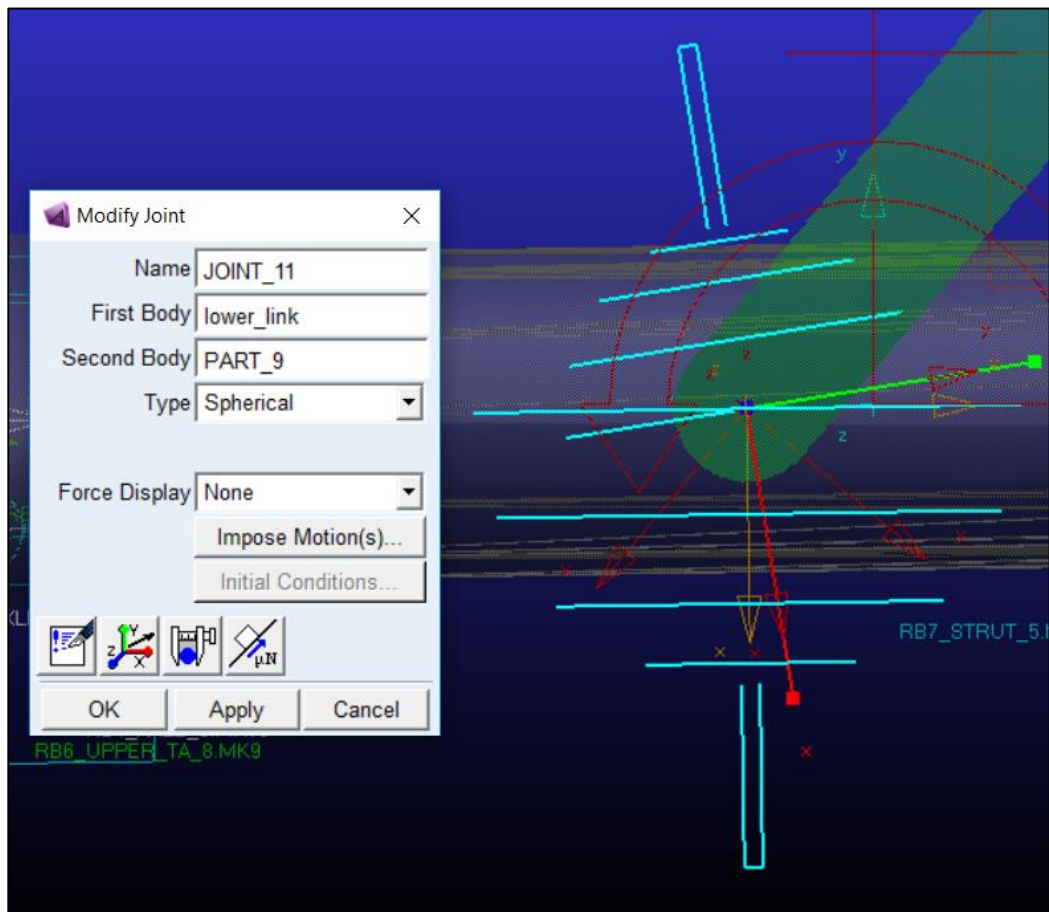
Figure 4.15: Spherical Joint between Lower link and Part_9.
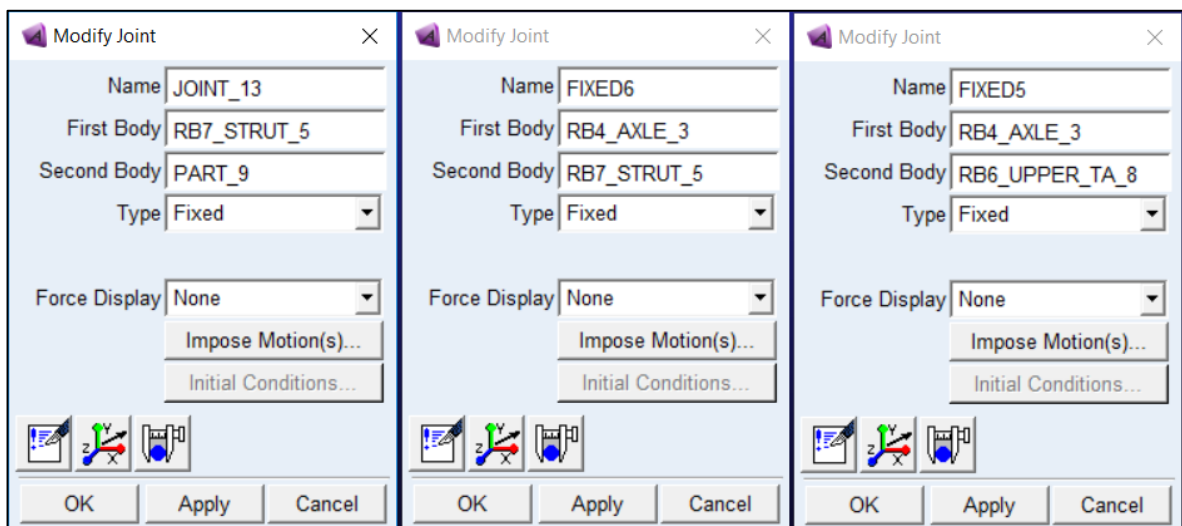
Figure 4.16: Fixed Joint between Strut and Part_9, Strut and Piston, Piston and Upper Torque arm.
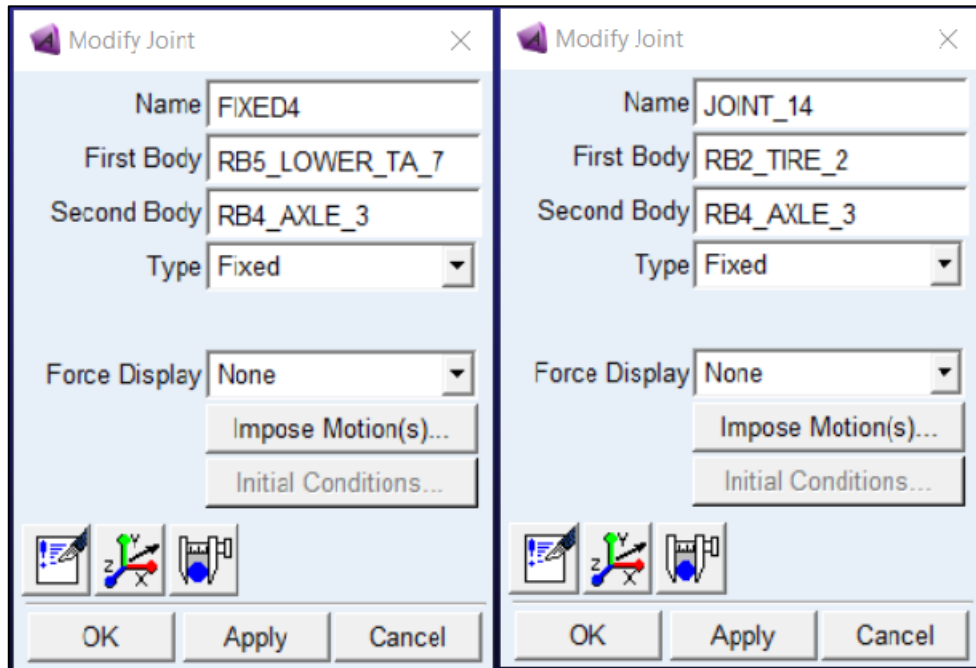
Figure 4.16: Fixed Joint between Lower Torque arm and Piston, Wheel and Piston.

After setting the constraints it is necessary to introduce a motion law to allow the the landing gear extraction. A rotational motion is chosen, it is applicable to a revolute and a cylindrical joint; the right-hand rule determines the sign of the motion. The z-axis of the first part must be aligned with the z-axis of the second part at all times. The angle is zero when the x-axis of the first part is also aligned with the x-axis of the second part. The speed of the motion can be directly expressed in displacement units per second or with a mathematical function into "Function Builder".

Figure 4.17: Constraints and Motions.

In the landing gear model the motion has been set according to the revolute joint between the upper connecting rod and the wing, moreover the type of motion is described by function "step5". The "step5" function provides approximation to the step function with a quintic polynomial. It has continuous first and second derivatives. Its third derivative is discontinuous at $x = x_0$ and $x = x_1$.

In the function builder the "step5" function takes the following form:

$$step5(x, x_0, h_0, x_1, h_1) \qquad\qquad (4.3.1)$$

Where:

- x is the independet variable.
- x_0 is a real variable that specifies the x initial value in the function.
- x_1 is a real variable that specifies the x final value in the function.
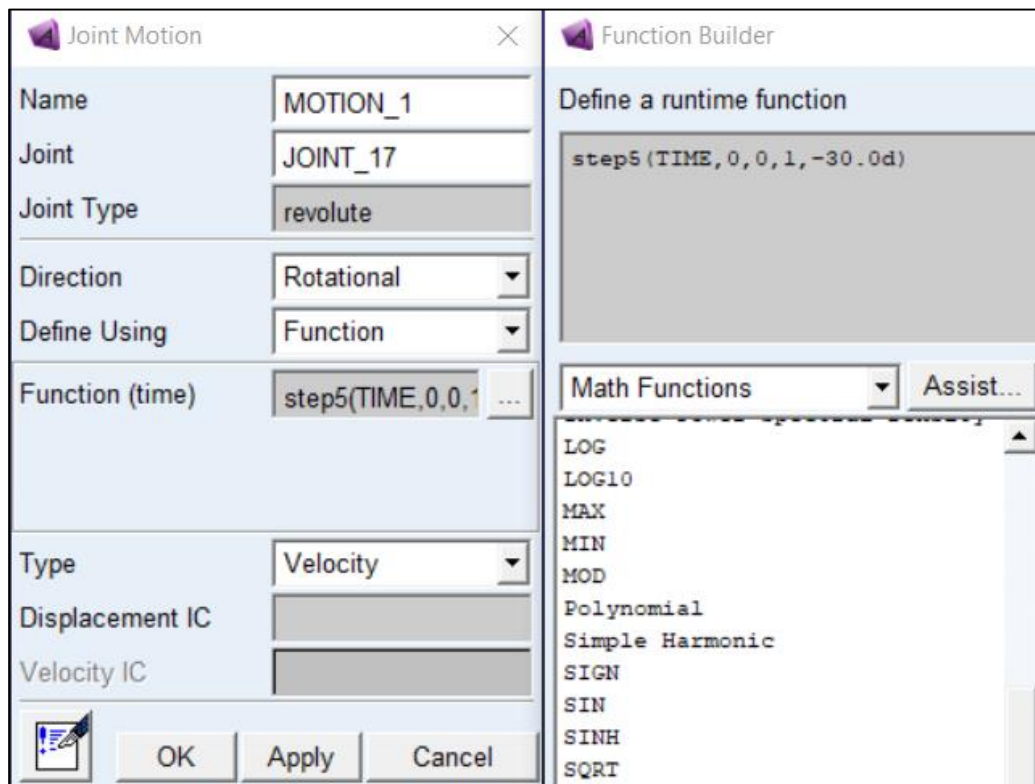- h_0 is the step initial value.
- h_1 is the step final value.

Figure 4.18: Rotational joint motion on the left and the step5 function on the right.

In this case the independent variable is the time, in which the initial and final value in the function are 0 and 1 second while the initial and final value of the "step5" are 0 and -30 degrees.

4.4 Forces and Co-simulation setting description

Adams offers different types of forces through which it is possible to simulate a large variety of cases. There are three main categories:

- Applied forces
- Flexible Connectors
- Special forces

The applied forces are divided into axial forces and torques, they can have from one to three components; alternatively it is possible to create a general force having 6 components (three axial and three torques). To create an applied force is necessary to specify the application point and its direction; the application can be between two parts or to one part and the ground. Regardless of the choice Adams creates two marker on the selected parts, the first one (action body) receives the action force while the second one (reaction body) receives the reaction force. The magnitude can be defined as a costant value or a mathematical function defined as a combination of displacements, time, velocities, other applied forces or user-defined variables.

Instead of using applied forces, it is possible to consider using the flexible connectors (spring damper, bushing etc…), they let to connect two bodies in a compliant way. In contrast to joints, which are rigid connectors, flexible connectors do not absolutely prohibit any part movement and, therefore, do not remove any degrees of freedom from the model. Special forces simulate specific cases such as the contact between two bodies or the load distributed on the nodes of a flexible body.

In the landing gear model a "Bushing" has been used between "Part_9" (whose marker are on the strut) and the wing. A bushing is a linear force that represents the forces acting between two parts over a distance, for both translational and rotational (torque) forces applied by the bushing is necessary to chose the three stiffness coefficients, three viscous- damping coefficients (the force due to damping is zero when there are no relative translational velocities between the markers on the action and reaction bodies) and three preload constant force value. As it is possible to observe in the following image, a high stiffness has been set in terms of translation along the three axes and rotation around the x and y axis, while the value 0 related to

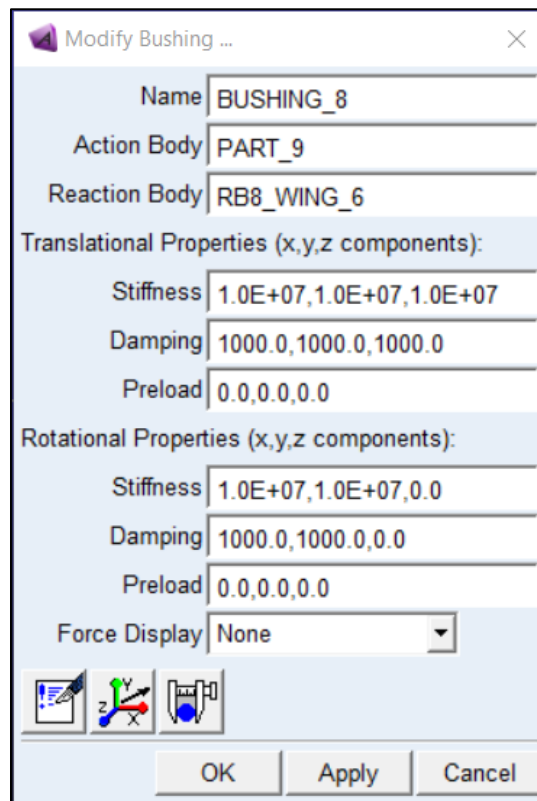the rotation around the z axis is indicative of a compliance so that the carriage can rotate.

Figure 4.19: Bushing details.

With the current settings it would already be possible to carry out a simulation, however to perform a co-simulation it is necessary to introduce further forces called "GForces". These forces are general forces (3 force and 3 torque components), whose components are currently vacant pending the information passed by the co-simulator; for each parts interested in the co-simulation is necessary to create a different "GForce".

Figure 4.20: Tree of Forces.

For the landing gear model three "GForces" have been created, two of them relative to the "cm" of connecting rods and one relative to the landing gear leg (marker_11098).
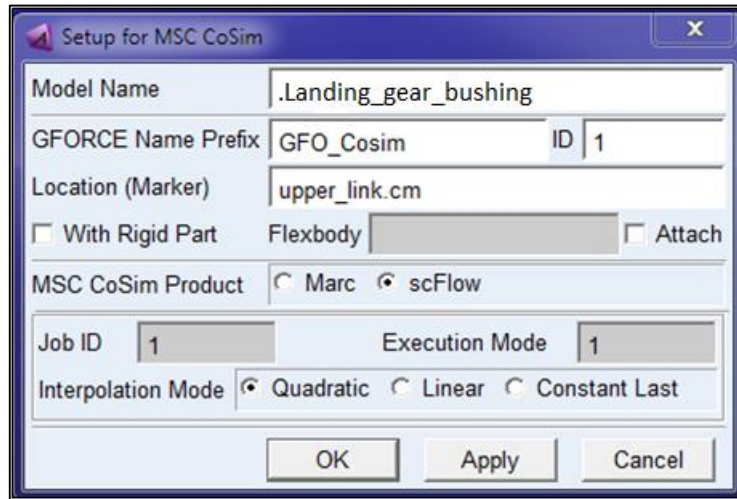
Figure 4.21: GForce setting.

The ID is the identifier of the created GForce, this will be appended to the end of the GForce name, the ID of each of the GForces must be different because it will be necessary to insert them correctly in ScFLOW.

Job ID specifies the ScFLOW Job ID to which this GForce will correspond. Setting this field is useful when co-simulating between one Adams process and multiple scFLOW processes, therefore, one want to instruct MSC CoSim which GForces in the model correspond to interaction with which ScFlow process.

Execution Mode defines the order in which the processes participating in the co-simulation proceed. In a co-simulation, the software with higher execution mode number starts first. Also, if this number is set to 0, the application software stops when it detects the termination of the communication partner software. If this number is greater than zero, an application software moves forward until the end of its process using the extrapolated data sent from the MSC CoSim process even if the communication partner has terminated.

4.5 Measures and Simulation script

The creation of measures allows, in the post processing phase, to monitor the temporal trend (or other independent variables) of the various quantities of interest.
The following measures have been taken into consideration for the simulation carried out:

- Rotations in degrees relative to revolute joints.
- Angular velocities of revolute joints.
- Angular acceleration of revolute joints.
- Landing gear leg displacement along 3 axis.
- Landing gear leg velocity along 3 axis.
- Landing gear leg acceleration along 3 axis.
- The three components of force discharged on the bushing.
- The three components of torque discharged on the bushing.
- The torque needed to perform the motion set on the upper rod.

In addition to the aforementioned measures, in the post-processing section, it is possible to monitor each type of quantity relating to each part or joint in the model, including the unknown aerodynamic forces of the co-simulation.
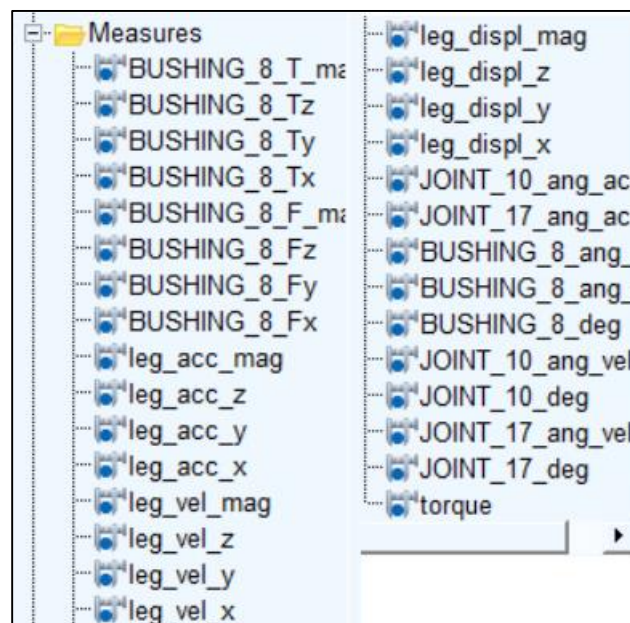
Figure 4.22: Tree of Measures.

The last step is the creation of a simulation script, the chosen simulation is the dynamic one with a duration of 2.5 second and 0.0005 second of time step. The choice of this time step is not random, but linked to the time step in scFlow; this equivalence allows to choose a co-simulator interpolation method different from the constant one and to obtain results as the aerodynamic forces transmitted in Adams coherent with the real ones calculated in scFlow.
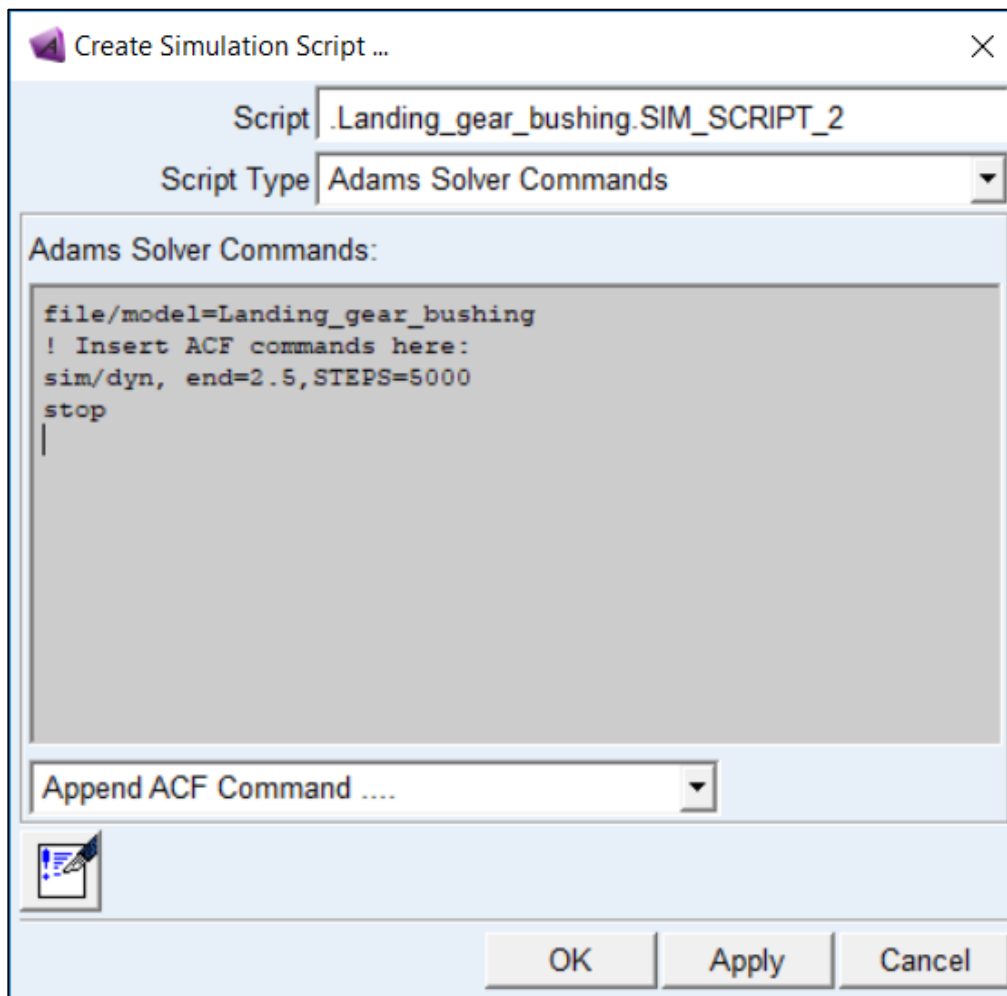
Figure 4.23: Simulation script.

Chapter 5

scFLOW: set up of CFD analysis

5.1 Parts Preparation

5.1.1   Refining of the CAD

The preliminary phase necessary to obtain a good CFD calculation is the preparation of the model. This step can be performed within the scFlow interface using simple geometries and working them through different tools or by importing a CAD model. In the present analysis the model previously prepared in Adams was imported, however in order to be adapted to a CFD analysis it requires a cleaning phase since the presence of holes, edge walls or too detailed parts can lead to problems in the calculation phase. The starting model is analogous to that seen in Adams with distinct and separate parts between them.
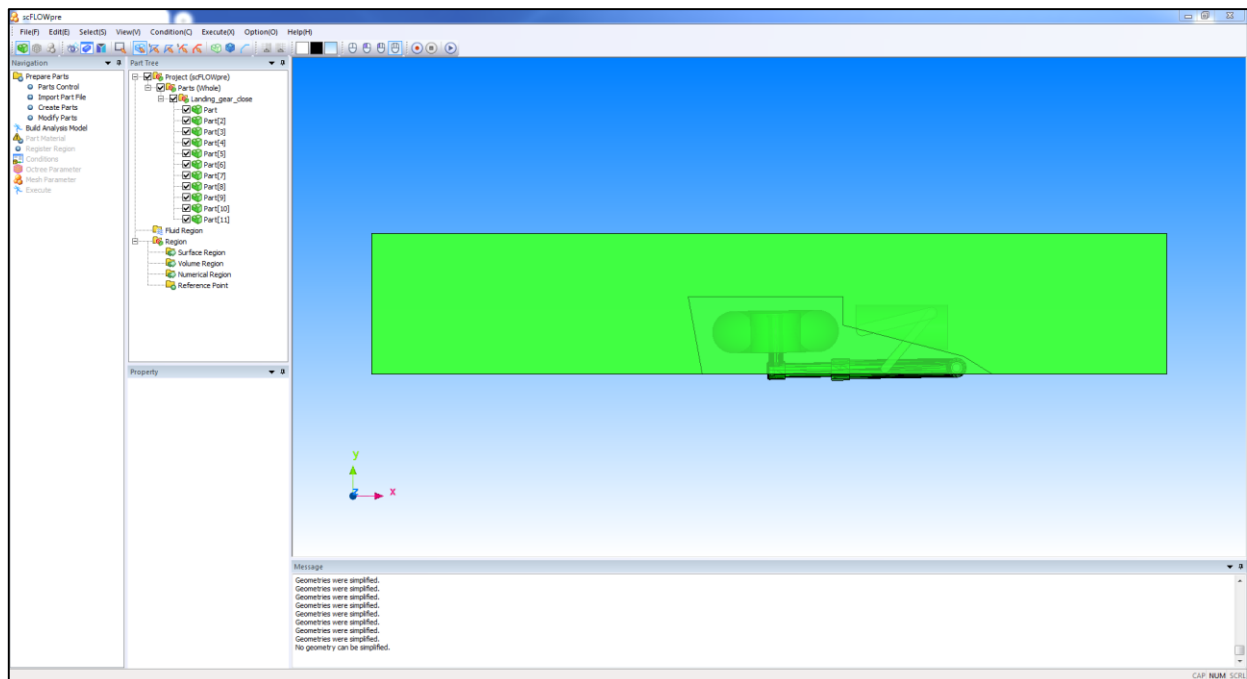
Figure 5.1: Starting model.

After importing the model it is essential to set the type of movement that the parts can perform; for the following analysis it is necessary to admit both displacements and rotations, they are made possible through the definition of auxiliary meshes called "overset mesh". The overset meshes are constructed in relation to the different moving parts and during the calculation phase they will move inside the main mesh which remains fixed.
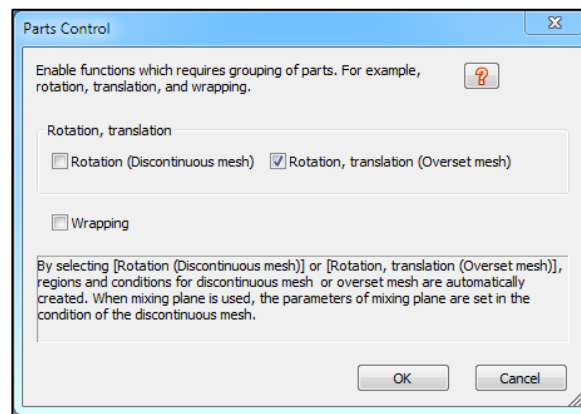
Figure 5.2: Setting the type of movements.

The purpose of the present fluid dynamic analysis is to evaluate the forces acting on the landing gear and then have an estimate of the drag coefficient, for this type of analysis in order to lighten the calculation it is necessary to sacrifice parts that would require a too detailed mesh. In the model under consideration, for example, the torque arms have been eliminated thus sacrificing a small aliquote of resistance in exchange for a lower computational cost.

The next step is to unify all the parts which move in the same way; in the Adams model we can distinguish three different groups that have different movements, the two connecting rods and the landing gear leg. Consequently it is necessary to make the leg a single part differently from how it appears in Adams, however before doing this it is important to eliminate any type of hole, cut or irregularity in order to obtain a smooth surface.

For example in the following image is displayed the refinishing operation relative to the strut.
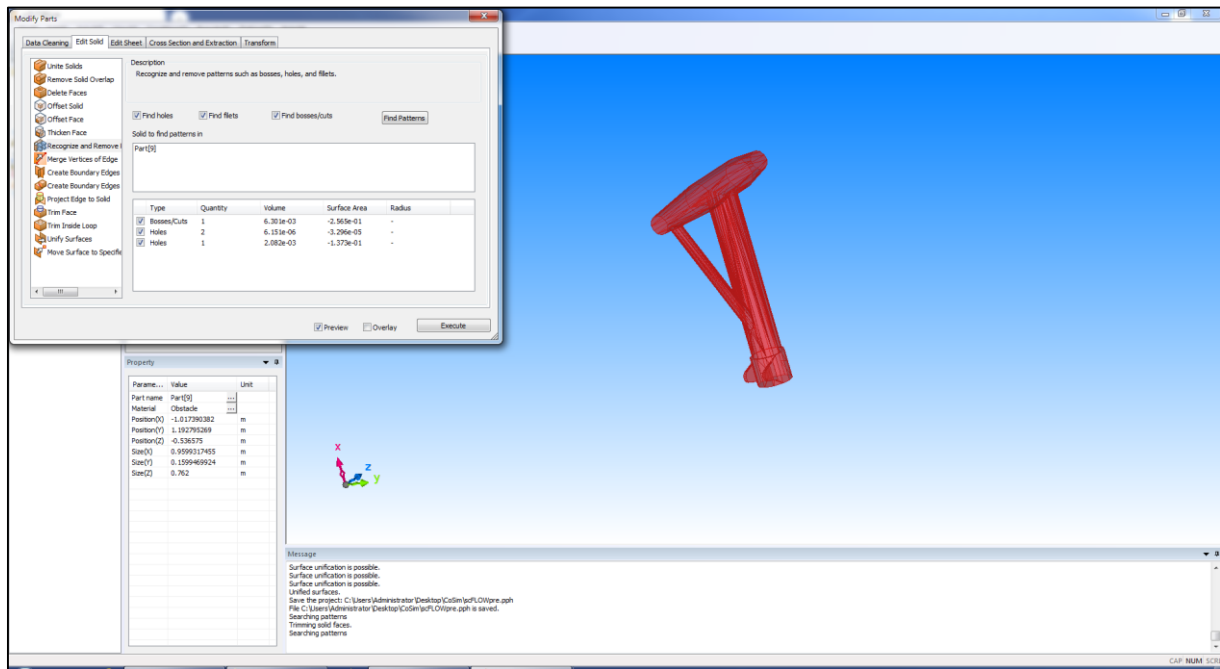
Figure 5.3: Refinishing process of the strut.

After this operation, repeated for each part, it is possible to unify all leg elements.
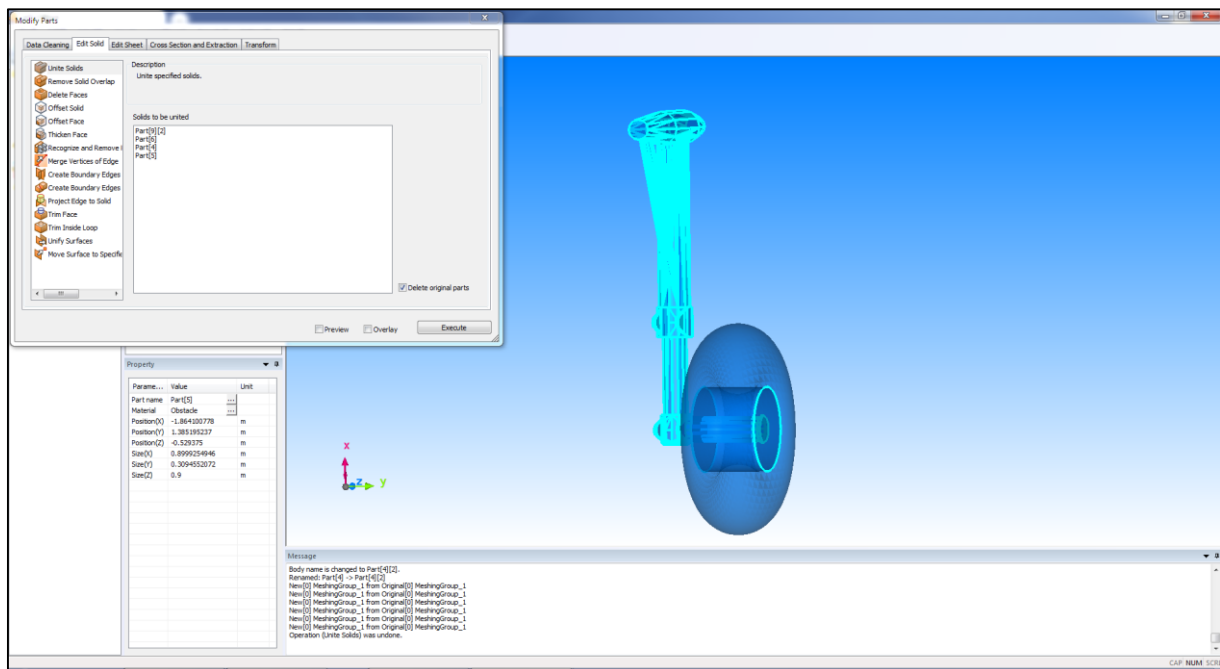
Figure 5.4: Union of different leg parts.

5.1.2   Domains definition

Once the work on the parts is finished, it is necessary to create the main domain and the secondary ones related to the moving parts. The main domain has a rectangular section with dimensions correlated to the wheel diameter, furthermore the wing block is subtracted from the starting cuboid because it is superfluous for calculation purposes.
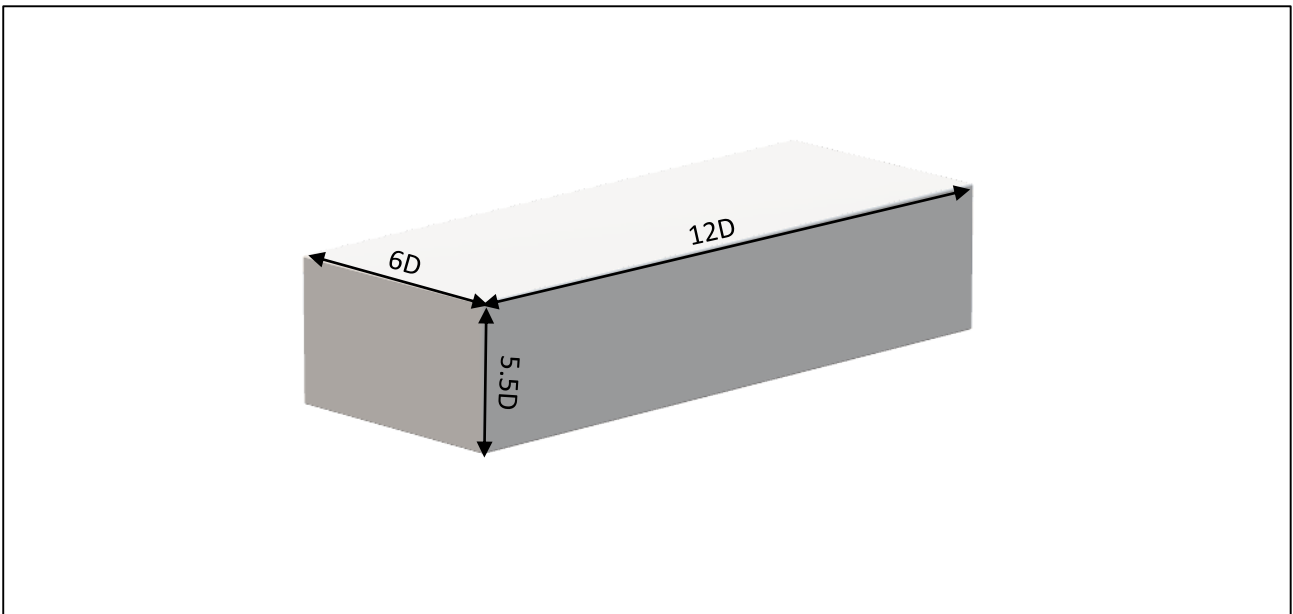
Figure 5.5: The computational domain.

The secondary domains necessary for the overset meshes are created starting from the reference elements; for the connecting rods a domain of similar geometry is generated but of approximately doubled size, while for the landing gear leg a cuboid is generated. From these domains the physical parts of the reference elements are subtracted in order to obtain voids that will subsequently be interpreted as disturbing elements (obstacles) within the fluid domain. The subtraction of bodies is permissible because for the purposes of the fluid dynamics calculation only the "wet" surfaces are of interest while all that is inside the bodies is not relevant.
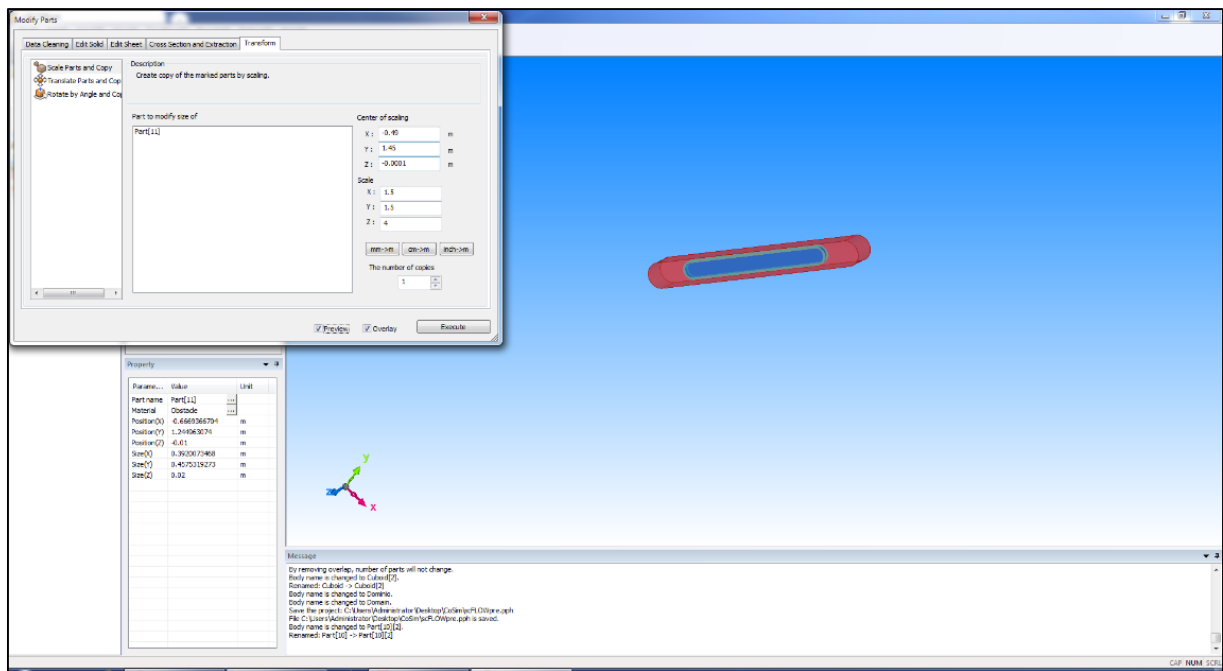
Figure 5.6: Connecting rod domain.
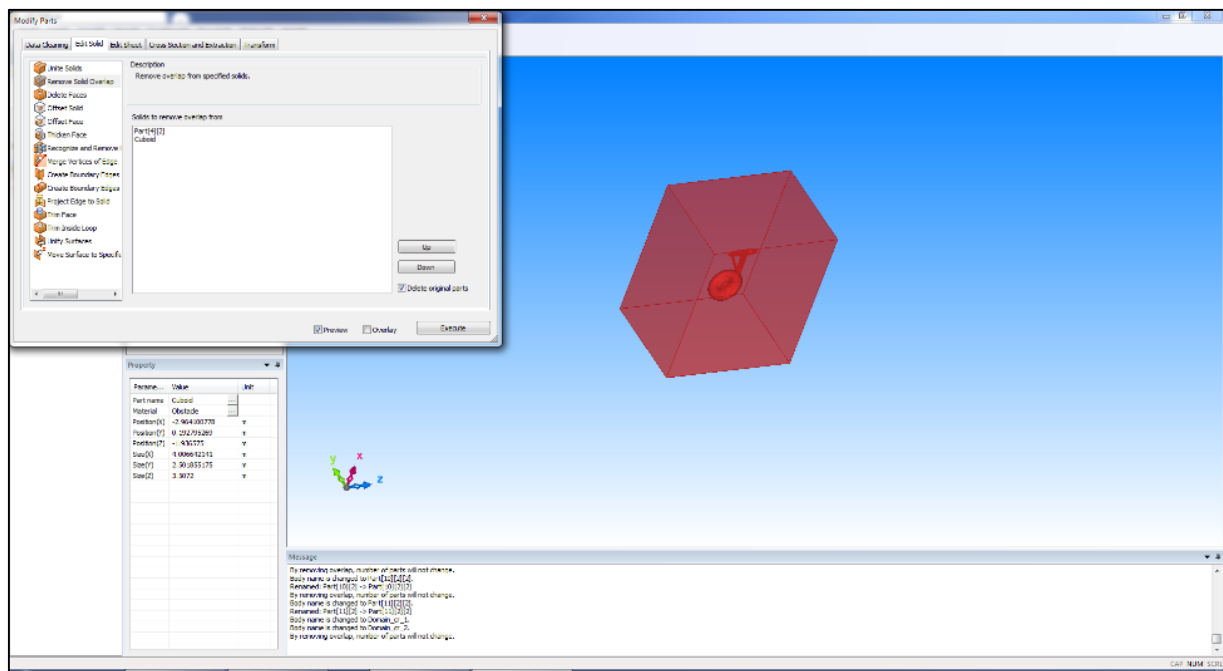
Figure 5.7: Landing gear leg domain.

51

The last step is to create a distinct cuboid within the main domain with dimensions slightly larger than the leg domain. It is called "Fit zone" and it will be useful during the mesh creation phase to work more easily on the grid size in that particular area.
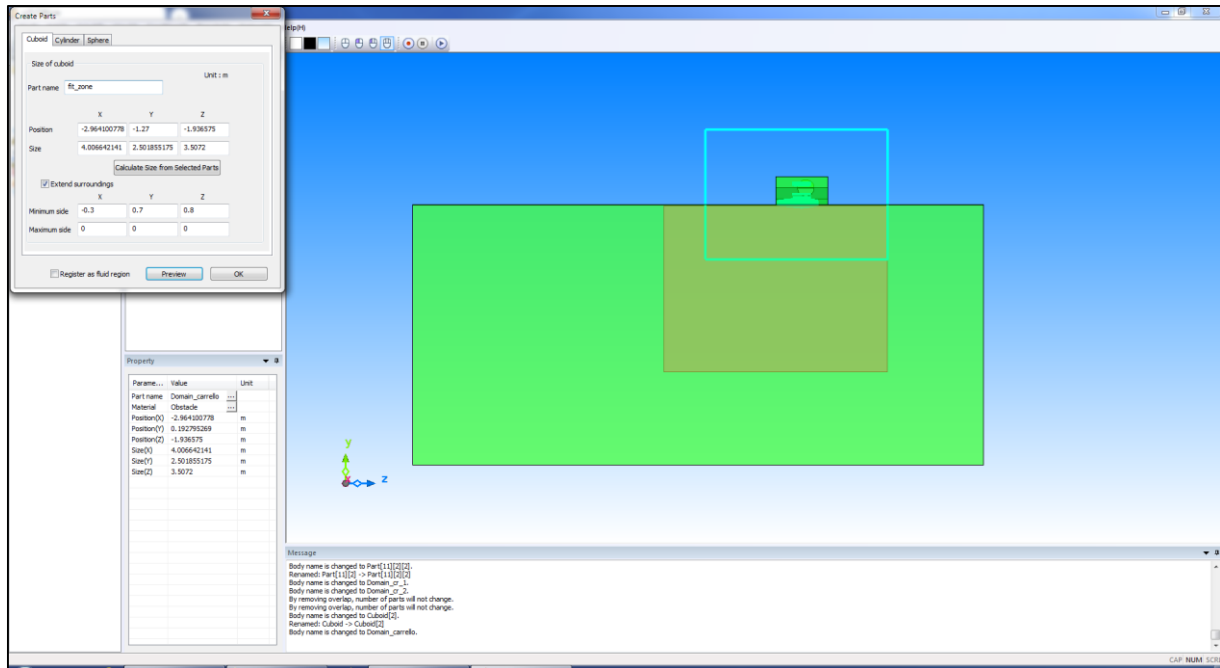
Figure 5.8: "Fit zone" creation.

At this point, having defined all the necessary elements, it is necessary to differentiate the main calculation domain from those related to overset mesh. This step allows to work with four distinct meshes during the mesh setup phase.
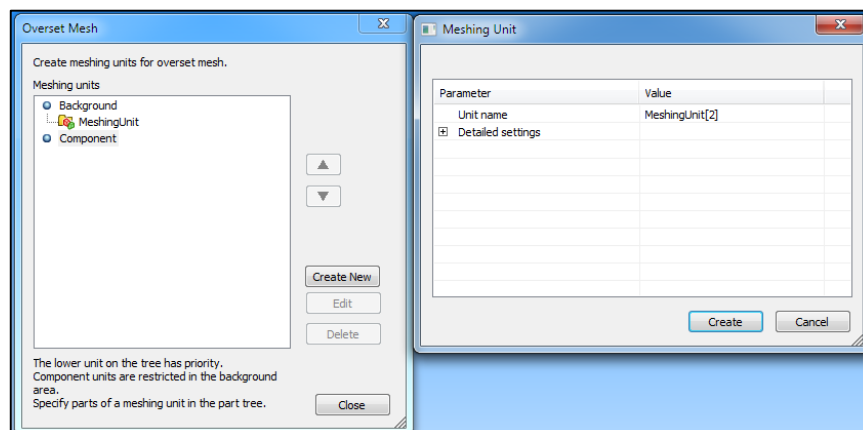
Figure 5.9: Meshing units creation for overset mesh.

Once the first phase related to the preparation of the model to work on is complete, it is possible to proceed with the building of the analysis model. This step is made automatically by scFLOW, now the parts divided into a material part (green) and void one (blue) appear in the tree.
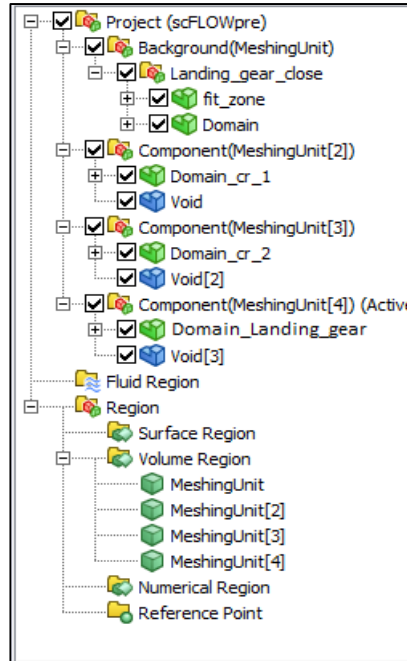
Figure 5.10: Analysis model parts tree.

5.2 Build of Analysis Model

This phase represents the core of the CFD analysis defining the set of equations used, the time step, the initial conditions, the type of boundary conditions and the connection between the mobile elements being examined in the two calculation codes. Initial values of quantities such as the pressure and temperature have been chosen with reference to the extraction condition of the landing gear at a height of about 1000 meters.

5.2.1   Part Material and Register Region

The materials choice allows to define the type of fluid domain and the disturbing elements of the current immersed in it. For the defined domains the air (incompressible) has selected in material chart while for other present elements the "obstacle" is left. The choice of "obstacle" allows to the software, when generates the calculation grid, to leave that particular area unchanged and therefore devoid of mesh; by operating in this way the imposed equations will not be resolved in those points (unless a no slip condition which imposes zero speed on the surface) and therefore the air flow will deviate and overcome the obstacle. The voids in the figure 5.11 are related to the two connecting rods and the landing gear leg previously subtracted from the created domains.
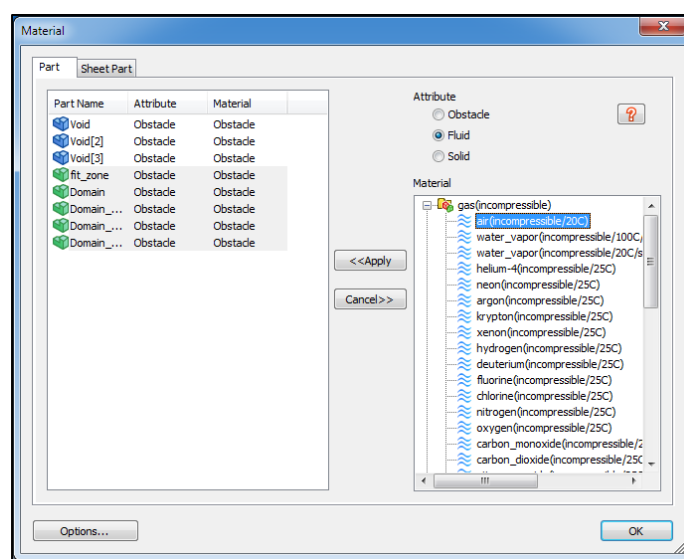
Figure 5.11: Materials choice.

Following the choice of materials there is the definition of the different regions, a useful phase to later attribute the boundary or wall conditions.

The registered regions are:

- Inlet – the entrance to the domain where the air current will enter
- Outlet – the domain exit
- Wall – the upper wall
- Simm – the side wall adjacent to the landing gear
- Free_slip – the side wall and the lower one far enough from the landing gear
- Surf_cr_1 / 2 – the surfaces of the two connecting rods
- Surf_landing_gear – the surface of the landing gear leg

5.2.2   Analysis Condition

In the following section the type of analysis and the relative data have been chosen. The chosen analysis is a transient "flow" analysis in which moving elements through the overset mesh and a coupling with Adams are allowed. Flow analysis has based on an incompressible flow, so the energy equation has denied during the calculation, and a SST $k - \omega$ turbulence model. The simulation time is 2.5 seconds with an operating time step of $5 \cdot 10^{-4}$ seconds.
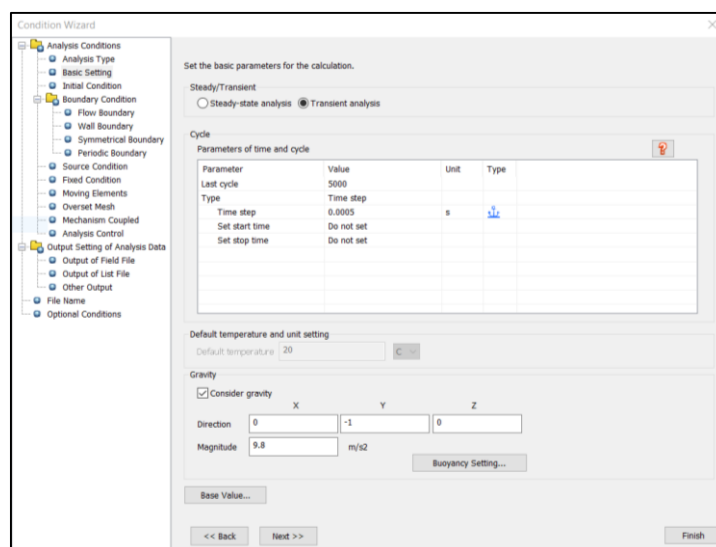
Figure 5.12: Set of time step and number of cycles.

As anticipated, initial conditions were set within the domain in terms of flow velocity, temperature and pressure at an altitude of about 1000 meters, in particular:

- $T_i = 8.5\ C$
- $P_i = 89876\ P_a$
- $V_z = 30\ m/s$

5.2.3 Boundary Condition

Boundary conditions are numerical conditions to be applied on the boundaries of computational domain, in the present case one relative to the inlet and the other relative to the outlet of domain. At the inlet a flow rate has been set with a speed along the z axis of $30\ m/s$, while on the outlet a relative static pressure (outflow) has been set.
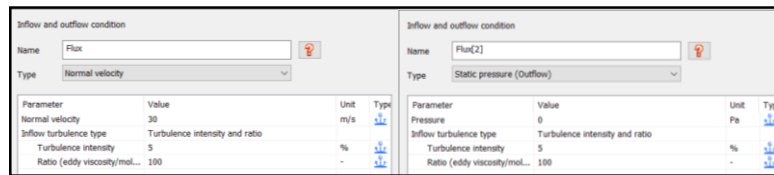
Figure 5.13: Inflow and outflow Condition.

Additional conditions on the walls of the domain and on the surfaces of the landing gear have been applied. In particular, a no slip condition have been applied on the upper wall and on the surfaces of the landing gear elements, forcing the flow to have zero speed in contact with the surfaces. On the wall adjacent to the landing gear a symmetry condition has been set, thus implicitly simulating the presence of a specular model. Finally, on the remaining walls, distant from the model, a free slip condition have been set so as to simulate free air.

A final step is necessary to properly couple the two calculation softwares and then the interest elements and quantities.

Initially the moving elements conditions have been set, however how the elements move have not been specified; the movement of the three different considered elements is in fact extrapolated by the co-simulator from Adams.

For each element, intended as a surface, has been set a type of movement "Mechanism coupled (Adams)" by remembering to insert the relative element ID which is an output of the created Gforce in Adams. The operation has been repeated for each moving element, by setting for each of them a specific ID and the reference surface on scFLOW correlated to Adams part in which the GForce was created.
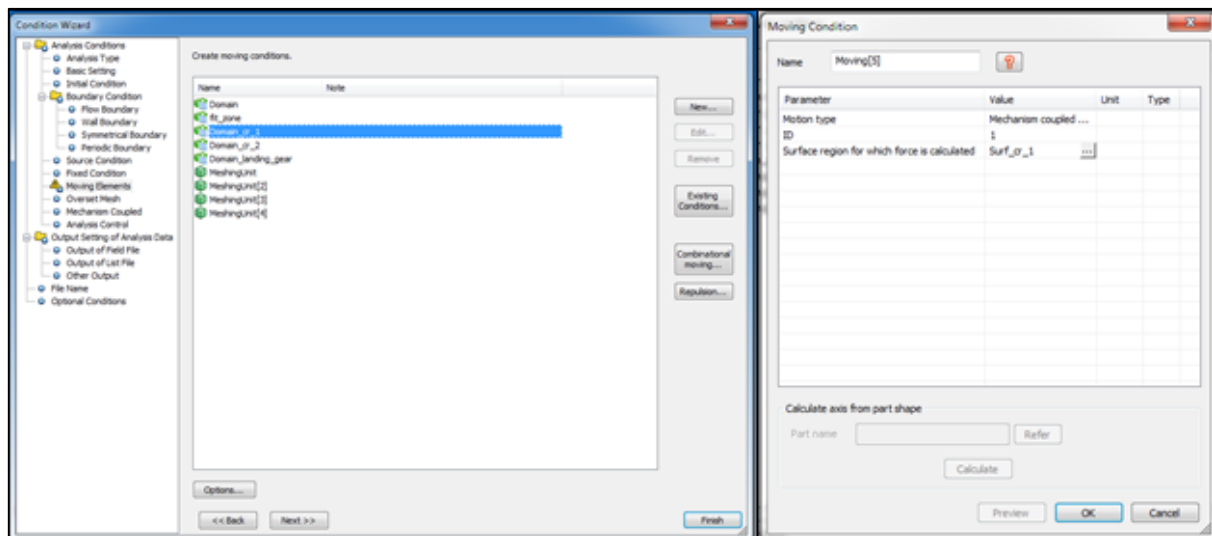
Figure 5.14: Moving condition on the upper connecting rod.

The right coupling of the calculation requires that the used units of measurement and the reference system orientation are equivalent between the two codes.

It is possible in fact to manipulate the orientation of the axes so that they are aligned and in a congruous way in both software.
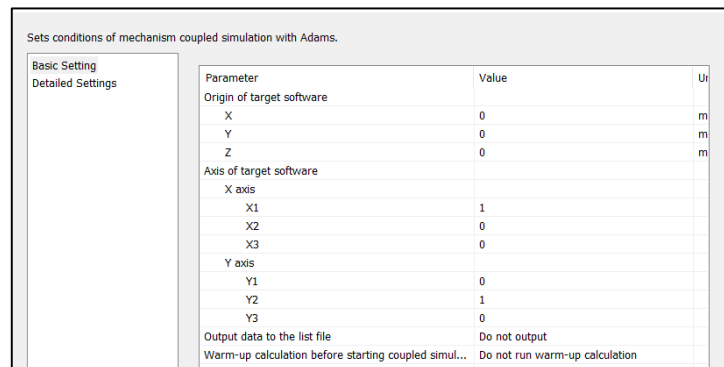
Figure 5.15: Axis Orientation.

Finally, before working on the mesh, the type of co-simulation was chosen. For the present analysis, two-way coupling has been chosen for bilateral communication, terminating the data exchange at the end of the fluid dynamic simulation time. To observe what the differences were, two simulations have been performed, varying between them the temporal interpolation method between "Constant Last" and "Quadratic".
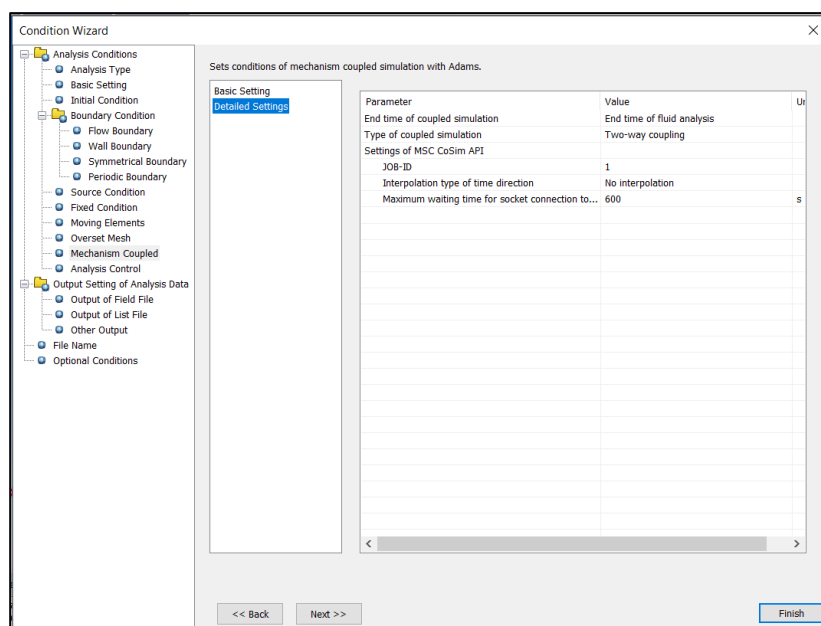
Figure 5.16: Co-simulation with interpolation method "Constant Last".
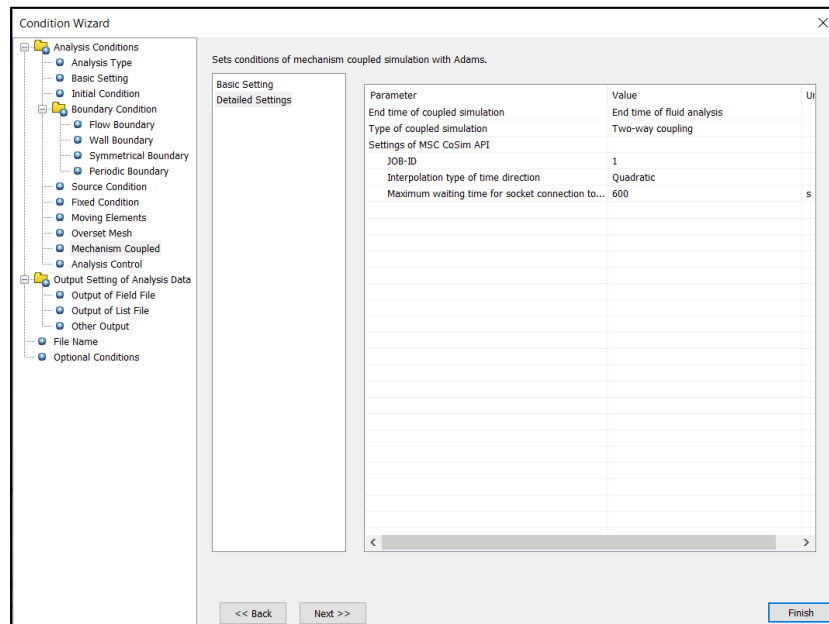
Figure 5.17: Co-simulation with interpolation method "Quadratic".

5.3 Build of Octree and Mesh

scFLOW adopts mesh-adaptation refinement function. In the function, an octree is reconstructed based on an analysis result, and mesh is generated from an original model geometry. This method represents model shape well, because mesh is reconstructed from the original model geometry data.

In adaptive mesh refinement of scFLOW, analysis mesh is automatically generated from model geometry and the appropriatethickness of boundary layer elements of walls is calculated from the surrounding elements. These functions enable scFLOW to generate mesh completely automatically.

The main work has made on octree, in particular for each domain an octree is generated in which is initially defined automatically a maximum and minimum size of the cells that can be suitably modified if necessary. Furthermore, taking as a reference the registered regions or surfaces, it is possible to refine the starting grid by introducing one or more layers of more accurate dimensions.

On the main domain the work was done on the upper wall and in the area where the landing gear has positioned during extraction ("fit_zone"). On the upper wall 6 layers has been inserted starting from a thickness of $3 \cdot 10^{-4}$, while in the area below the compartment a thickness of $3.5 \cdot 10^{-3}$ has been set.
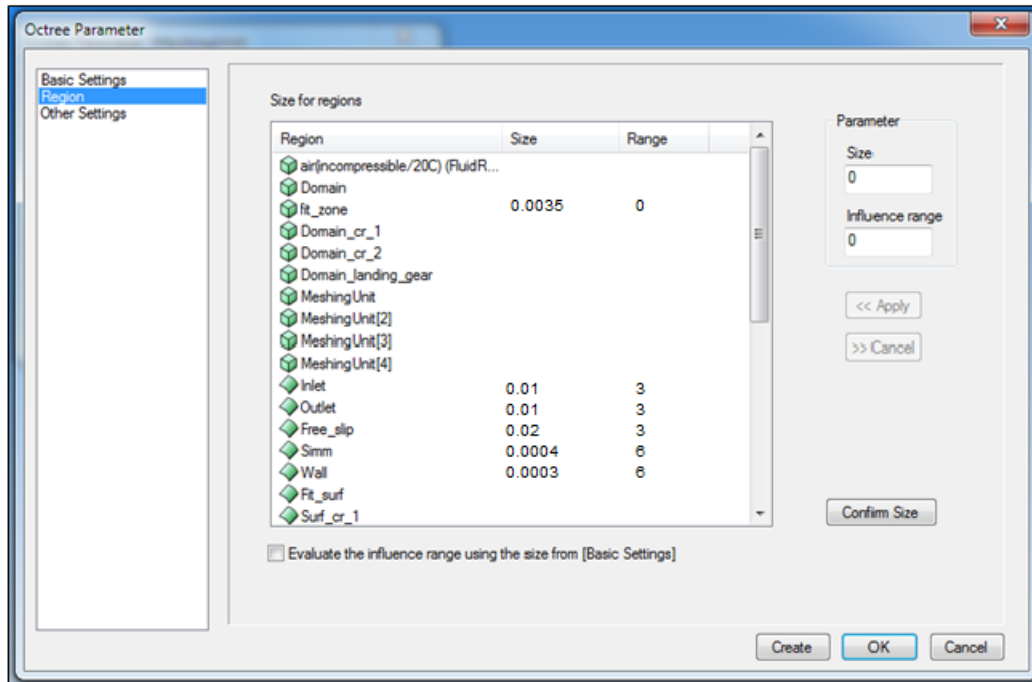
Figure 5.17: Parameters for prism layer insertion.

Similar work has been done on the walls of the connecting rods and the leg of the landing gear. In particular, 6 layers have been inserted on the leg starting from a thickness of $2 \cdot 10^{-4}$, while in the domain a coherent size with that set in the main domain "fit_zone" has been chosen. This choice is linked to the need to have a coherent overlap of the cells during the rotation of the landing gear.

For the two connecting rods, similarly to what has been done with the landing gear leg, a thickness of $1.5 \cdot 10^{-4}$ has been set by inserting 6 surface layers.
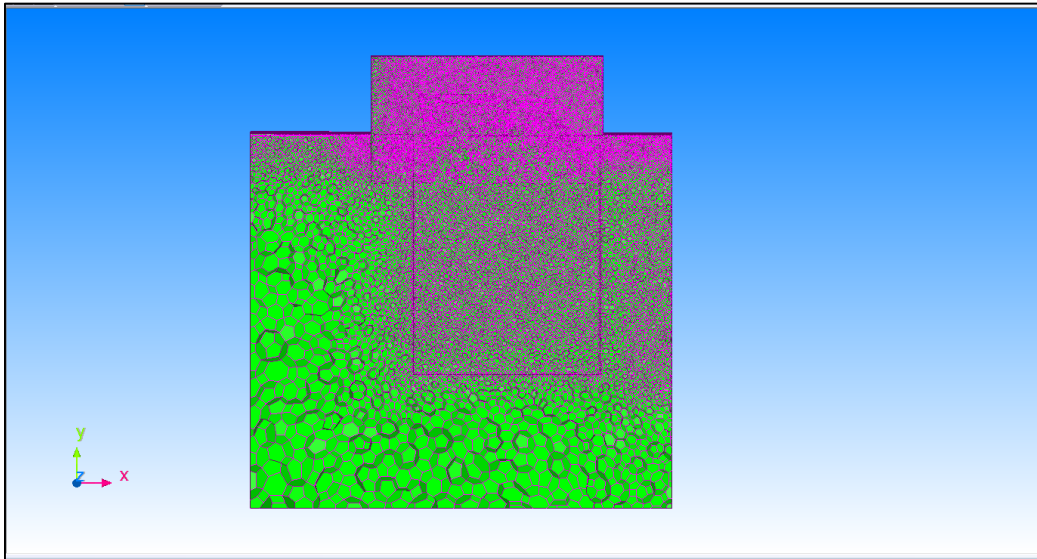
Figure 5.19: Main domain mesh Section 1.
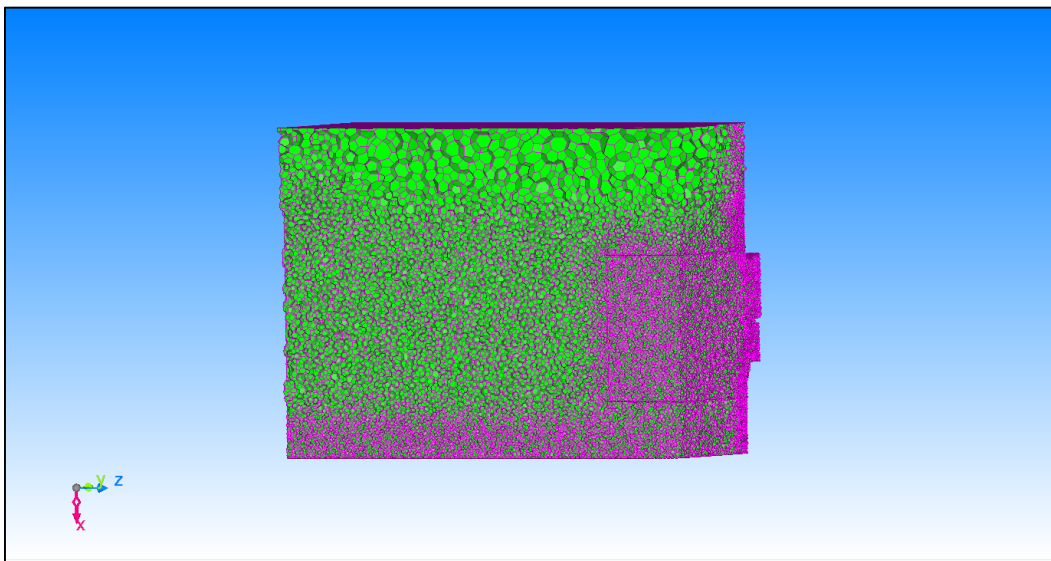
Figure 5.20: Main domain mesh Section 2.
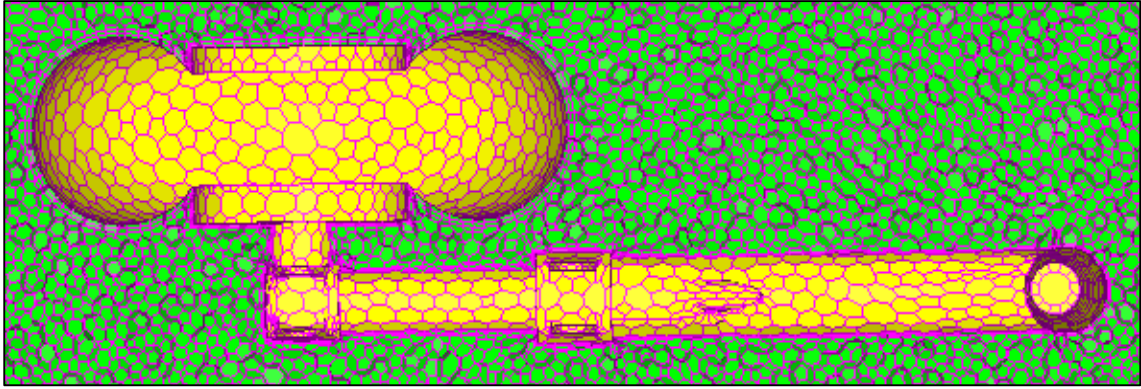
Figure 5.21: Landing gear leg mesh.

Once the mesh is generated, executing the program, it gets the file (.sph) to be started in the co-simulator together with the Adams analysis file (.acf). Starting the calculation using the co-simulator, the scFLOW Solver is launched in which the equations are solved taking into account the established conditions and the expected convergence criteria. The analysis ends with the post-processing operations in which the results of both software can be displayed.

Chapter 6

Results

In this chapter the results of the two coupled analysis will be presented.

The first section will be dedicated to the fluid-dynamic analysis of the landing gear in which the obtained results can be compared with experimental ones collected by Dr. Ing. S. F. Hoerner. This comparison allows to understand the accuracy of the current analysis and therefore possible improvements for future work developments.

In the second section a comparison between Adams results will be presented, the first ones considering the influence of the aerodynamic forces and the second ones relative to a dynamic analysis without coupling.

At the end a estimator of the percentual error will be evaluated between the calculated quantities and the trasmitted ones through the co-simulator. This process allows to verify if the coupled analysis is accettable or the errors between the trasmitted quantities could lead to erroneous results.

6.1 scFLOW Results: Landing gear fluido-dynamic post-processing

The starting point of a fluid-dynamic analysis is the estimation of the Reynolds number with which is possible to understand if the working fluid is in a laminar or turbulent regime. By considering a velocity of 30 m/s and the wheel diameter as the characteristic dimension the followed Reynolds number is obtained:

$$R_e = \frac{\rho V D}{\mu} = 1.2 \cdot 10^6$$

this value, related with the experimental ones around a cylinder, is relative to a turbulent flow regime.

The boundary layer around the wheel is completely turbulent and characterized by high kinetic energy. This higher rate of kinetics around the wall of the wheel allows to counteract the adverse pressure gradients and therefore the separation. It is not a coincidence that in this configuration the separation point is attended for angles close to $100 \div 120$ degrees. The wake has characterized by a chaotic motion of particles with reminescence of the vortices.
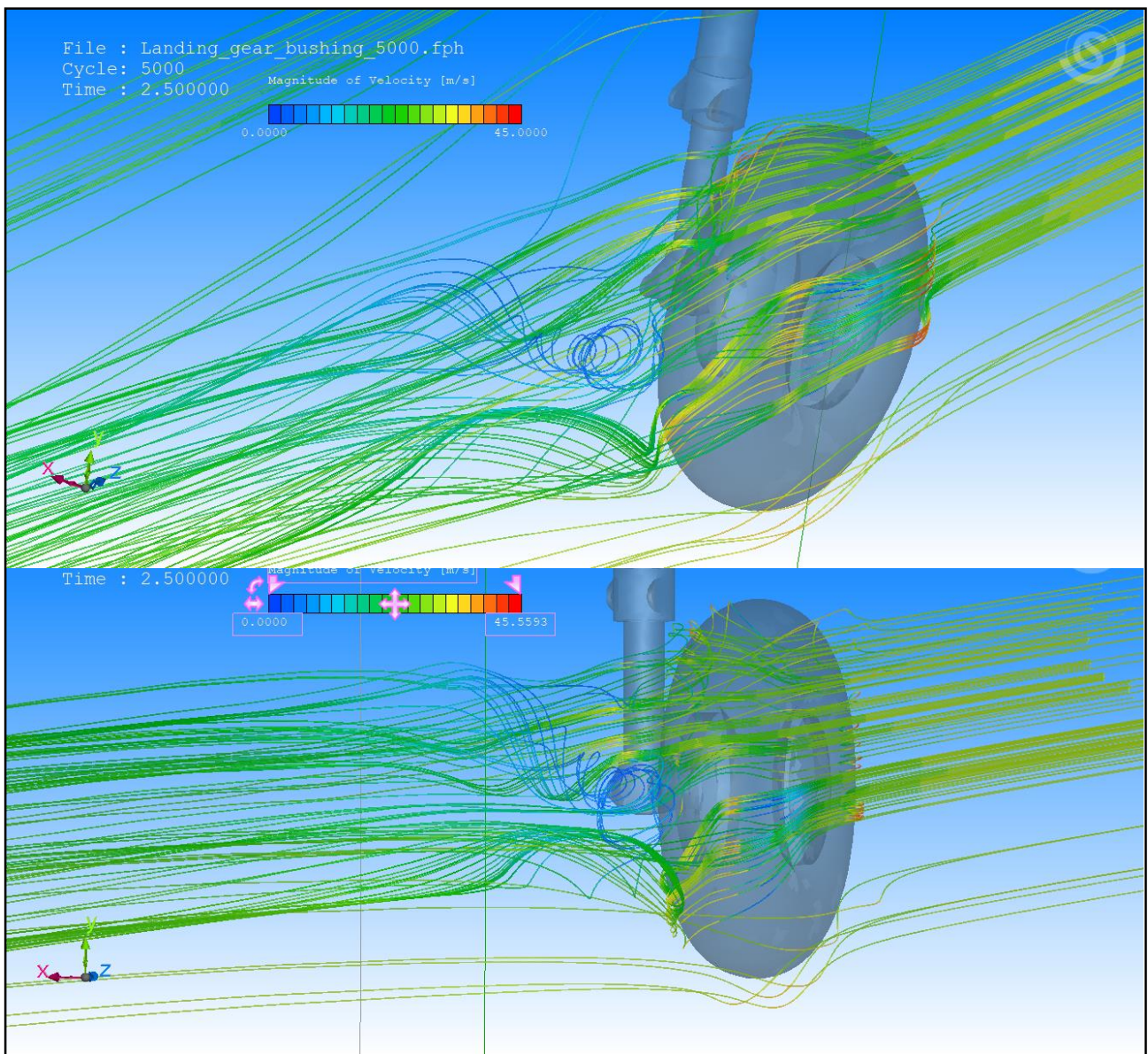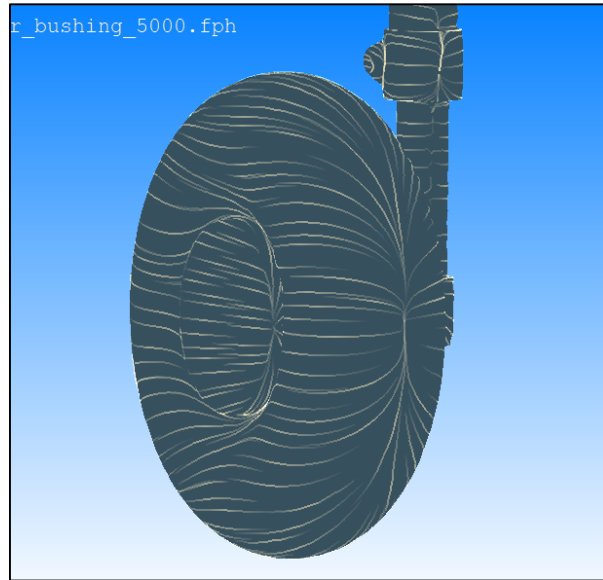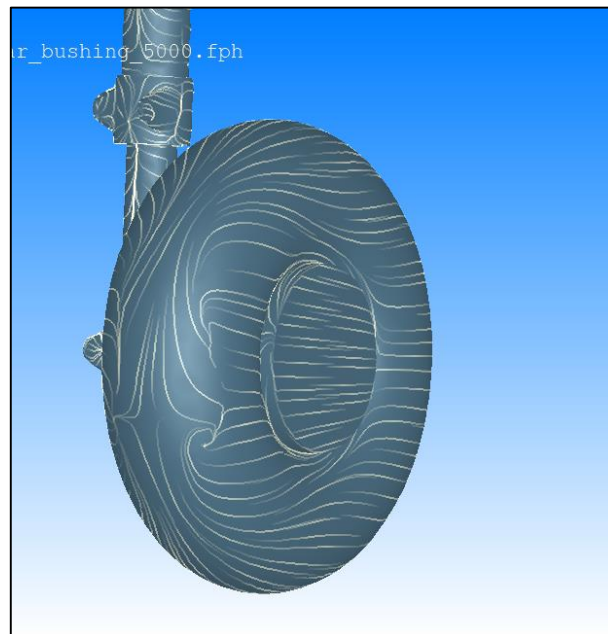

Figure 6.1: Streamline visualization in the wheel wake.

A first result can be presented in the *figure 6.2* and *6.3* in which the streamlines produced from the time averaged velocity field in the simulation and the oil flow visualization are plotted on the landing gear wheel.

Figure 6.2: Oil flow visualization and streamlines, front view of wheel.

Figure 6.3: Oil flow visualization and streamlines, rear view of wheel.

In *figure 6.2* a stagnation point of the flow is visible, while in *figure 6.3* it is possible to hypothesize a separation for an angle greater than 120 degrees in which the shear lines are not displayed. Certainly a more accurate wall mesh would have allowed to visualize the recirculation zones and local current separations in greater detail.
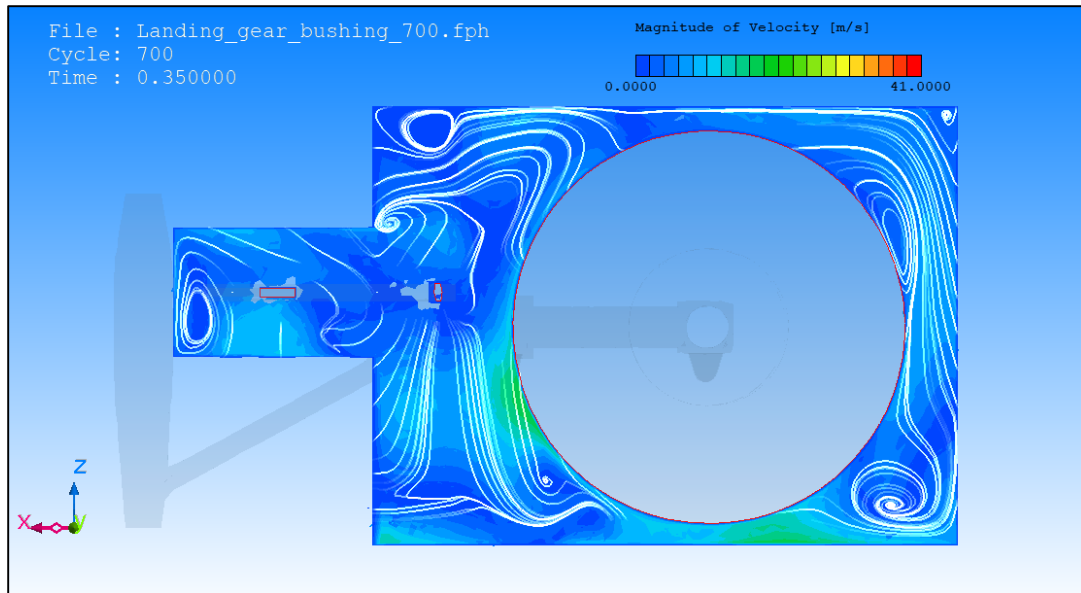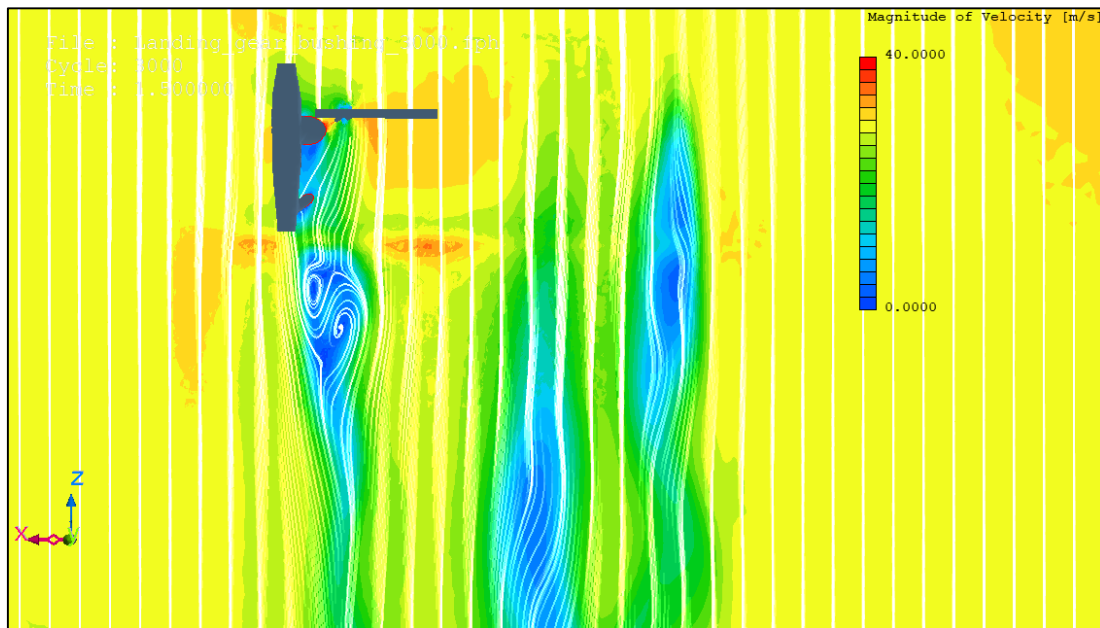

Figure 6.4: Contour of velocity and streamline visualization (y=1.5, t=0.35).
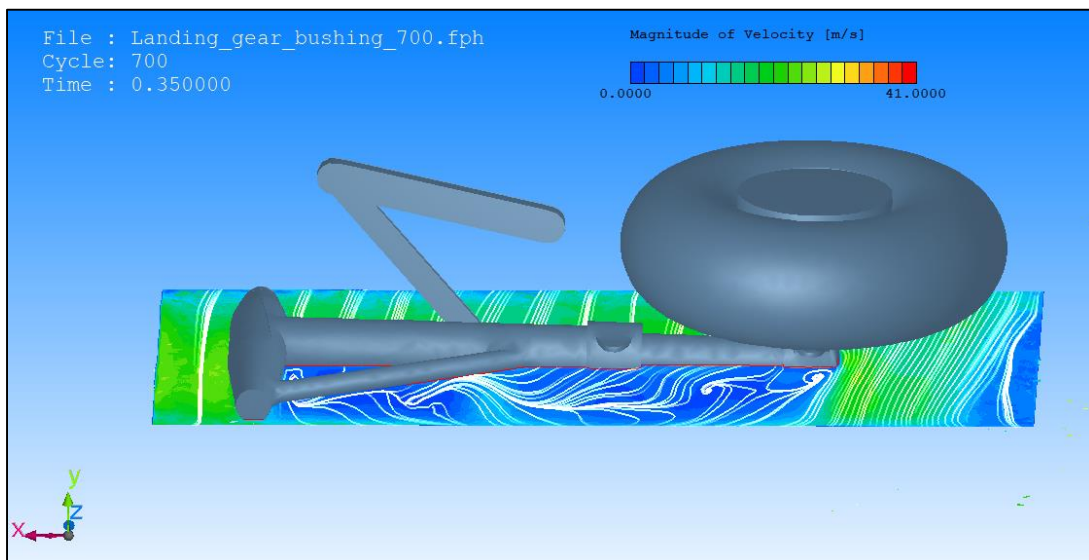
Figure 6.5: Contour of velocity and streamline visualization (y=1.25, t=0.35).
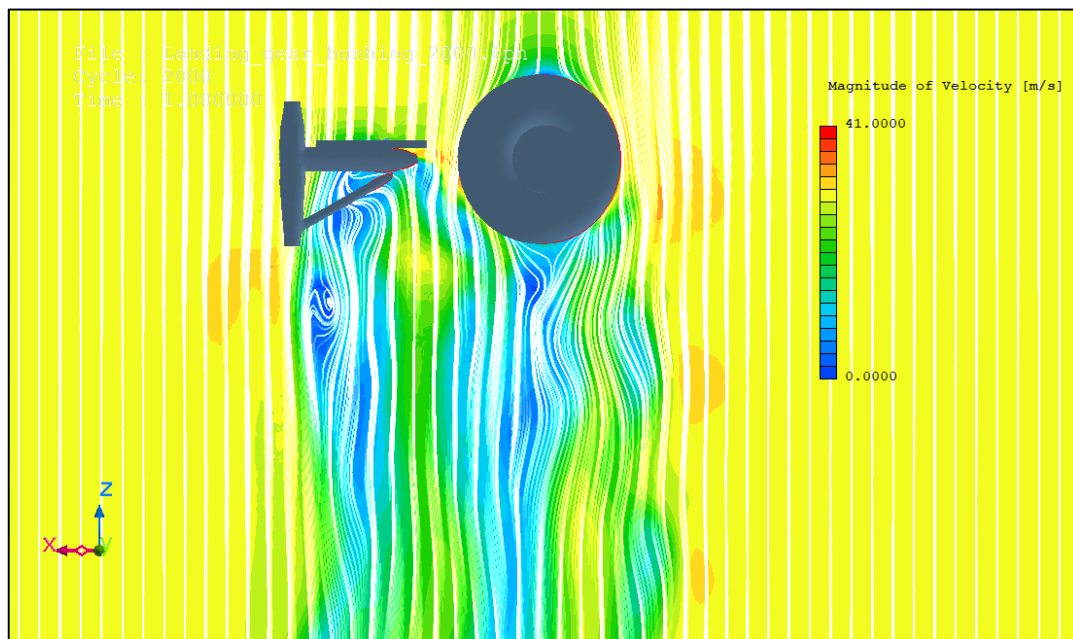
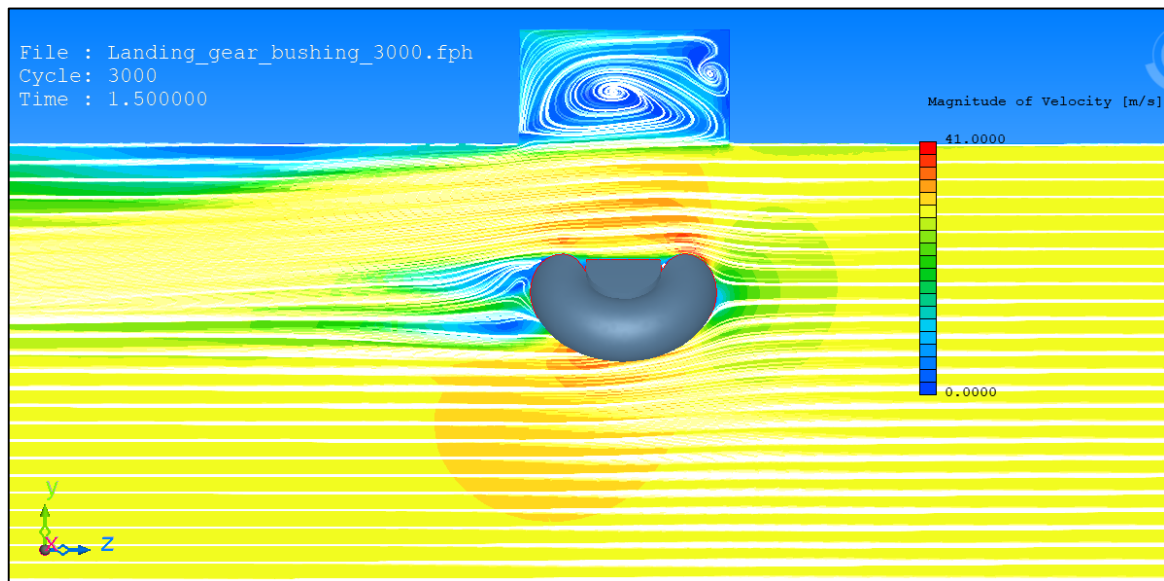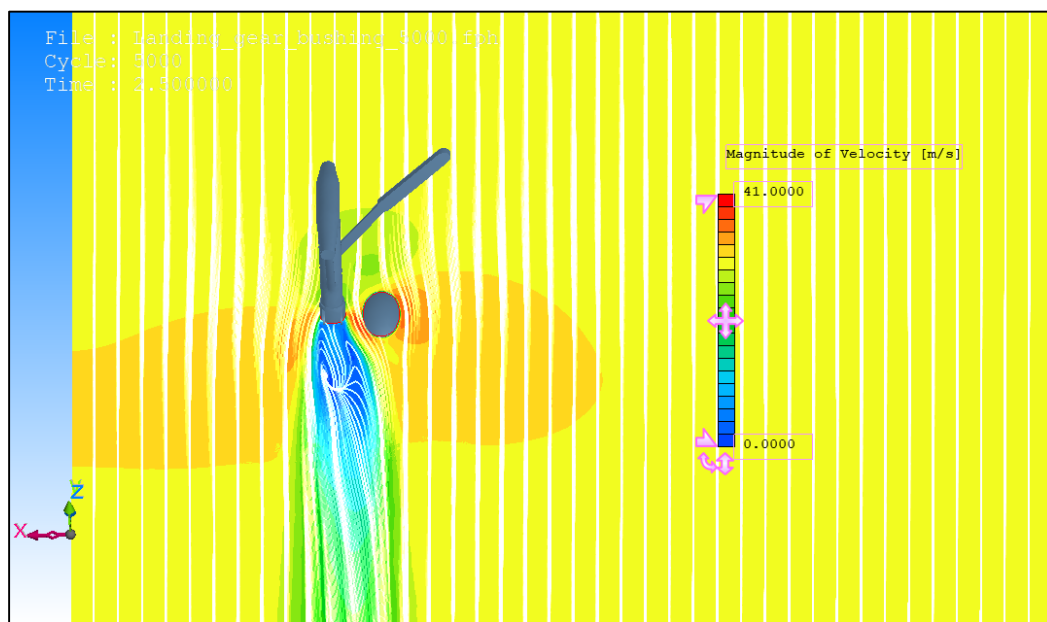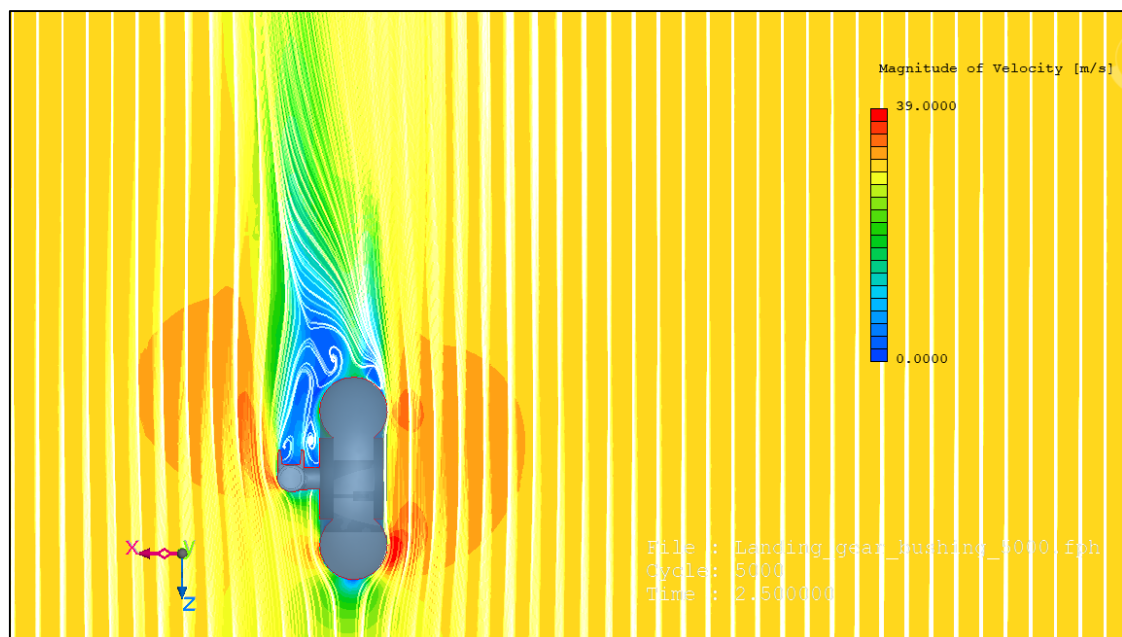*Figure 6.6: Contour of velocity and streamline visualization (y=1.1, t=1).*
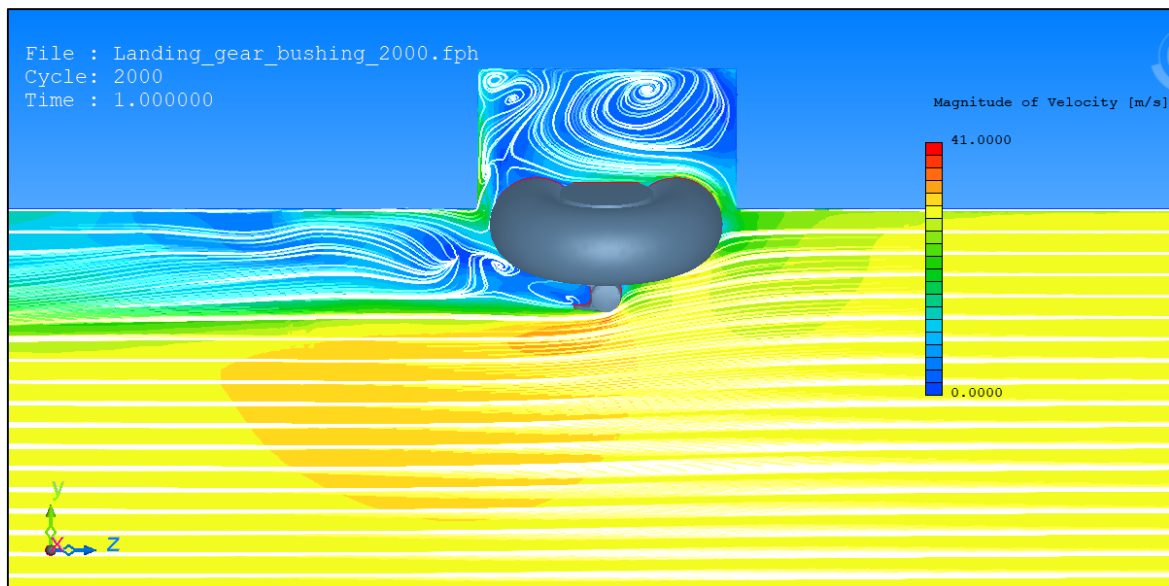
Figure 6.7: Contour of velocity and streamline visualization (x=-1.3, t=1).

Figure 6.8: Contour of velocity and streamline visualization (y=0.42, t=1.5).
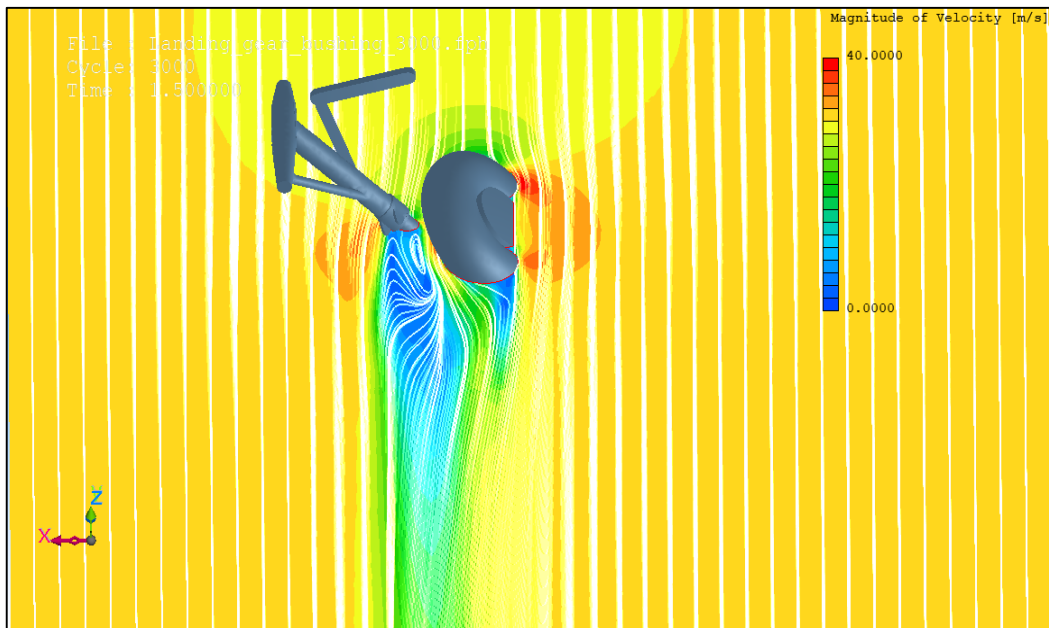
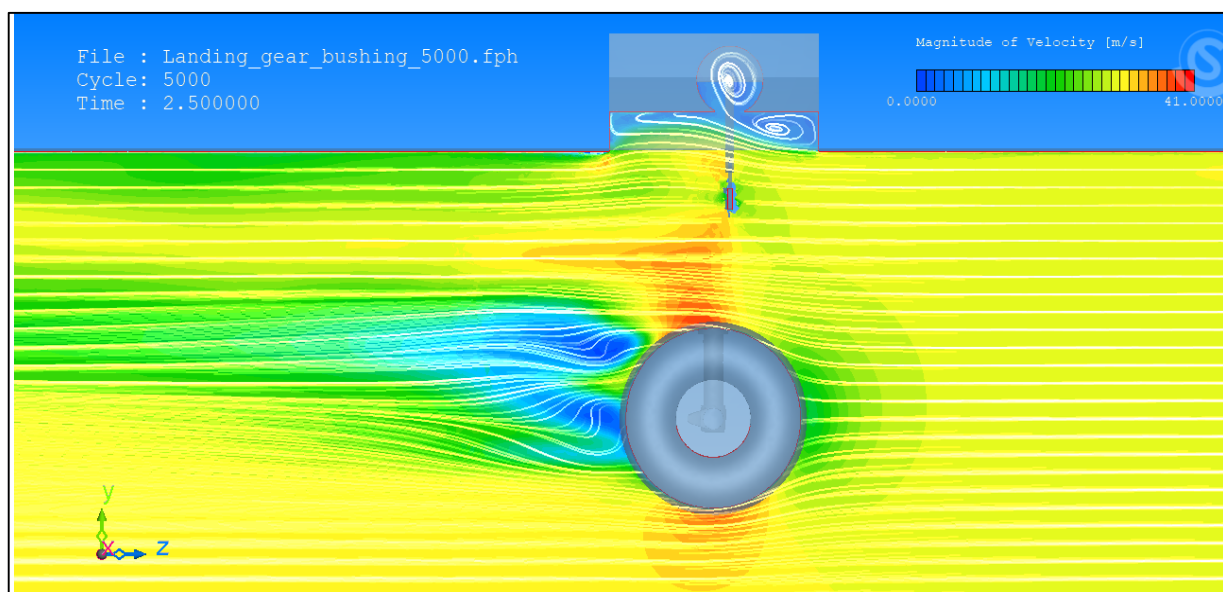*Figure 6.9: Contour of velocity and streamline visualization (y=0.6, t=1.5).*

Figure 6.10: Contour of velocity and streamline visualization (y=1.2, t=1.5).
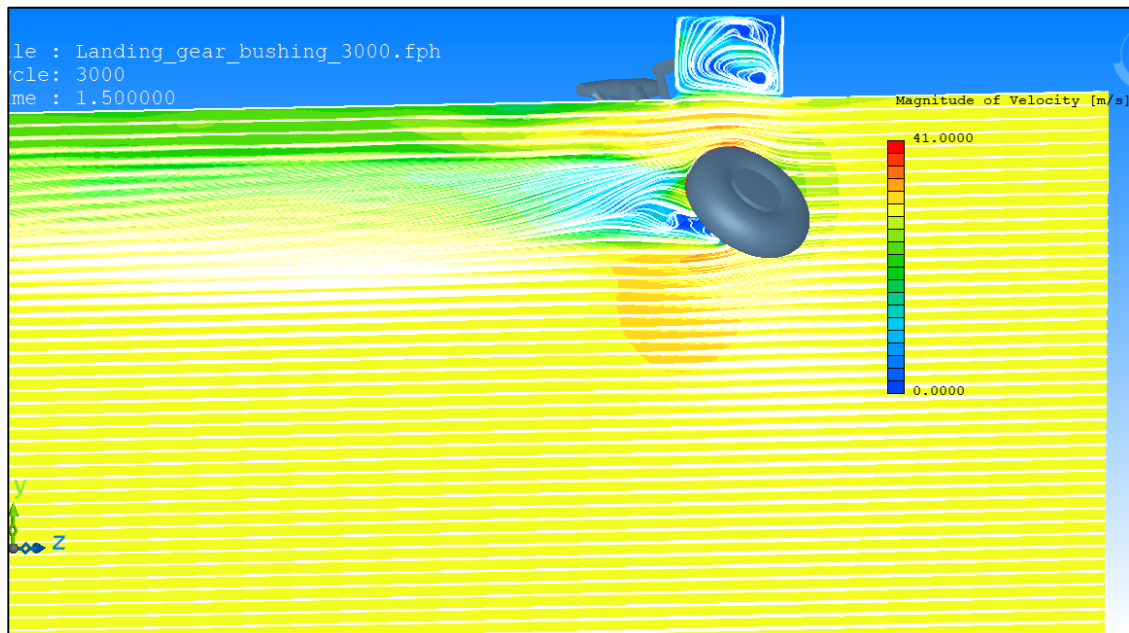
Figure 6.11: Contour of velocity and streamline visualization (x=-1, t=1.5).

Figure 6.12: Contour of velocity and streamline visualization (x=-1.2, t=1.5).

Figure 6.13: Contour of velocity and streamline visualization (y=0.4, t=2.5).

Figure 6.14: Contour of velocity and streamline visualization (y=0.01, t=2.5).

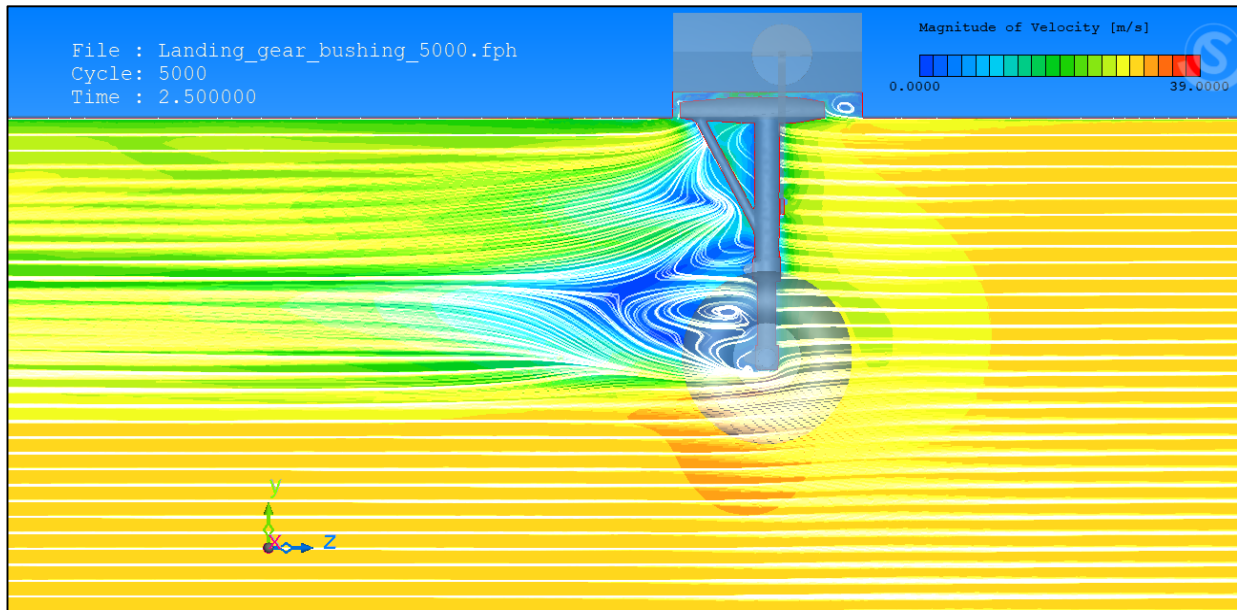*Figure 6.15: Contour of velocity and streamline visualization (y=-0.4, t=2.5).*

Figure 6.16: Contour of velocity and streamline visualization (y=-0.12, t=2.5).

From *figure 6.4* to *6.16* the velocity contour projected on the planes at different x and y location is represented. The images have been taken at four different times relative to four different positions of the landing gear, allowing us to appreciate the flow evolution in the wake. In a good approximation the simulation reflects the introduced flow field having a turbulent wake at rear in which vortical structures are distinguished. It is important to note that the results value (such as the acting aerodynamic forces) during the first moments of simulation can be compromised due to the landing gear compartment geometry. In fact in *figure 6.4* it is possible to notice the "corner flow" presence in the wall edges, they influence the pressure distribution on the body when there is not enough distance between it and the walls.

Figures 6.17 and *6.18* show pressure on the landing gear surface, the numerical values obtained from the pressure contour allow to evaluate the pressure coefficient along the central section of the wheel and the drag coefficient of the landing gear.
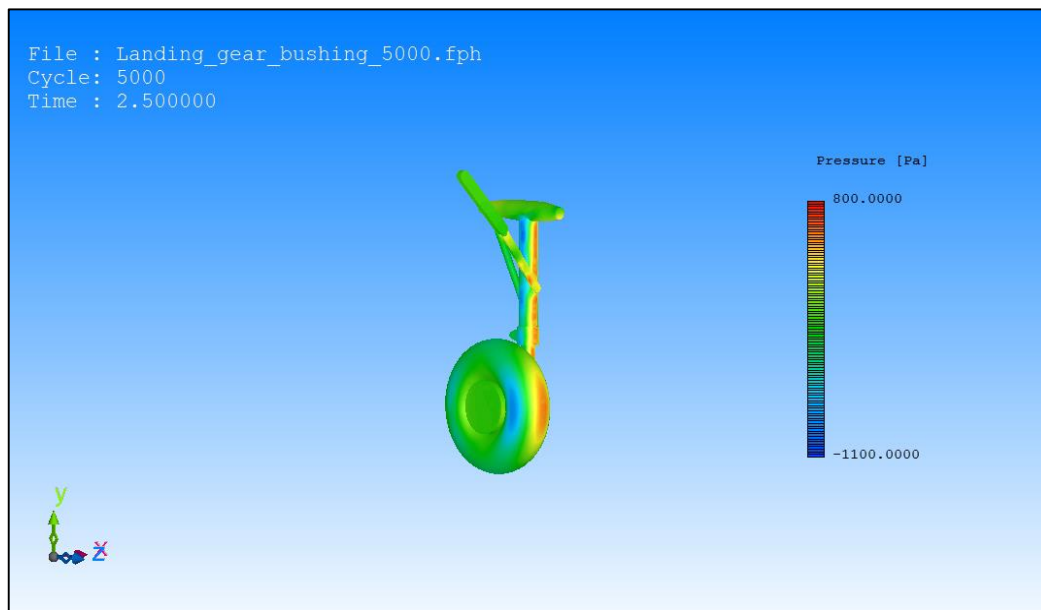
Figure 6.17: Pressure contour on the landing gear surface. Front view.
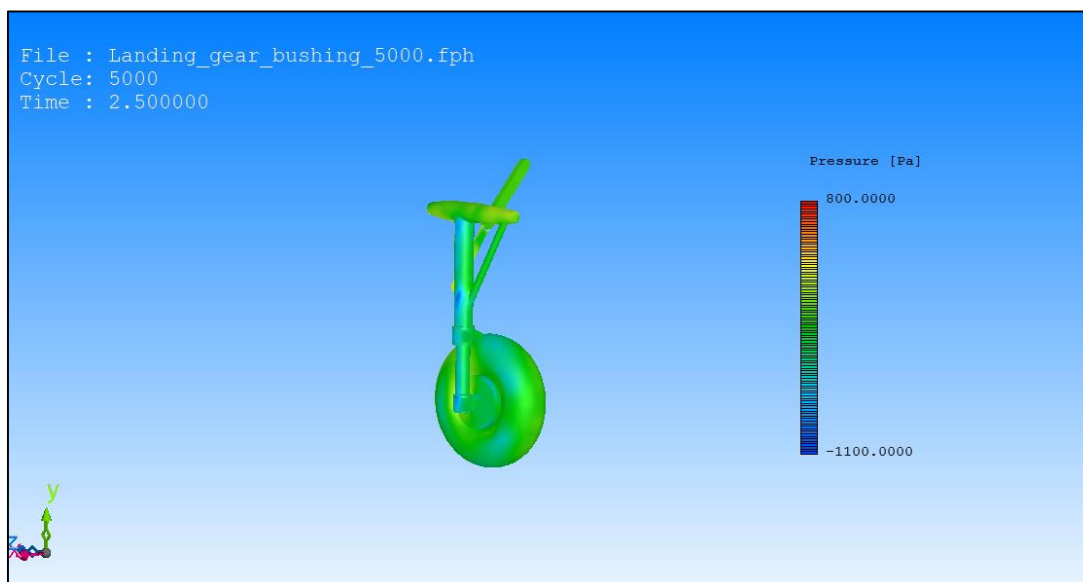

Figure 6.18: Pressure contour on the landing gear surface. Rear view.

Pressure is conveniently presented in a non dimensional form as the ratio of relative pressure to the free stream dynamic pressure.

$$c_p = \frac{P - P_\infty}{\frac{1}{2}\rho_\infty V_\infty^2} \qquad (6.1.1)$$

where P is the local static pressure at the point which is being evaluated and P_∞ is the free stream pressure.

The pressure coefficient has been calculated function of the θ angle and considering the pressure distribution on the central section of the wheel. *Figure 6.19* shows how theta is defined.
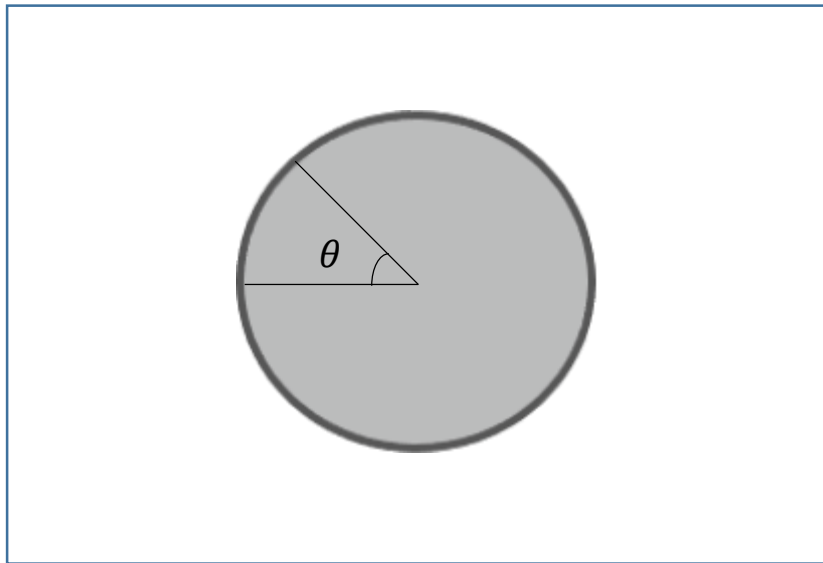
Figure 6.19: Definition of θ.

The obtained result has been compared with [11] in which experimental wind tunnel test and simulation results are presented. With good approximation the trends are quite similar, the differences can be linked to different factors such as a different Reynolds number or a different and more detailed mesh.
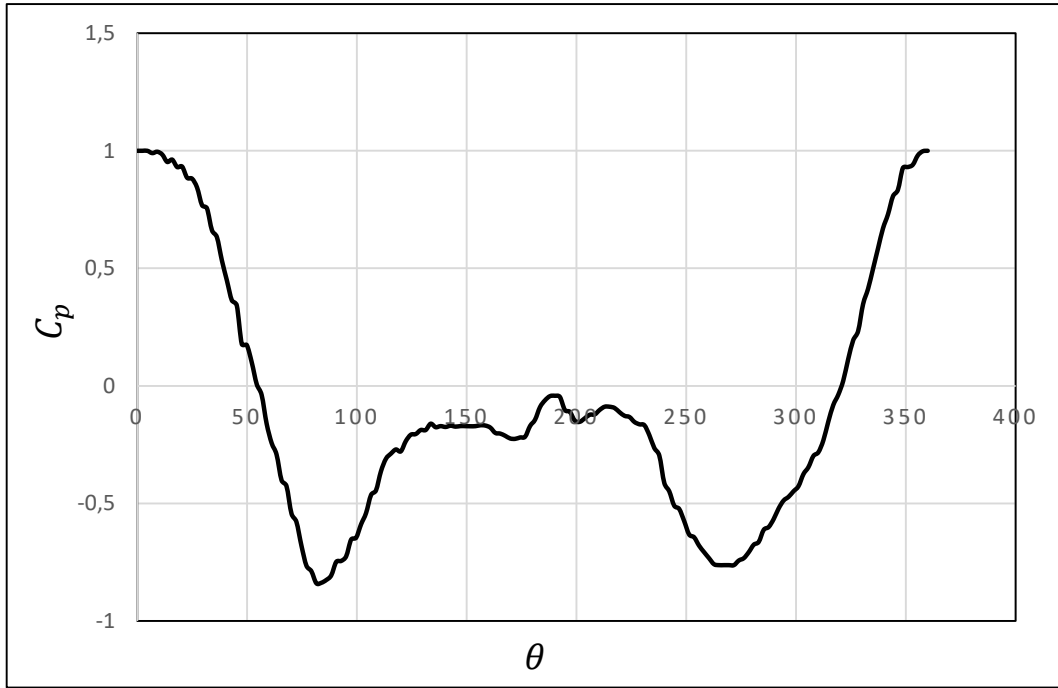
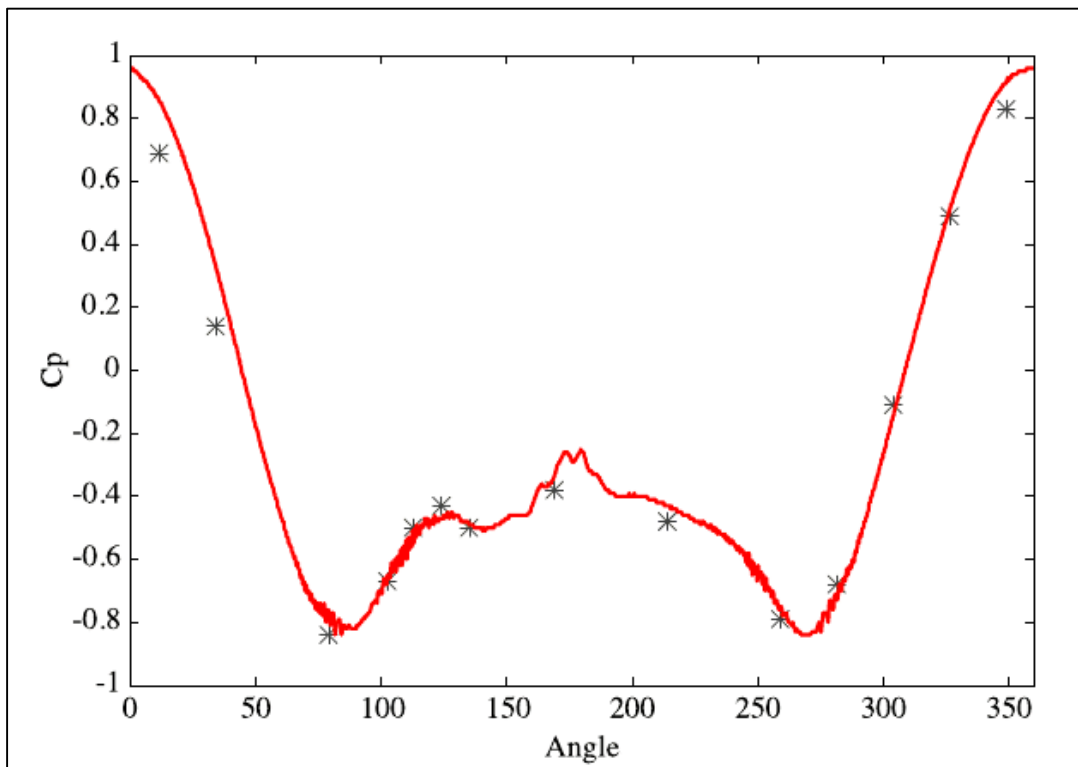*Figure 6.20: Cp along the circumference of wheel.*

*Figure 6.21: Mean pressure coefficient around wheel. Experimental results (*) and simulation results (—). (from Numerical Simulations of Flow over a Landing Gear with Noise Reduction Devices usi*ng the Lattice-Boltzmann Method)

In the first region near the leading edge the pressure begins with a maximum value at the stagnation point then decrease up to a minimum value, while the airflow velocity increases along the surface. This is the favorable pressure gradient region ($dp/d\theta < 0$), there is no risk of separation in this region.

After a minimum point the pressure begin to increase along the surface, while the velocity decrease. This is the pressure recovery region, or unfavorable adverse-pressure gradient region ($dp/d\theta > 0$). In this region there is a risk of separation if the pressure gradient is high enough. After a certain point on the $C_p(\theta)$ graph in this adverse pressure gradient region if there is a constant pressure region, this region may be an indication of separation.

For a sure prediction of the separation point should be necessary to value the $C_f(\theta)$ and find where the value is equal to zero.

The last presented result, for the present CFD analysis, is the estimate of the landing gear drag coefficient. It can be defined as:

$$C_D = \frac{F_z}{\frac{1}{2}\rho_\infty V_\infty^2 S_w} \qquad (6.1.2)$$

where S_w is the wheel frontal surface.

The choice of this reference surface is in agreement with what has cited by [12], in particular: "The drag coefficient of airplane wheels and landing gears may conveniently be based upon the area S_w, equal to tire width times outer diameter. Referring the drag of the whole landing gear to that area, the size of these parts and their drag is properly considered to be proportional to wheel and tire size".

For the drag coefficient calculation the pressures along the landing gear surface have been integrated, the obtaining result of this calculation is the resultant force that projected along the z axis has given the drag force component.

The force F_z has been plotted as a function of time and therefore throughout the extraction process.
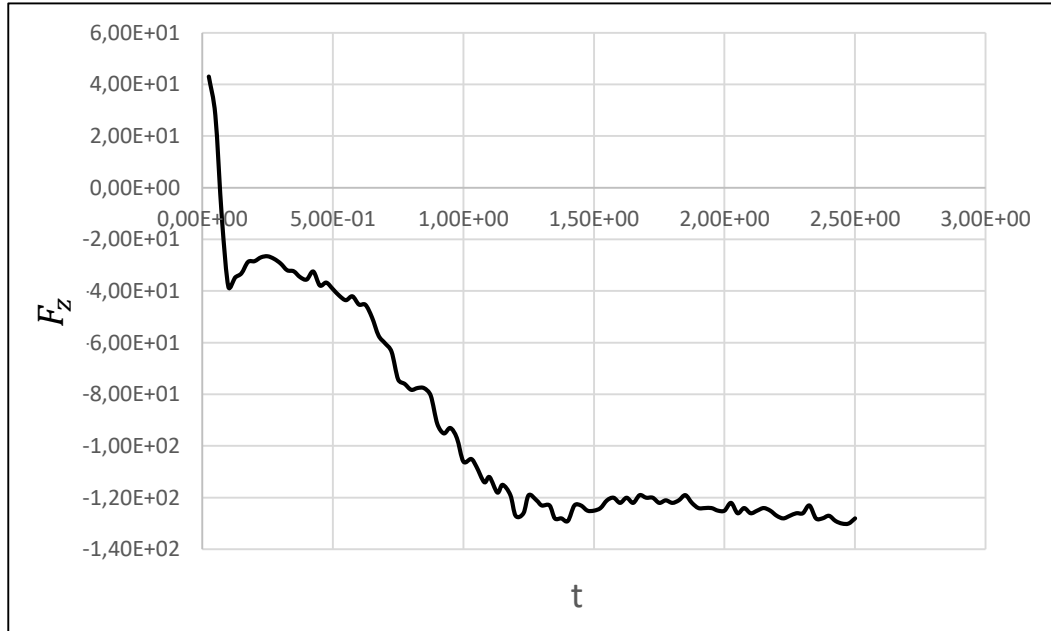

Figure 6.22: Drag Force during the landing gear extraction.

The negative value of the force is correlated to the positive direction of the z axis which is contrary to that of the current motion.

The *figure 6.23* shows the growth of the drag coefficient during the entire landing gear extraction process. To estimate the quality of the performed simulation, only the last value which represents the drag coefficient in the completely extracted position has been used. As a comparison the results proposed by [11] and [12] have been taken into consideration. The results proposed by [11] are related to statistical and experimental data collection while those of [12] of a numerical simulation using L-B method (Lattice-Boltzman) and wind tunnel tests.
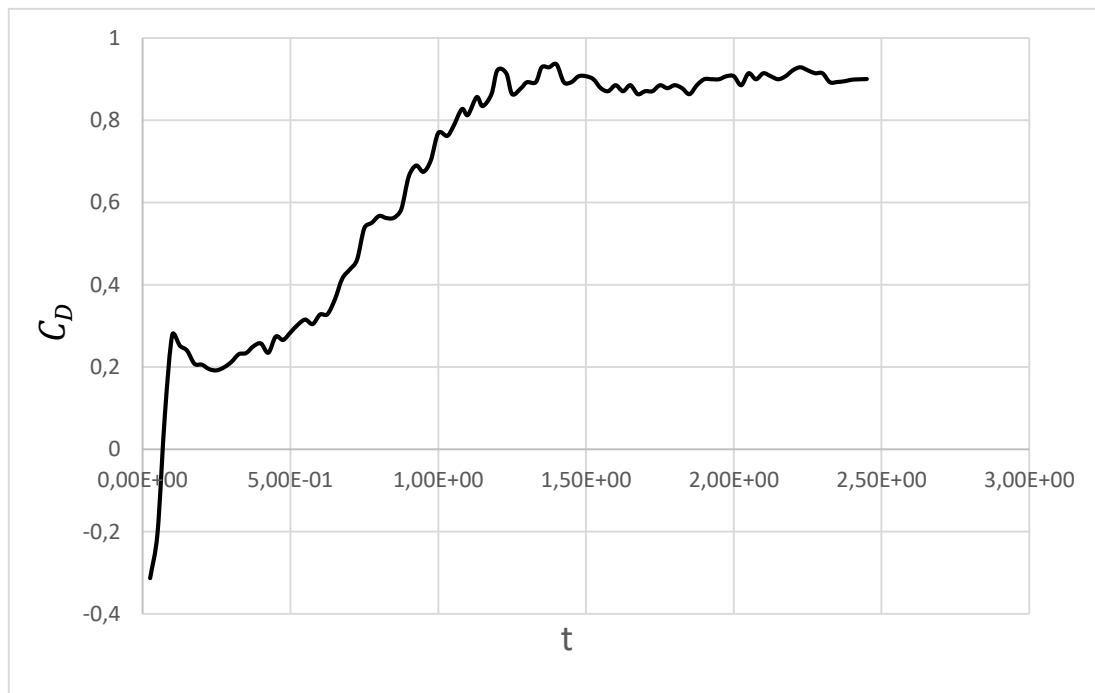
Figure 6.23: Drag coefficient during the landing gear extraction.

|	CURRENT SIMULATION	[12] STATISTICAL DATA	[11] SIMULATION	[12] W.T.
C_D	0.9	$0.6 - 0.8$	0.751	0.750

Considering a reference value of 0.8 the error committed is 12.5%, one of the possible causes is certainly related to the mesh structure which in fundamental areas, for the calculation purpose, have not a sufficient detail level. However the considered analyzes have been carried out at different speed and Reynolds numbers, this factor can certainly influence the results similarity.

6.2 Adams Results: Influence of aerodynamic loads on the extraction mechanism

In this section the results collected from the multi-body analysis will be presented, putting in evidence the effect that aerodynamic loads have on the entire landing gear extraction process. The first graph presented on the left refers to a coupled analysis while the second one on the right refers to an uncoupled analysis, the comparison allow to appreciate the differences between the two analysis.

This simulation shows the landing gear extraction from the under wing compartment, the process takes place through the rotation of the upper connecting rod which allows the movement of the entire mechanism.

The following figures represent the extraction process from the closed position to the extracted one:
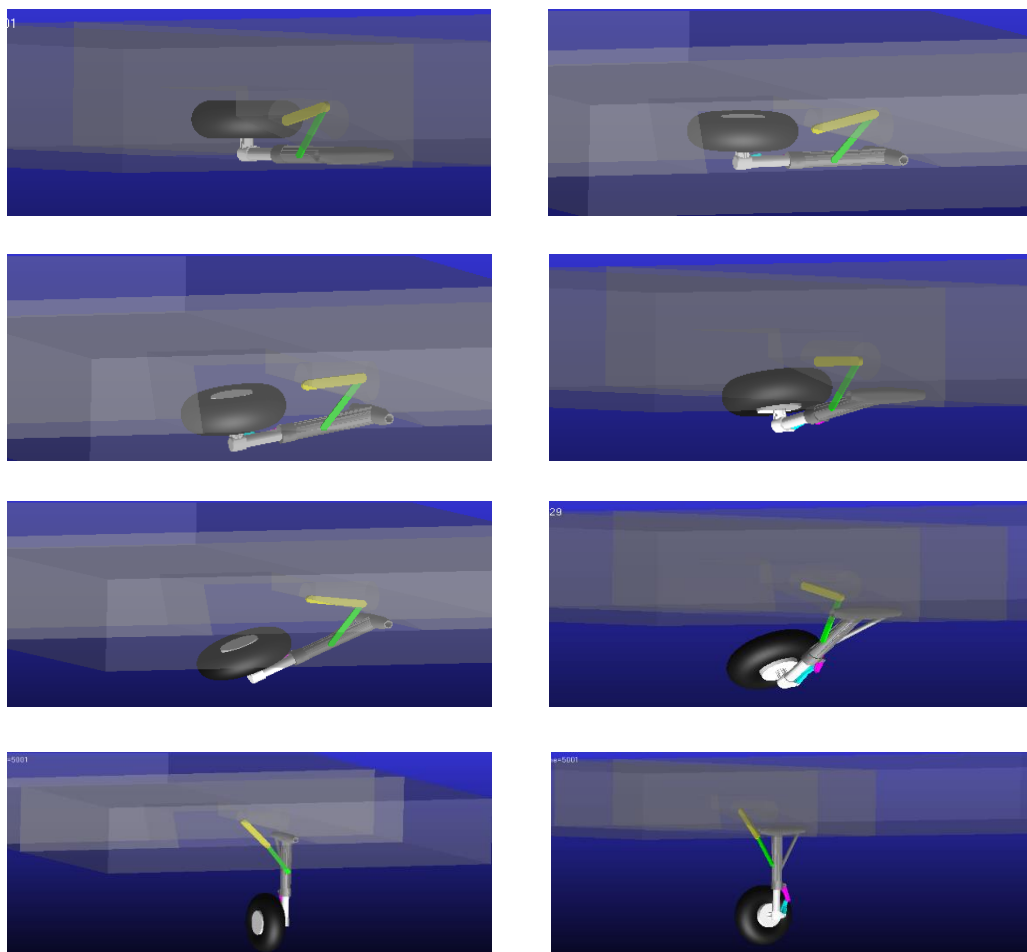
Figure 6.24: Landing gear extraction process, from the close position to the full opened.

Having performed a co-simulation, a first result which can be shown is the time trend of aerodynamic loads on the three interested parts.
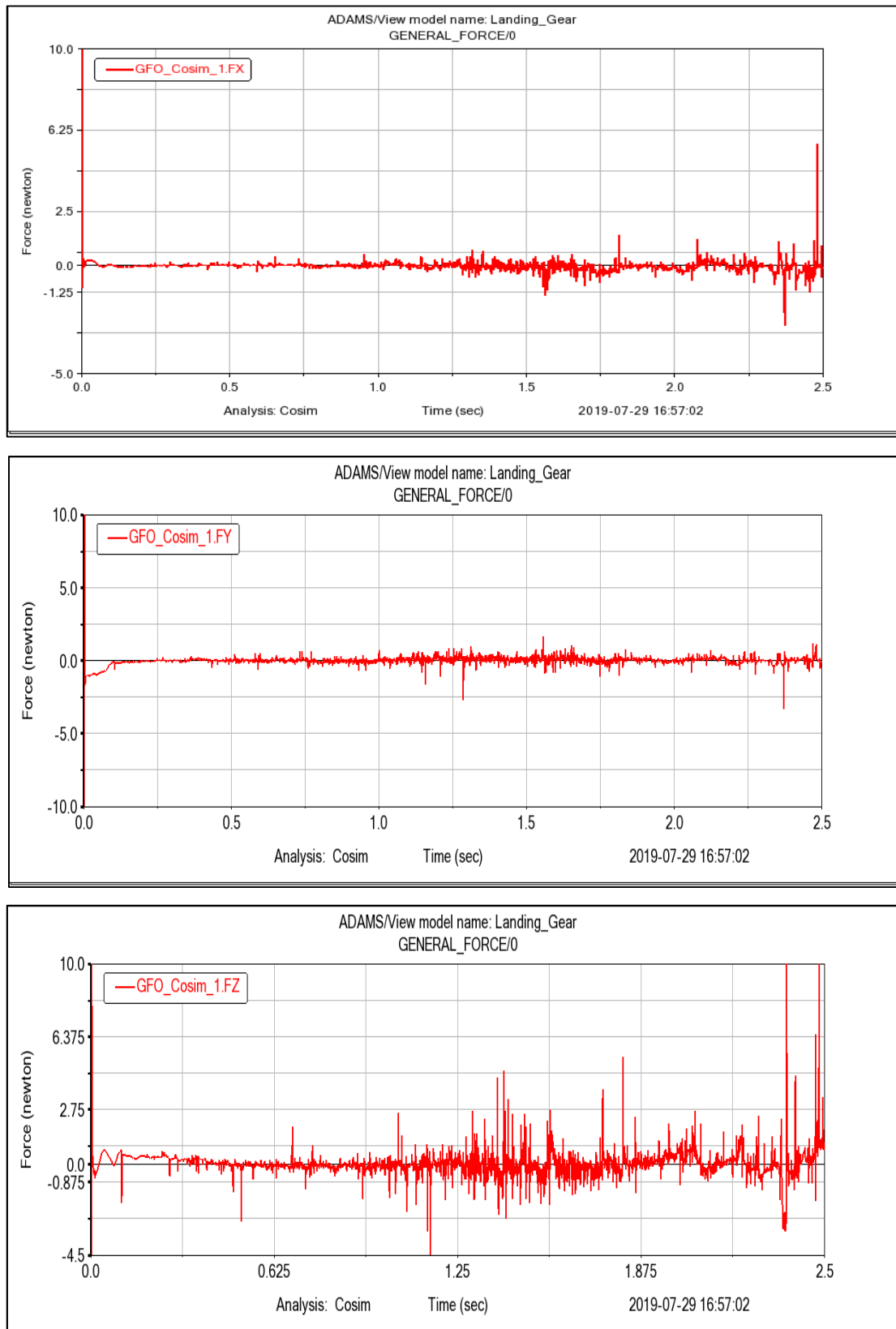

Figure 6.25: The three aerodynamic force component along X, Y and Z axis on the upper connecting rod.
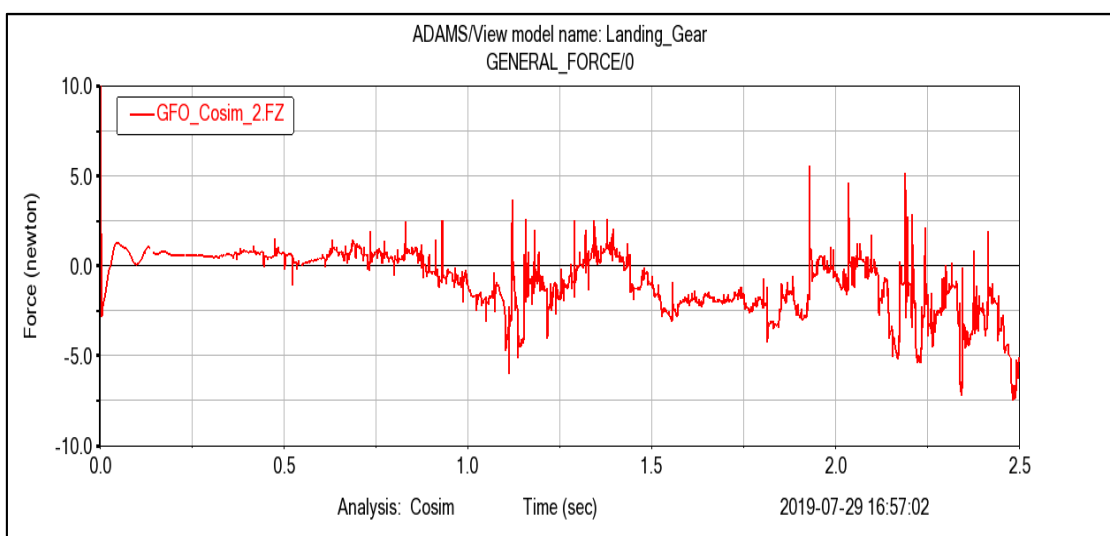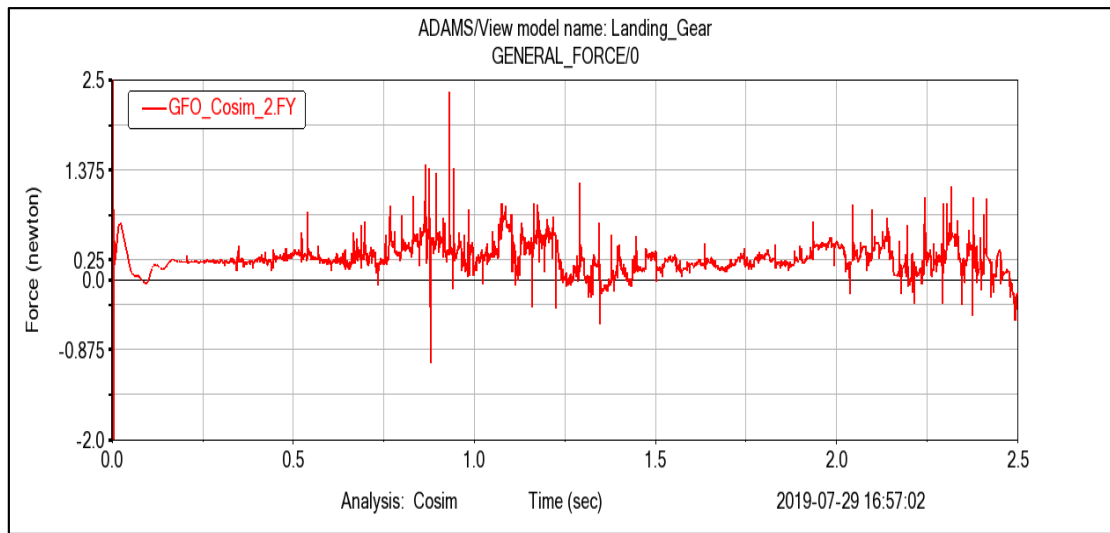
80

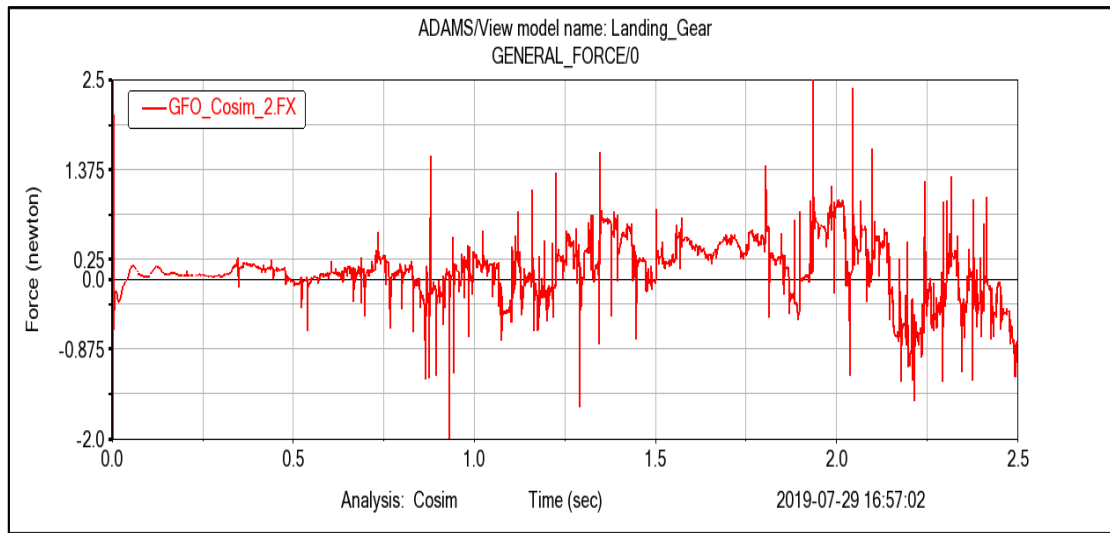*Figure 6.26: The three aerodynamic force component along X, Y and Z axis on the lower connecting rod.*
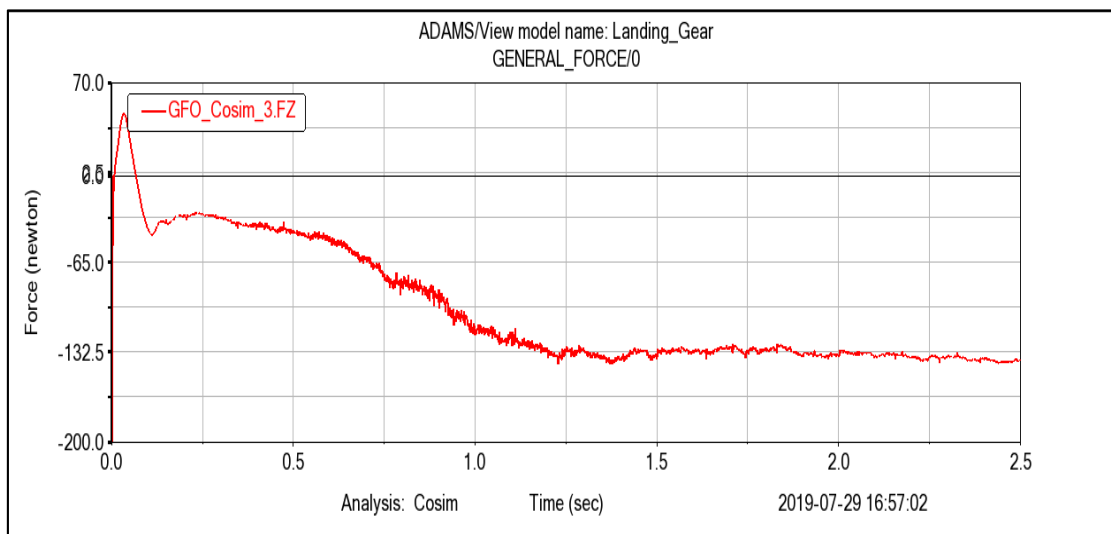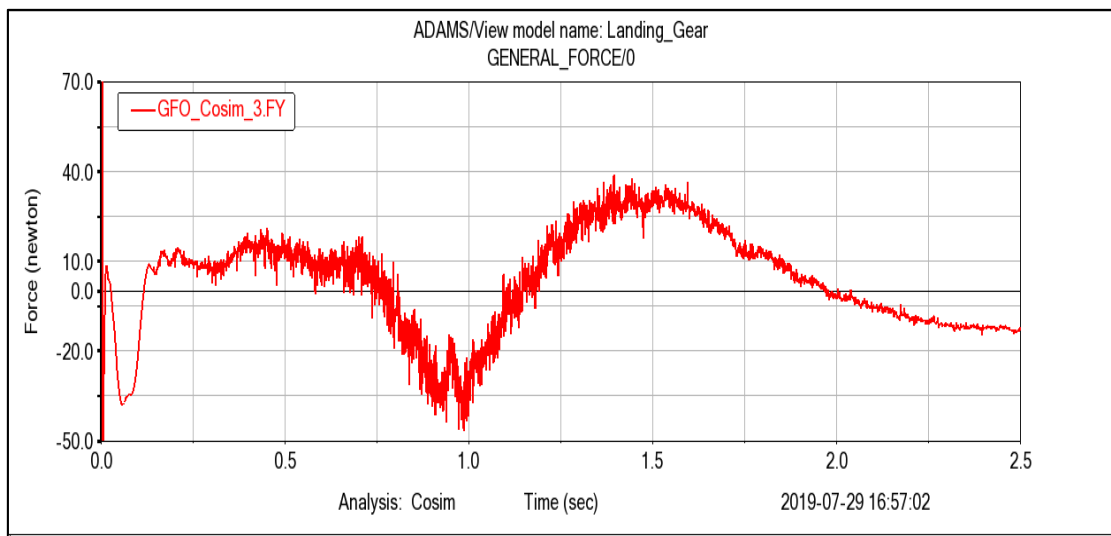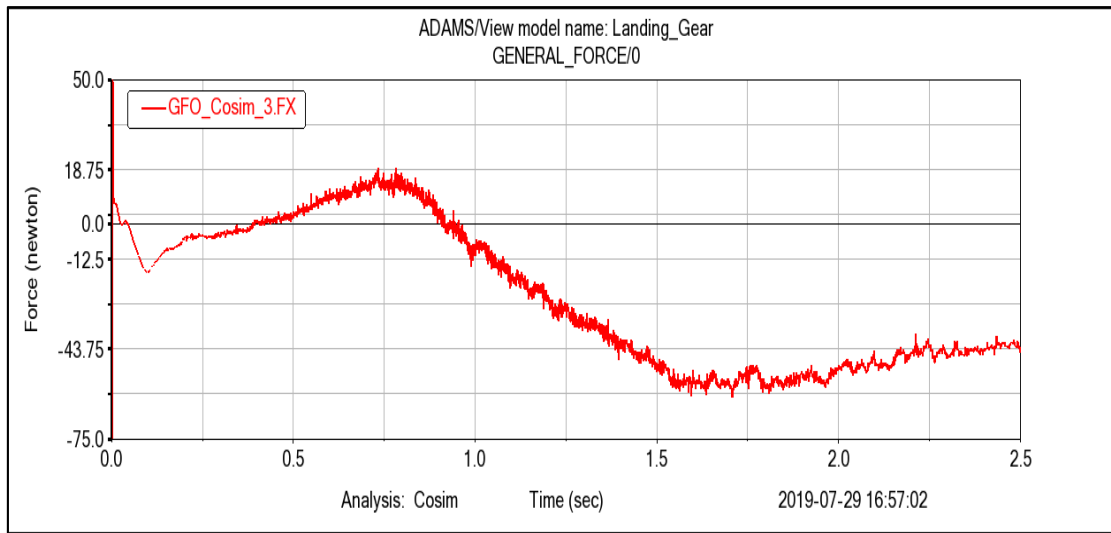
Figure 6.27: The three aerodynamic force component along X, Y and Z axis on the landing gear leg.
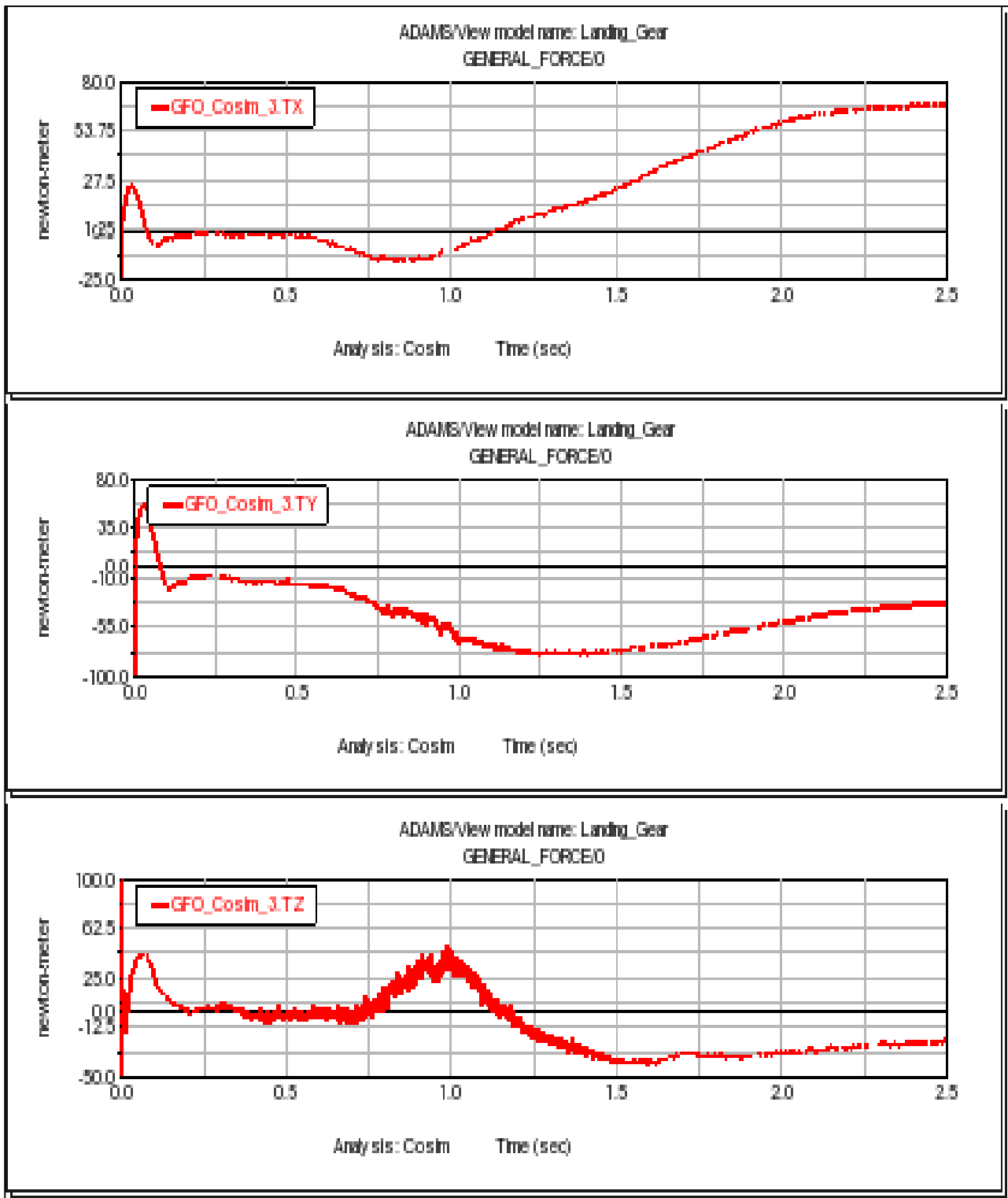
Figure 6.28: The three aerodynamic torques component around X, Y and Z axis on the landing gear leg.

The forces upon the two connecting rod can be almost neglected, infact the two parts for the entire simulation are covered by the compartment. A comparison can be done considering the force acting along the z axis upon the landing gear leg, this force is the drag resistance and its trend and values are very similar to that shown in *figure 6.22.* Introduced the aerodynamic loads which modifies the forces and torques necessary to satisfy the imposed motion law, it is interesting to show in which way they have changed and verify if the different trends are imputabled to the transmitted load. The data which will be presented are relative to the four main connectors present in the analysis, the first one is the bushing which belongs to the family of flexible connectors, the second one is the spherical, the third and the last one are two revolute joints which allow only the rotation around one axis.
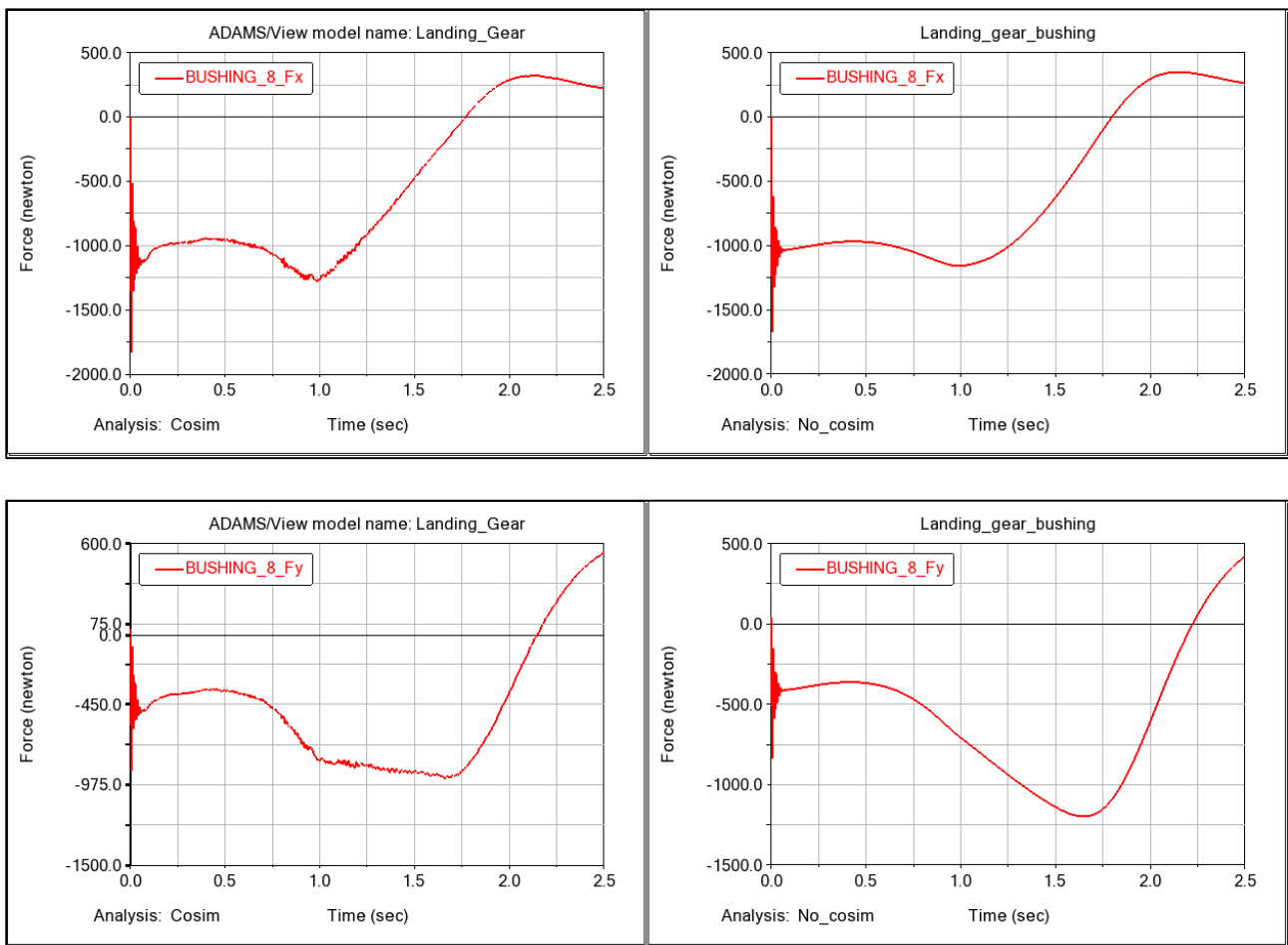
− Starting from the bushing:

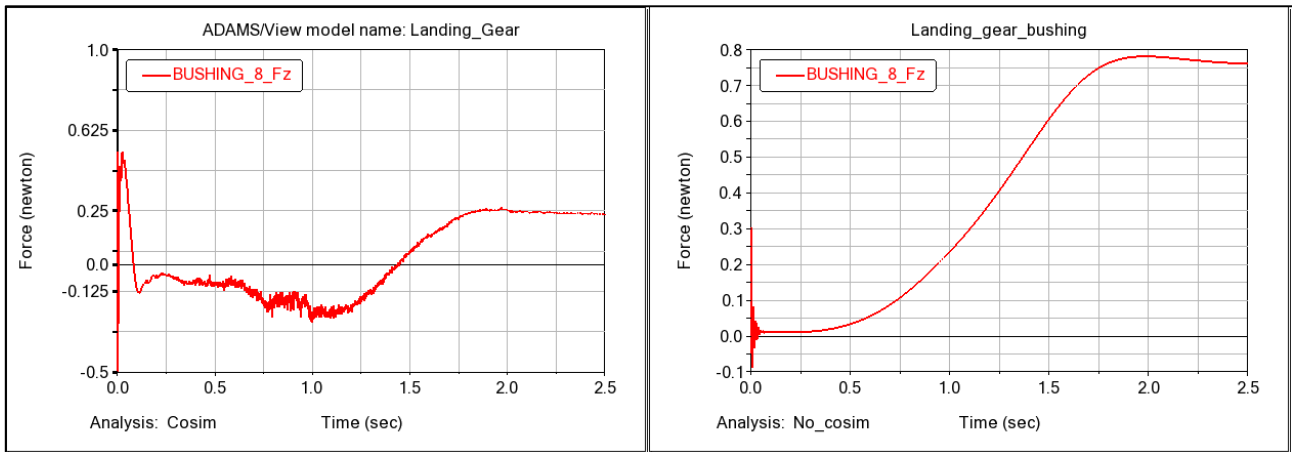*Figure 6.29: Force components along X and Y axes acting on the bushing.*

Figure 6.30: Force component along Z axis acting on the bushing.
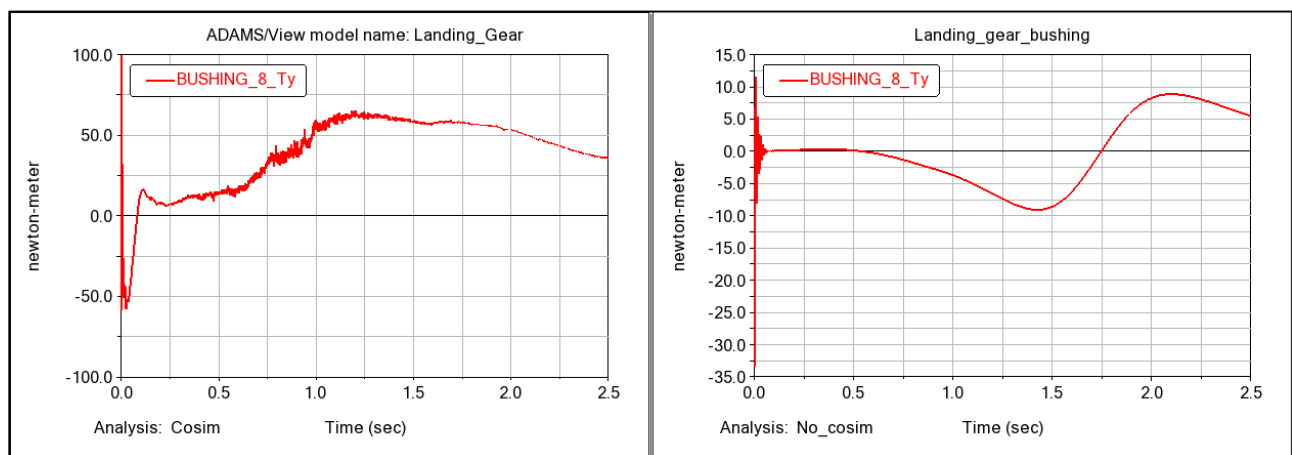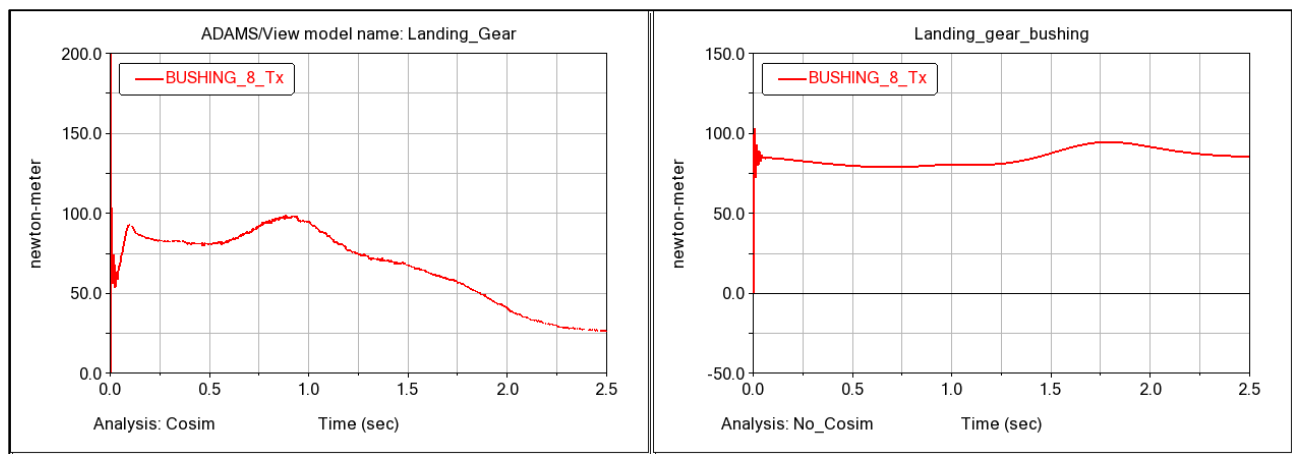

Figure 6.31: Torque components around X and Y axes acting on the bushing.
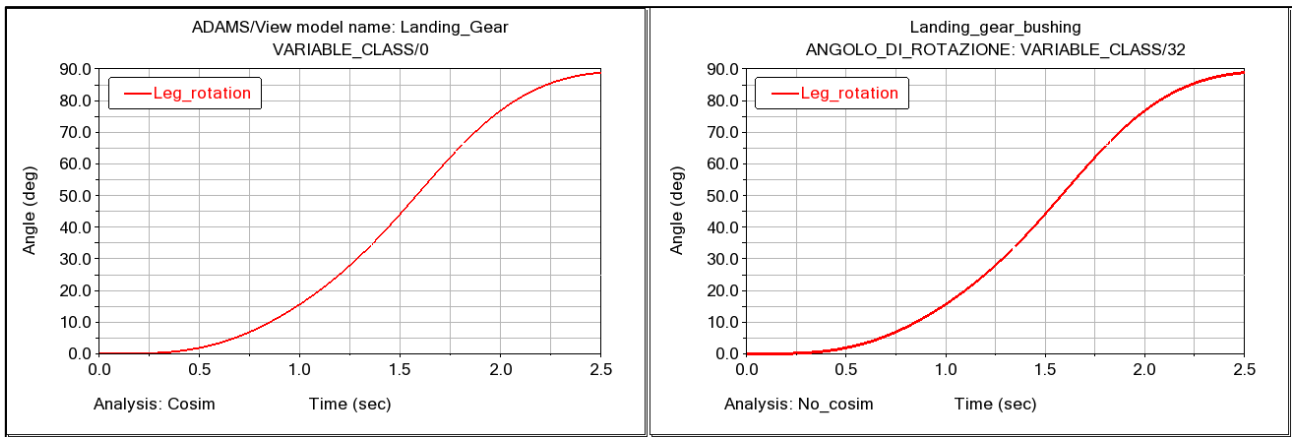
85

Figure 6.32: Angular rotation of the landing gear leg.

‒ The spherical:
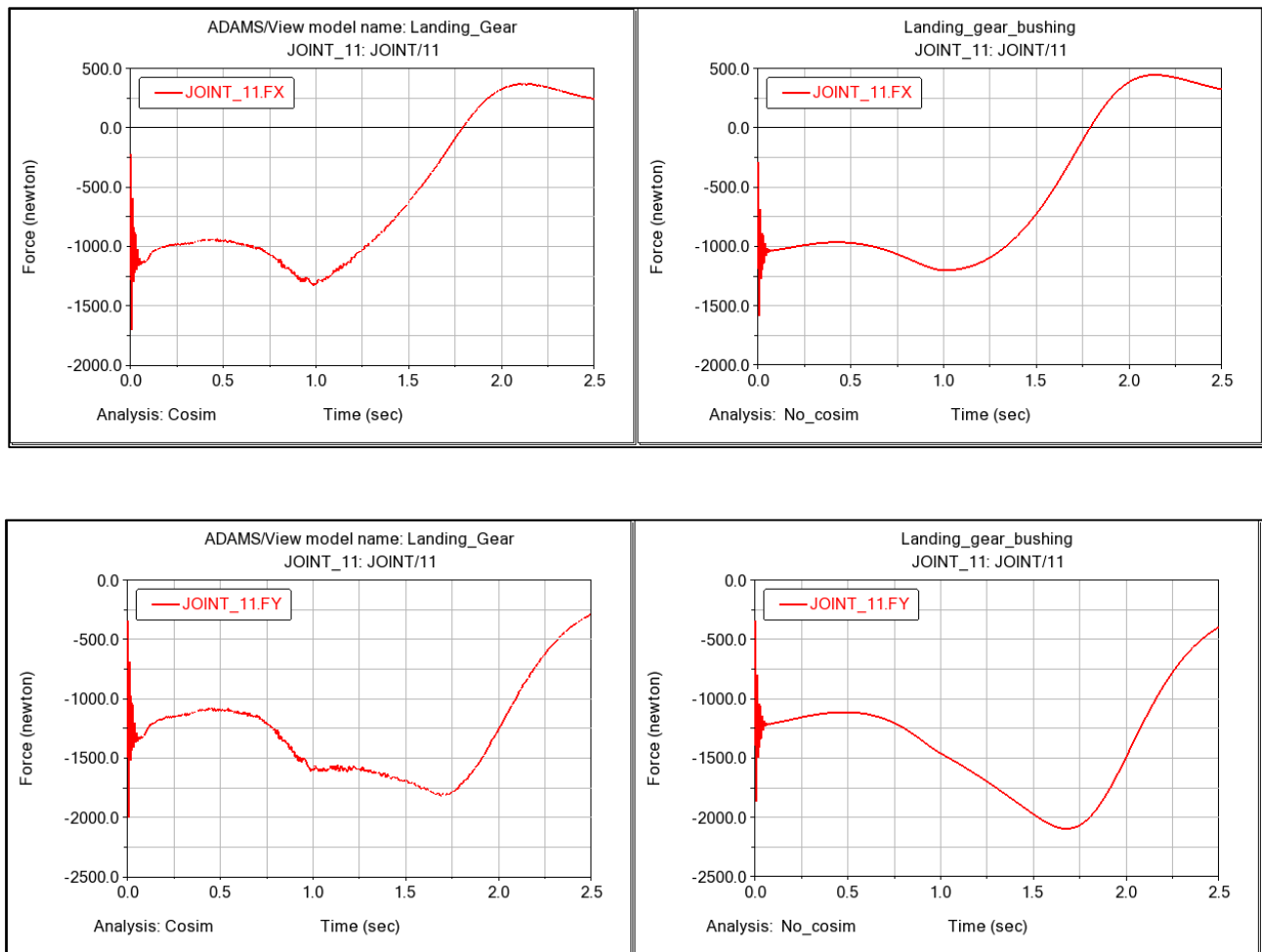
Figure 6.33: Reaction components along X and Y axes of spherical joint
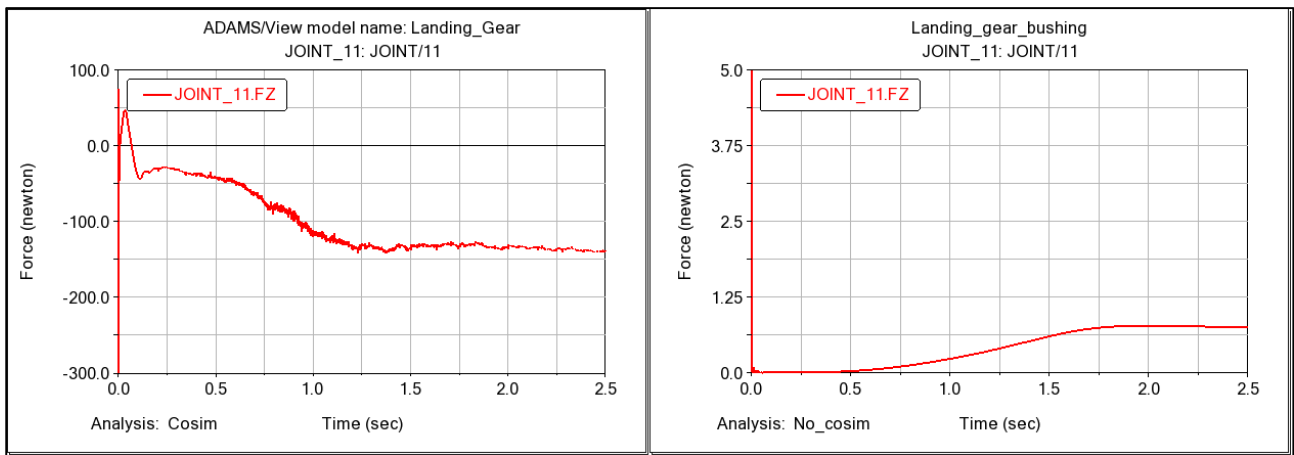
Figure 6.34: Reaction components along Z axis of spherical joint

– The revolute joint between the upper and lower rod:
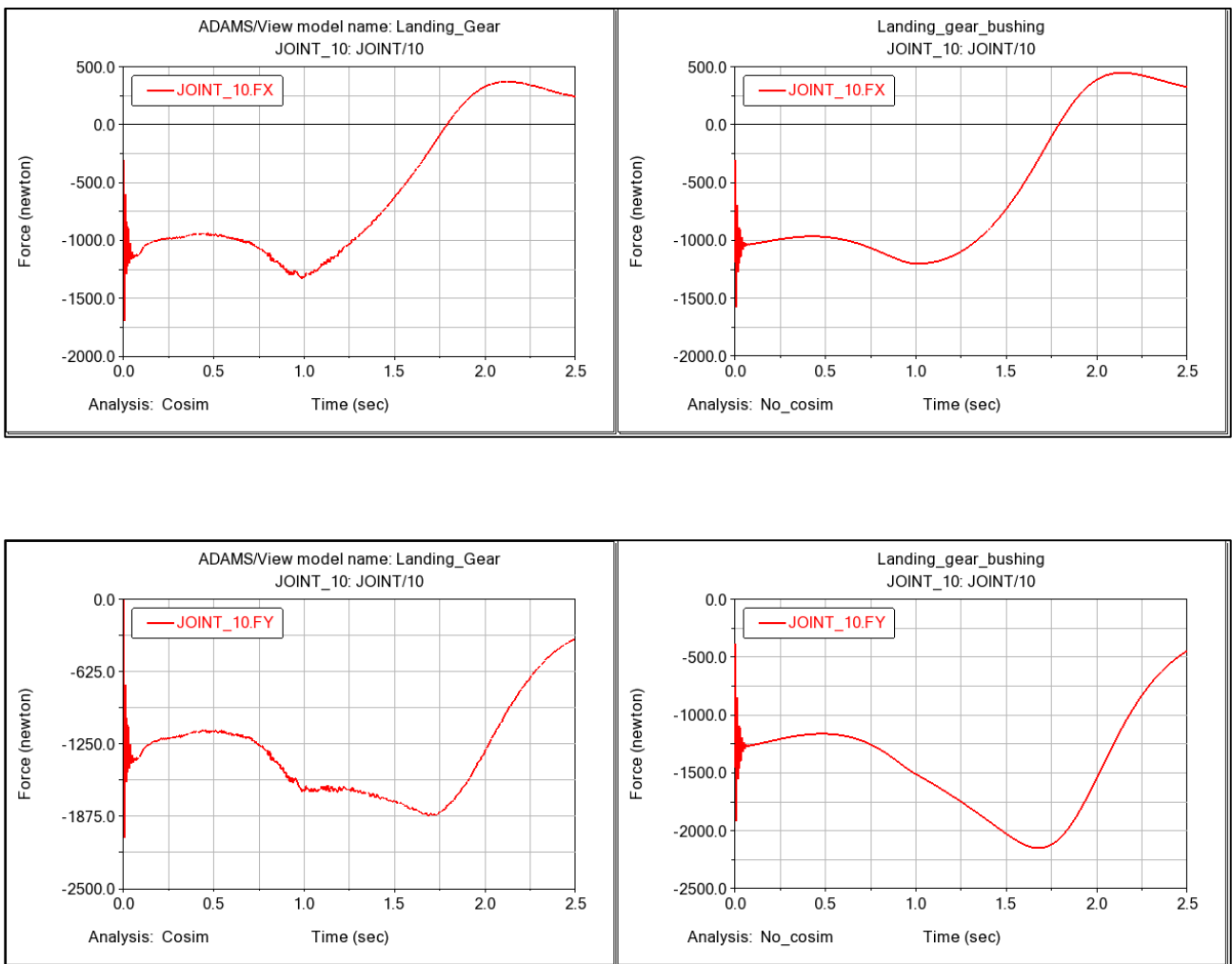
Figure 6.35: Reaction components along X and Y axes of lower revolute joint.

Figure 6.36: Reaction component along Z axis of lower revolute joint.
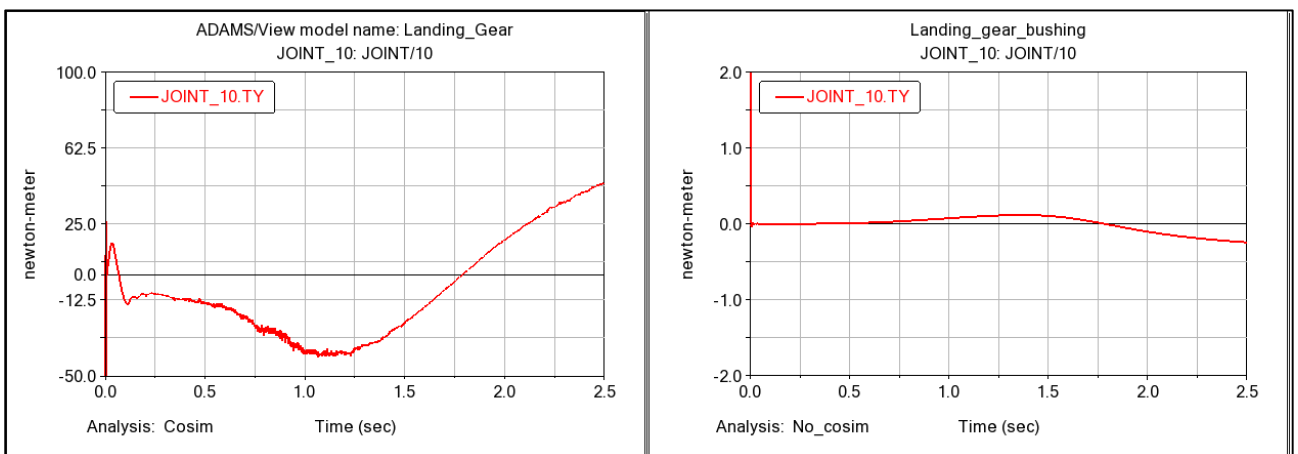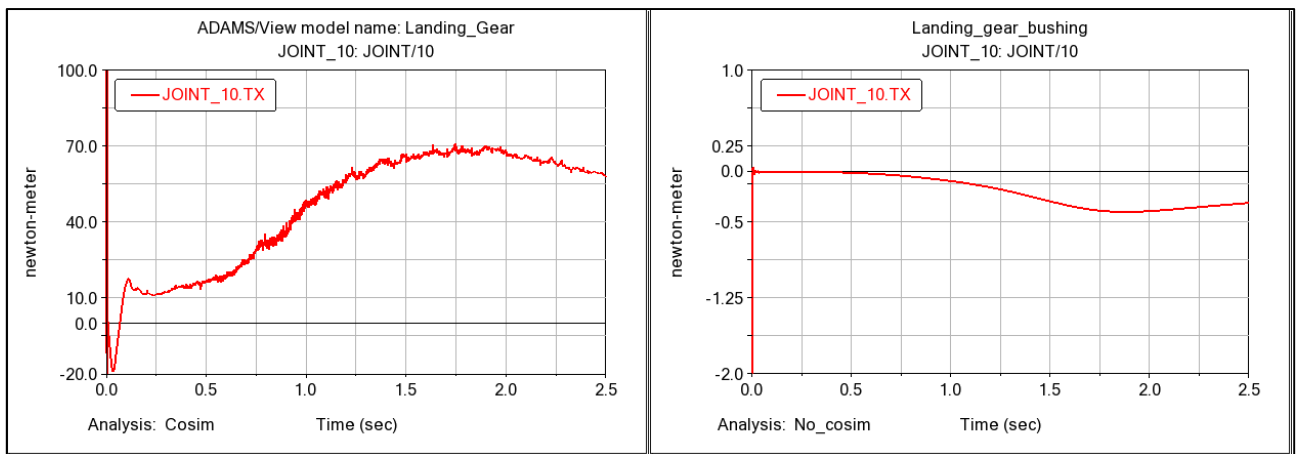
Figure 6.37: Reaction components around X and Y axes of lower revolute joint.

88

Figure 6.38: Angular rotation, angular velocity and angular acceleration of the lower revolute joint.

– The revolute joint between the upper connecting rod and the landing gear compartment:
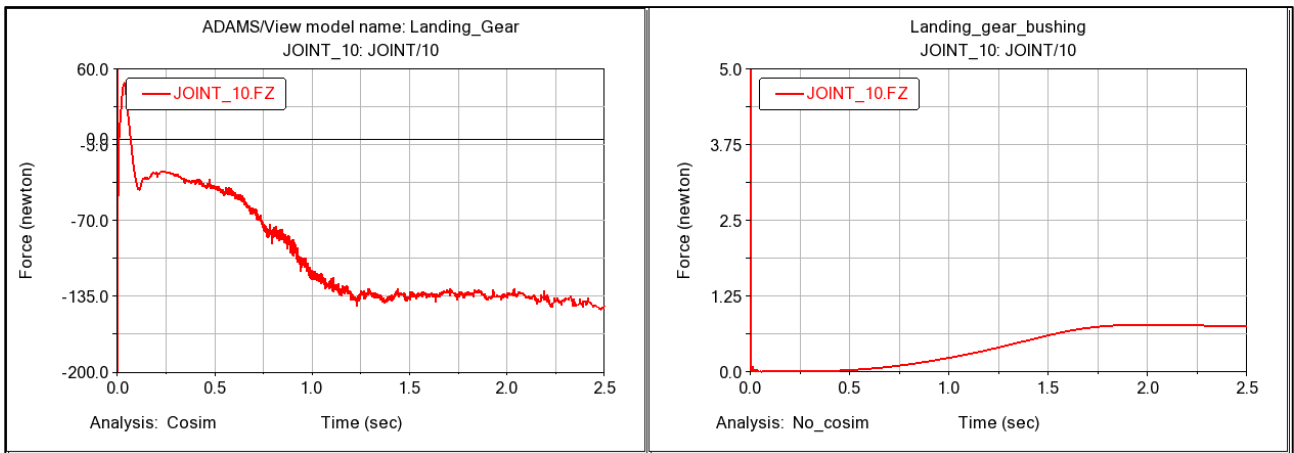

Figure 6.39: Reaction components along X, Y and Z axes of upper revolute joint.

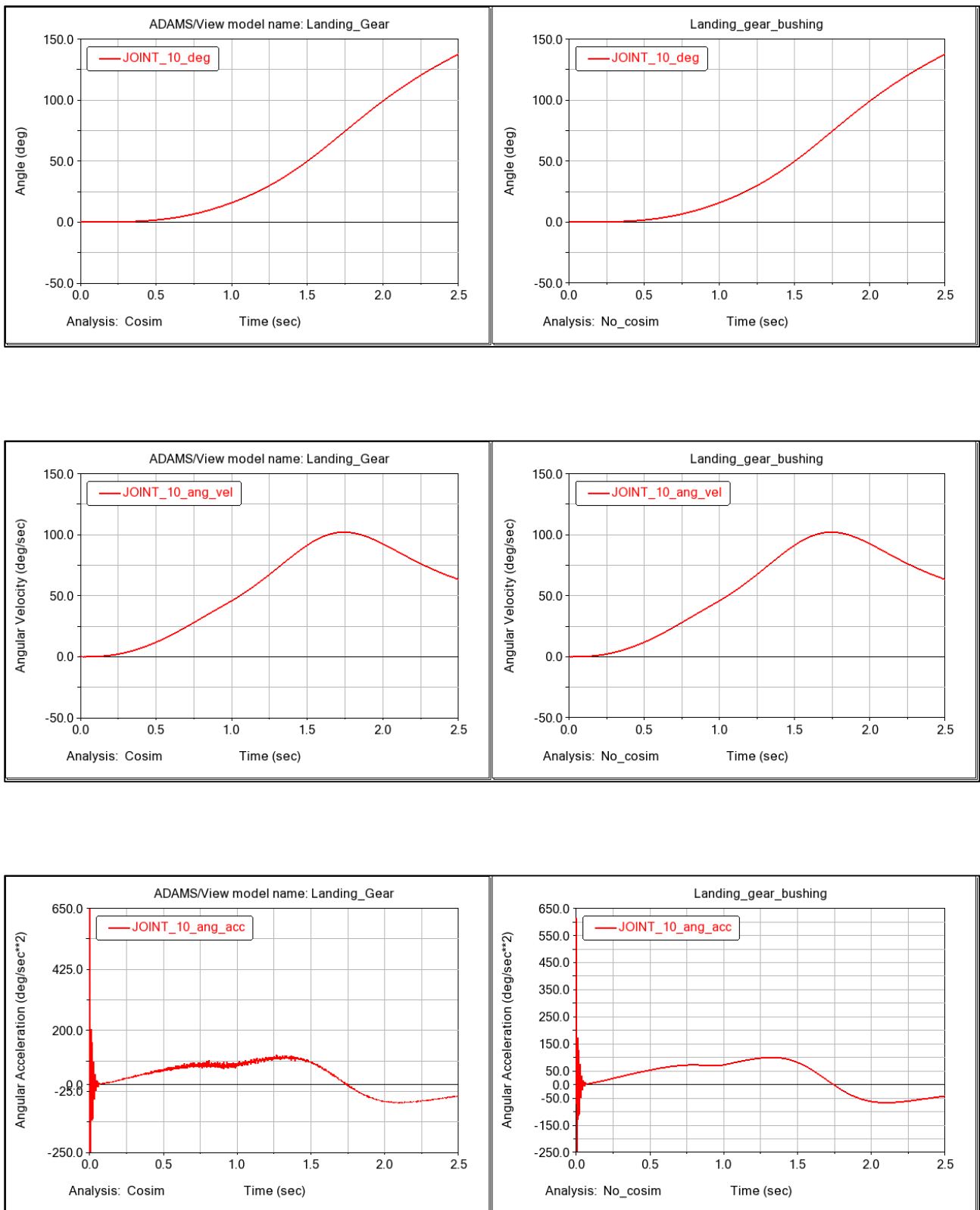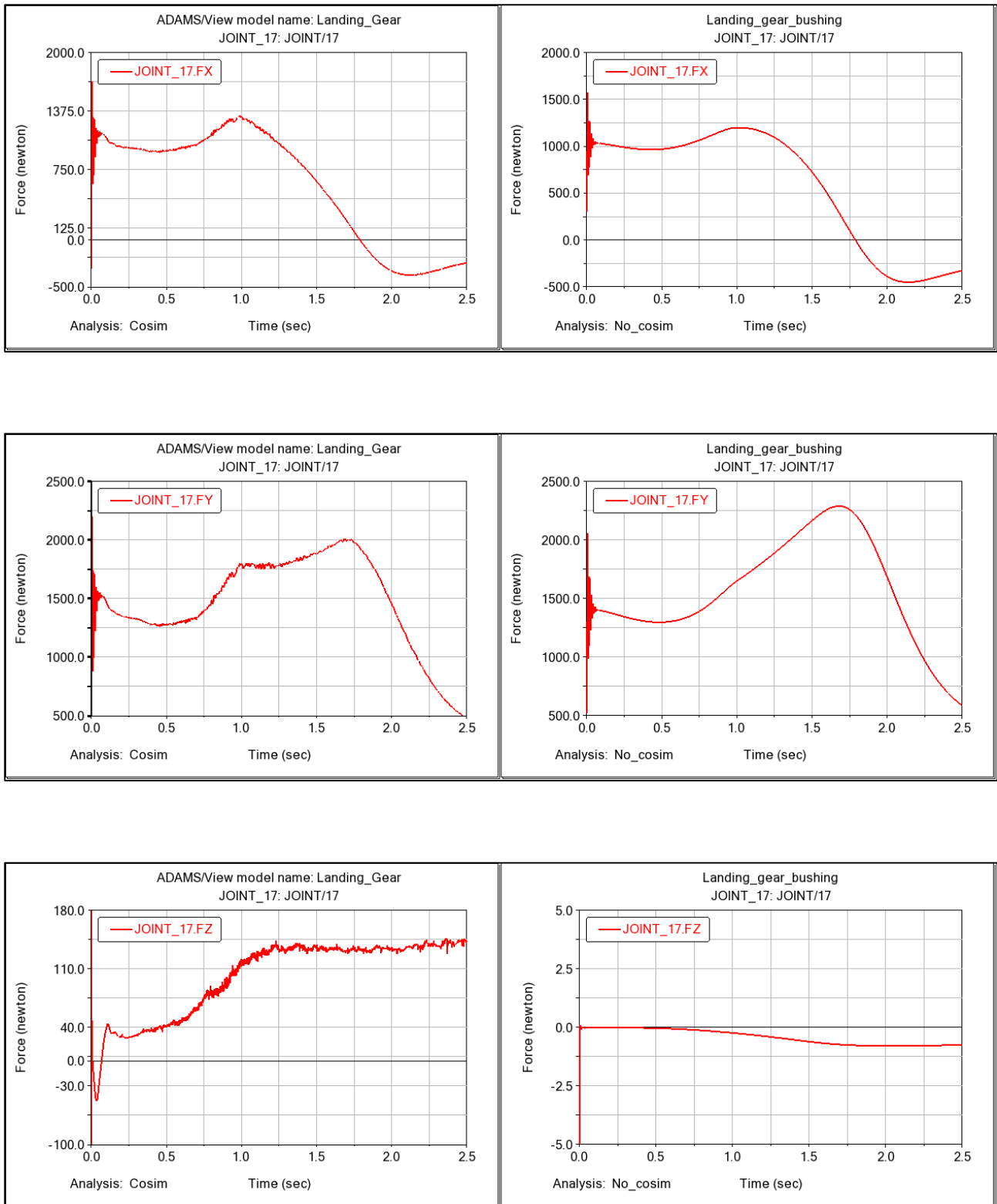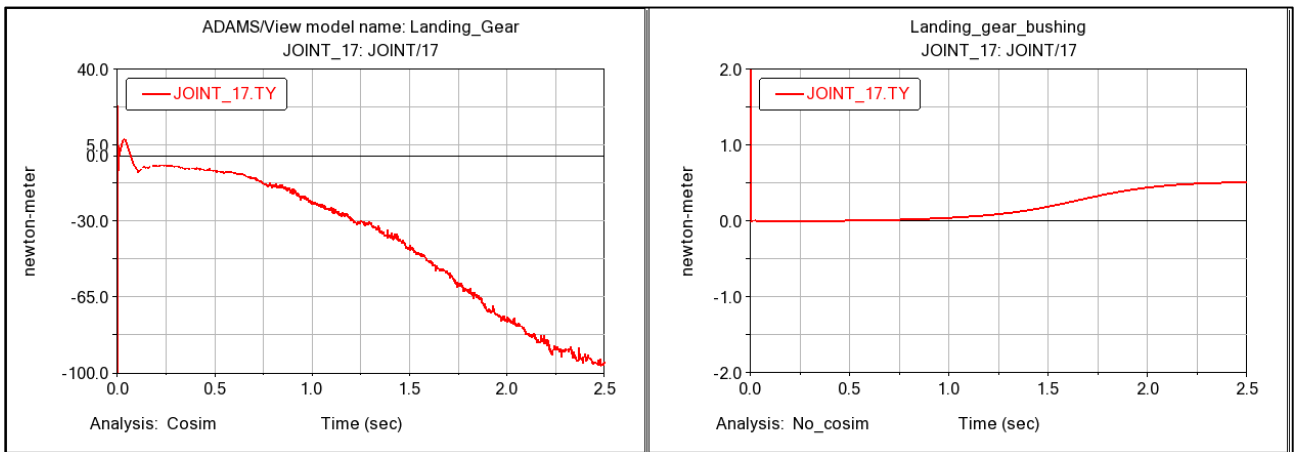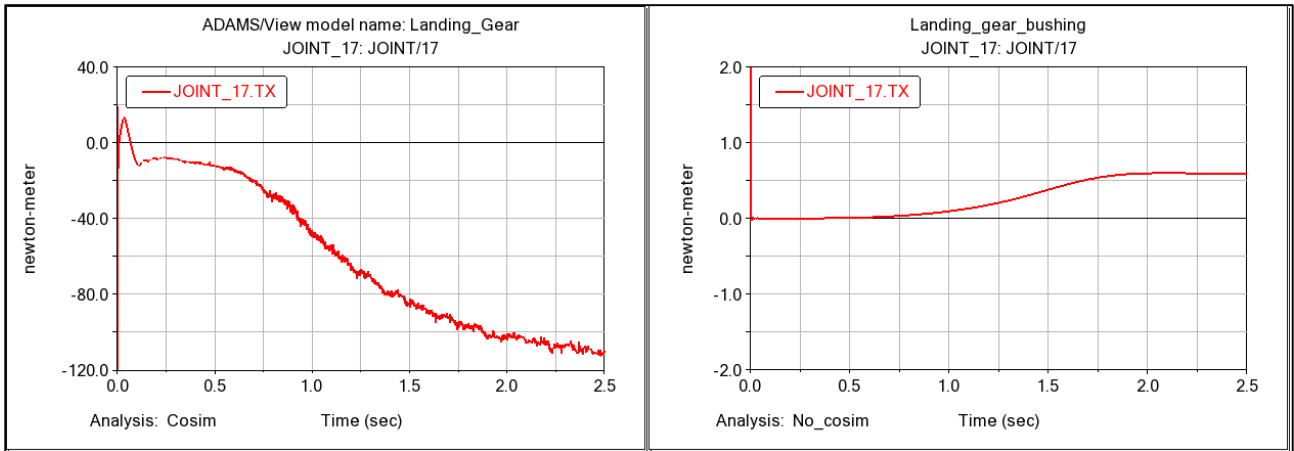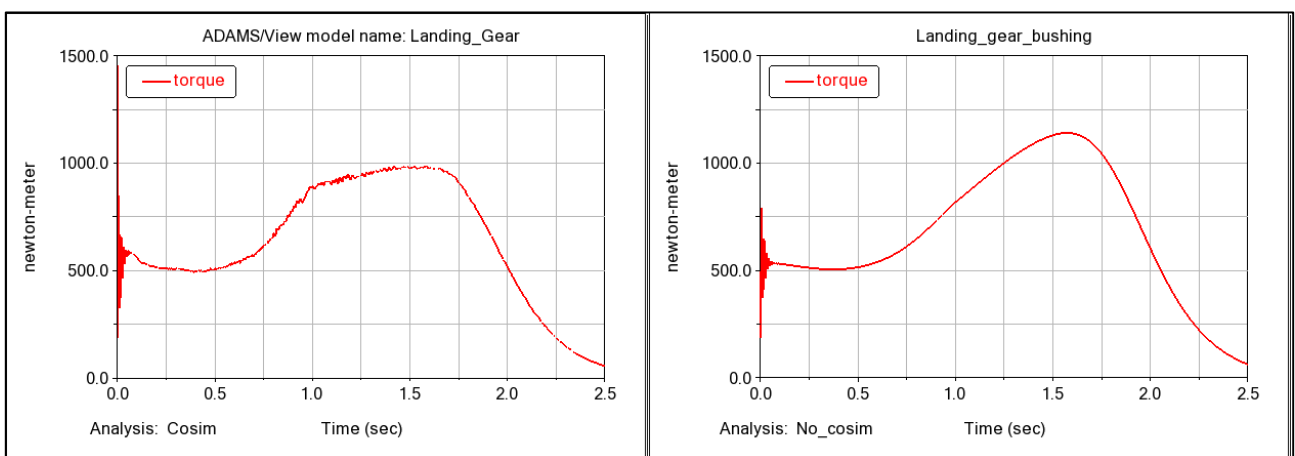*Figure 6.40: Reaction components around X and Y axes of upper revolute joint.*

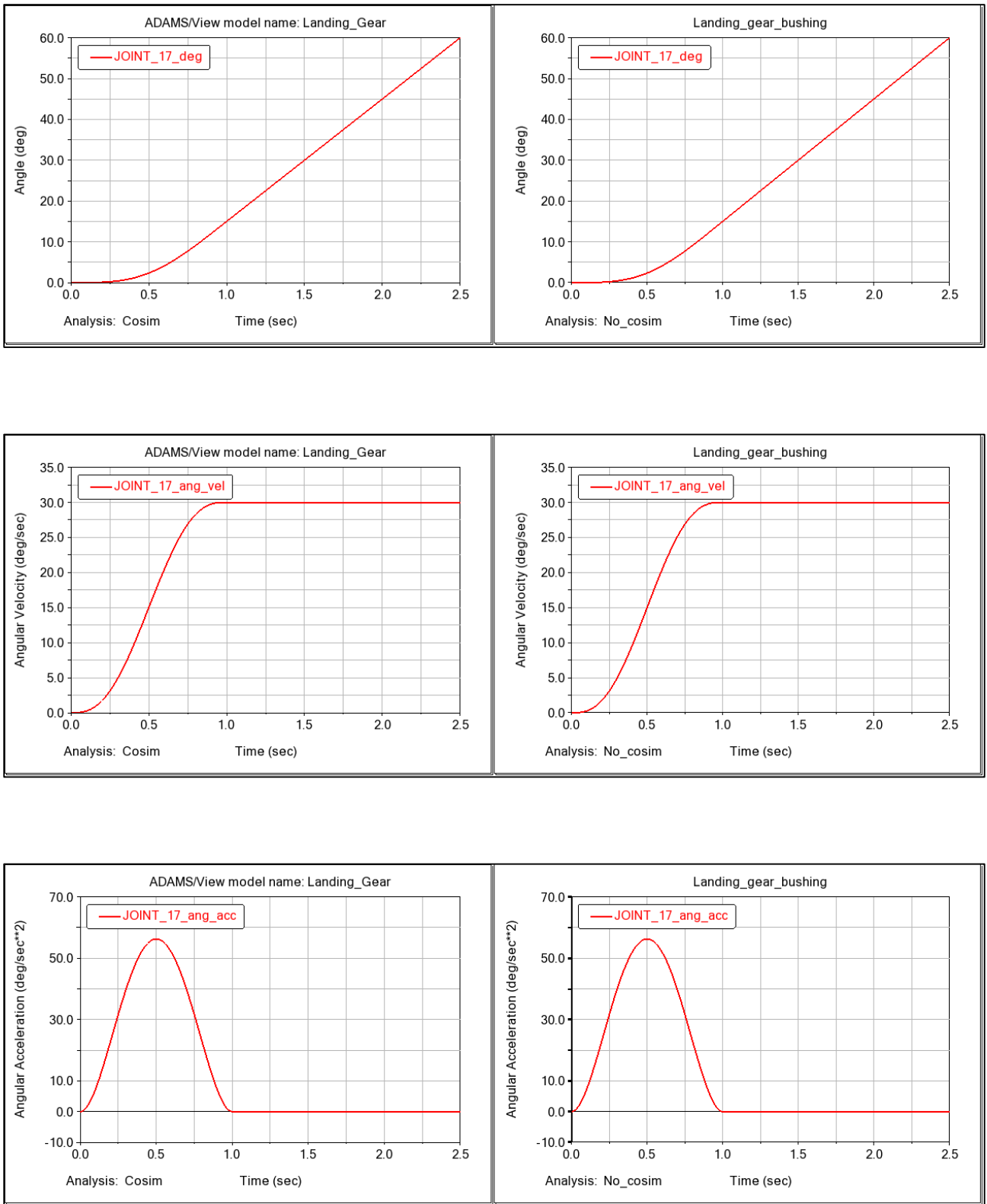*Figure 6.41: Torque acting on the upper revolute joint to obtain the desired rotation.*

Figure 6.42: Angular rotation, angular velocity and angular acceleration of the upper revolute joint.

Before analysing how the co-simulation can influence the results of a multibody simulation, it is interesting to pay attention to figures 6.32, 6.38 and 6.42. In these figures are displayed the angular rotation and velocity trends of the bushing and the two revolute joint, on the right there are the un-coupled results while on the left the coupled ones. In both configurations, the trends are equal despite in the two analysis different forces are applied. This result can be explained observing that the mechanism motion is defined through a motion law, according with previous theoretical description. The motion law allows to guarantee the same displacements or rotations in the chosen time laps for each load configuration. In fact, when a motion law has been applied is possible to find which would be the ideal force or torque to apply on the joint to obtain the same movement. For this reason, in the two simulations there are the same displacements, however in order to obtain them is necessary that the applied load and then the joint reactions change.

Focussing on the figure 6.41 is possible to appreciate how the applied torque changes in order to allow the rotation of mechanism when aerodynamic loads (figure 6.27 and 6.28) are applied. By considering the first section of the plot, from $t = 0\ s$ to $t\ =\ 1\ s$, in order to perform the requested rotation in the coupled analysis is necessary a major torque. In fact the slope of the curve is initially major reaching a value of $879\ N \cdot m$ at $t\ =\ 1$ s against $795\ N \cdot m$ of the uncoupled simulation. After this moment a rapidly slope change occurs, in fact differently from uncoupled simulation in which the torque reaches a maximum point over the $1100\ N \cdot m$, in the coupled one the aerodynamic load allow to obtain the same displacement with a torque maximum of $980\ N \cdot m$ at the same time ($1.57\ s$). The two plots, after the maximum point, show a concordant and decreasing trend in line with the almost completely extracted configuration of the landing gear. The consequences to have introduced in the model new loads and then a different necessary torque are the variation of the joint reaction. This can be observed by plotting the joint reaction resultant before and after the co-simulation.
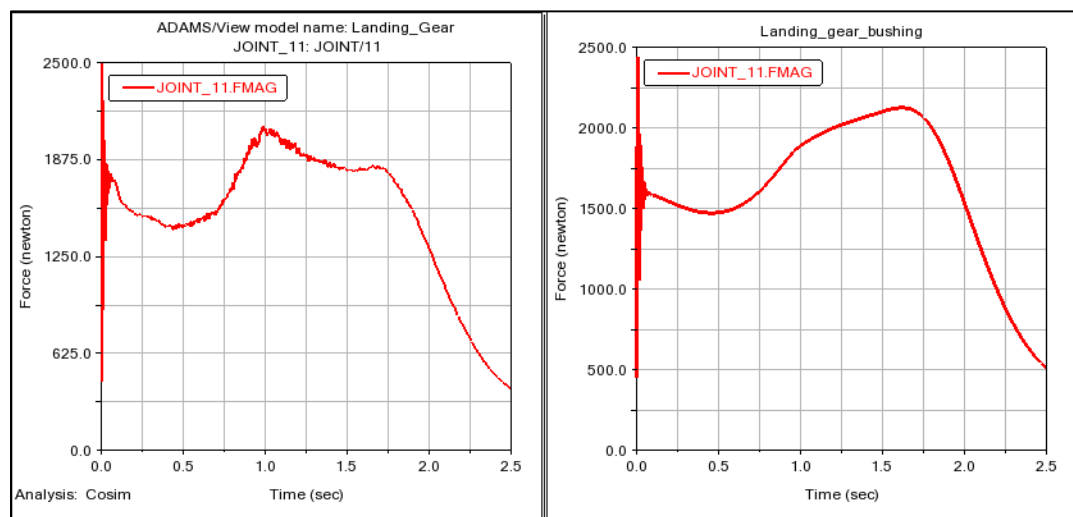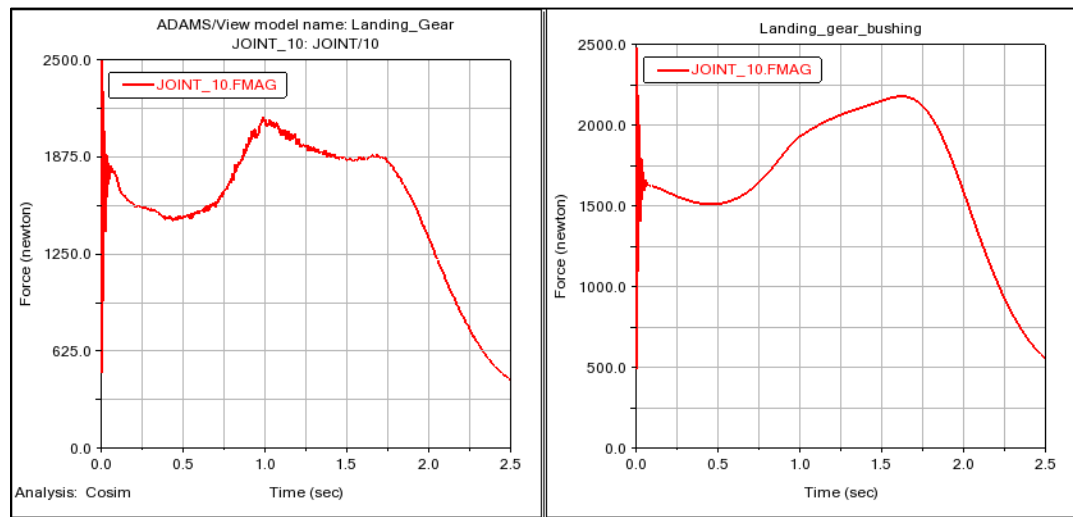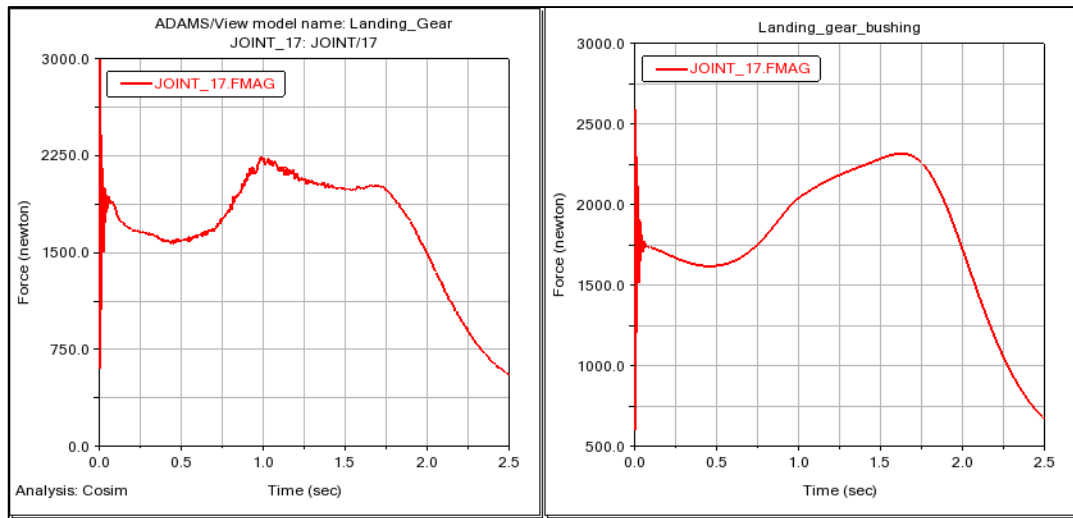
Figure 6.43: Joint reaction resultants, above that of upper rod revolute, in the middle that of lower rod revolute, below that of spherical.

The three-plotted trends are quite similar but between the two analysed cases there are some differences. The first section of the two compared plots, from $t = 0\ s$ to $t = 0.75\ s$, presents a similar trend in which the reaction first decreases reaching a minimum point and then increase. At $1\ s$ the reactions relative to the co-simulated model have a maximum point after which two decreases with two different slope are present, in which the first one is more soft than second. Different from the coupled analysis in the un-coupled one the maximum point is not at $1\ s$ but at $1.75\ s$, after which the reaction decrease starts. As happen for the analysed torque also for the reaction during this final section the trends return to be congruous.

6.3 Cosim Transmitted Quantities: Percentage Error

This last section has the purpose to investigate on the co-simulator work analysing the error margin between the calculated quantities by the "slave-code" and the transmitted one by the "master-code".

To observe if the trend of the error is the same or it change time-by-time two simulations with the same settings have been executed.

The chosen reference quantity is the aerodynamical force along the Z-axis because it rapresents the most important contribute acting on a landing gear.

The described analysis can be conducted introducing an estimator of the error, it is defined as:

$$\epsilon_\% = \frac{F_{z_t} - F_{z_c}}{F_{z_c}} \cdot 100 \qquad\qquad (6.3.1)$$

where F_{z_t} is the transmitted force by the co-simulatore, while F_{z_c} is the calculated one by the CFD code.

The obtained results have been reported on a plot in which the percentage error is on the ordinate axis while on the abscissas axis is reported the time of simulation.
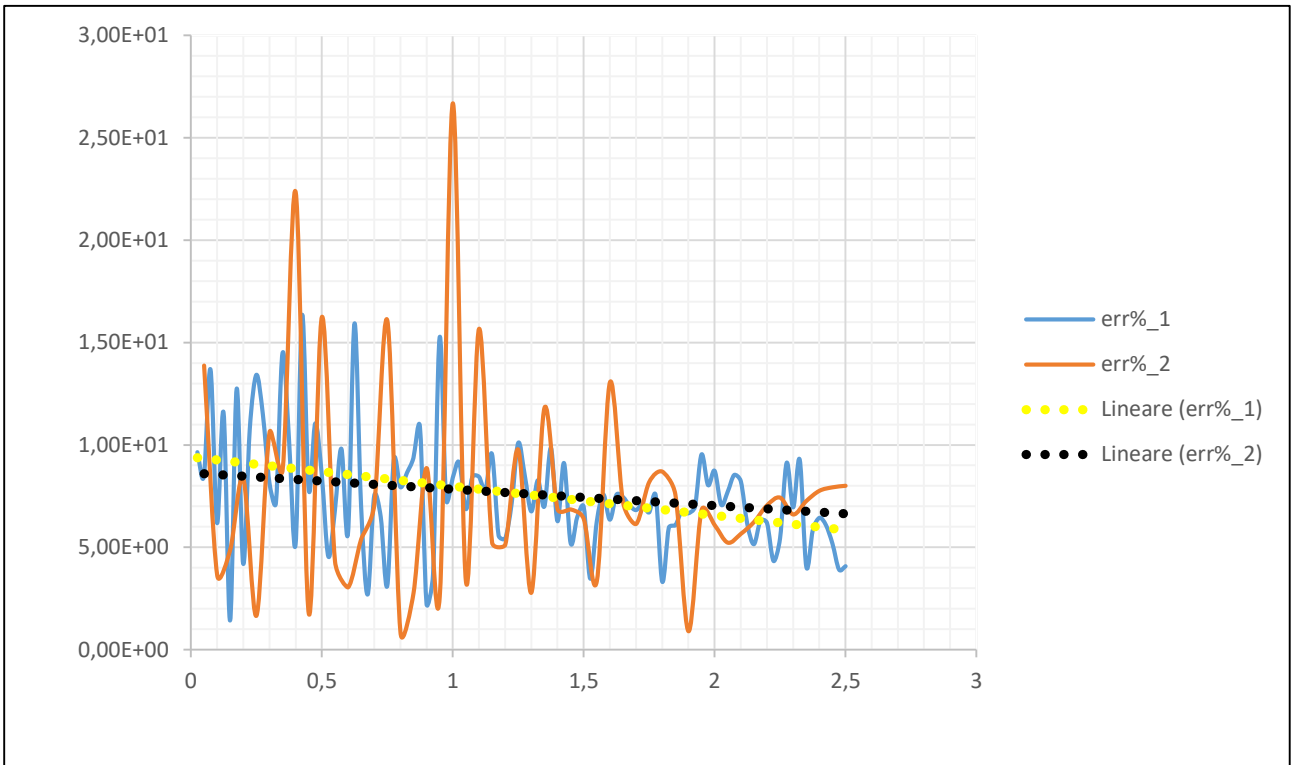
Figure 6.44: Percentage Error between the transmitted force and the calculated one, in blue the first simulation while in orange the second one.

The error trend in both the simulations fluctuates around the 5% and the10% decreasing with the passing of time, only in few isolated cases in the second analysis it increses over 20%. These few isolated errors do not represent a threat, in fact they represent only a neglected part of the entire sample.

Finally, as can be seen from the trend lines, the co-simulator transfers, in both the simulations, quantities which have congruent values between them and with the calculated ones by the code.

Conclusion

The present thesis represents the preliminary study of a landing gear whose results are obtained coupling the multi-body and CFD analysis. The main purpose of the work is to analyse how the mechanical loads during the extraction phase are influenced by the action of the aerodynamical forces. This analysis has been carried out at the MSC Software Company in Turin, thanks to technologies made available by them. In particular, for the calculation purpose three softwares developed by them have been fundamentals:

- MSC Adams
- scFLOW
- MSC Cosim

The first two are already known in engineering environment and used for the preparation of the relative models and the calculation execution while the third, still under development and testing, has been fundamental to perform a coupled calculation. His purpose is to allow the communication between the two softwares, transferring characteristic quantities such as displacements or forces from a code to another. It does not only transfer information but it decides also when to do it and in which way; principally if the set calculation time step on the two softwares is the same, the data are transferred each calculation step while if the temporal intervals are different the co-simulator sets through an interpolation model the data transmission in order to obtain the most efficient. The work can be divided in three main sections, the first two about models preparation of each calculation codes and a third about coupled calculation and post-processing of the results. Starting from the Adams model, based on the multibody theory, it is composed by different parts, each of them characterized by own concentrated mass. Each of the elements, which composes the landing gear, is appropriately linked to the previous and the following through kinematic and flexible joints, which allow to execute, based on their choice, specific displacements or rotations.

To execute a coupled analysis, in addition to base model, three general forces have been created on the interested parts. They initially have no value but they are subsequently filled with the aerodynamic force values by the co-simulator. At the end of the model preparation an uncoupled analysis has been execute in order to obtain elements which can be compared with the results that subsequently would be obtained.

At this point, because it is allowed by the two softwares, the developed geometry in Adams has been imported in the scFLOW environment, it has been adequately improved within the software itself in order to be correctly used for the CFD calculation. In particular, after the removal of redundant elements which could slow down or produce errors during the calculation, four domains have been generated, the first one fixed while the other three linked to the moving parts accordingly with the feature of the "Overset" mesh. Subsequently to this preliminary phase the calculation model has been made, it consists in a transitory analysis of incompressible flux using a turbulence model "$SST\ k - \omega$". In analogy with Adams, even in scFLOW, a further step to couple the simulations has been needed, in particular the surfaces which receive the displacements and on which the aerodynamic forces are calculated and subsequently transferred to Adams have been set. At the end of the model preparation phase a calculation has been launched through the co-simulation code, which has allowed to obtain the expected results.

Starting from the results obtained from the fluid-dynamic analysis, they appeared coherent with what the flow theory around blunt bodies reports. Infact from the velocity fields analysis it has been possible to appreciate a turbulent wake accordingly with the analysis Reynold number. A more adequate comparison has been made with the obtained numerical results, that are the drag coefficient and the pressure coefficient distribution around the wheel; they are coherent to those reported on reference texts or obtained through experimental and numerical analysis. The calculated error as distance from these reference results has not been more than 12.5%, it can depend on the built mesh that is not sufficiently detailed in order to describe all the phenomenology presented in the problem.

In Adams, differently, the results obtained by the coupled analysis has been compared with those relative to an uncoupled one. It has been evident how the presence of aerodynamics forces on the model has influenced the necessary mechanical torque for the landing gear extraction as well as the joint reactions of defined joints. In first analysis, considering the flow presence, the torque to supply for a correct extraction initially has resulted greater then the one evaluated in the uncoupled analysis while after a partial extraction of the landing gear the flow presence has had a positive influence on the necessary torque.

At the end a brief study on the co-simulator precision has been conducted, in particular one of the aerodynamic force component calculated by the numeric code has been compared with the one transferred by the co-simulator for each calculation step-time. The percentage error estimated as the distance between the two values never exceeded the 10%, except for a few cases.

Obviously the analysis carried out although it has proved to be sufficiently coherent, it presents different aspects which can be improved in order to obtain more accurate results. Starting from fluidodynamic analysis, as it has been specify, it would require a much more accurate calculation grid especially in the wall areas in which the involved phenomena such as the boundary layer need a lower dimension for a good simulation. Moreover, the used geometry represents a rudimental model of landing gear, it doesn't present a lot of details and then a subsequent simulation can be performed on a model which better reflects the real counterpart.

An aspect, which is no less important is relative to the co-simulator software, infact it is still in development phase, then it presents some analysis limits which preclude the possibility to perform more detailed simulation.

In conclusion, it can be assumed that the carried out work represents a good starting point for future analysis and moreover it puts in evidence the potential of this new technology. Infact, thanks to the co-simulator will be possible to perform numeric analysis, which combine different physic phenomena, producing more accurate result compared to the obtained ones through experimental approach.

Bibliography

[1] ADAMS Theory in a Nutshell, D. Negrut, B. Harris, 2001

[2] "https://it.wikipedia.org/ wiki/Fluidodinamica_computazionale"

*[3] Fondamenti di termofluidodinamica applicata,
SGEditoriali. G.Comini, G. Croce,E. Nobile, 2008*

[4] scFLOW User's Guide Analysis Method

[5] scFLOW User's Guide Analysis Method/Turbulent Flow

[6] https://it.wikipedia.org/wiki/Equazioni_di_Navier-Stokes

*[7-1] Wilcox, D., "Turbulence Modeling for CFD," Second Edition, CDW Industries, Inc.,
(1998).*

*[7-2] Menter, F., "Zonal Two Equation k-ω Turbulence Models for Aerodynamic Flows," AIAA
93-2906, (1993).*

*[7-3] Egorov, Y., Menter, F., "Development and Application of SST-SAS Turbulence Model in
the DESIDER Project," Hybrid RANS-LES Modelling, p.261-270., (2008)*

[8] MSC CoSim V1.6 (Beta) User's Guide, MSC Software Corporation, 2018

[9] "https://it.wikipedia.org/wiki/Carrello_d%27atterraggio"

[10] <Adams online help>, "mscsoftware.com"

*[11] Armstrong, Daniel; Najafi-Yazdi, Alireza; Mongeau, Luc; Raymond, Vincent; "Numerical
Simulations of Flow over a Landing Gear with Noise Reduction Devices using the Lattice-
Boltzmann Method",10.2514/6.2013-2114, 19th AIAA/CEAS Aeroacoustics Conference,
2013/05/27*

*[12] Hoerner, S.,F., "FLUID-DYNAMIC DRAG theoretical, experimental and statistical
information",1965*